

Highly dispersive magnons with spin-gap like features in the frustrated ferromagnetic $S = 1/2$ chain compound $\text{Ca}_2\text{Y}_2\text{Cu}_5\text{O}_{10}$ detected by inelastic neutron scattering

M. Matsuda,¹ J. Ma,^{1,*} V. O. Garlea,¹ T. Ito,² H. Yamaguchi,² K. Oka,² S.-L. Drechsler,³ R. Yadav,³ L. Hozoi,³ H. Rosner,⁴ R. Schumann,⁵ R.O. Kuzian,^{6,7} and S. Nishimoto⁸

¹*Neutron Scattering Division, Oak Ridge National Laboratory, Oak Ridge, Tennessee 37831, USA*

²*National Institute of Advanced Industrial Science and Technology (AIST), Tsukuba, Ibaraki 305-8562, Japan*

³*Institute of Theoretical Solid State Physics, IFW Dresden, Helmholtzstraße 20, D-01069 Dresden, Germany*

⁴*Max-Planck-Institute of Chemical Physics, Nöthnitzer Str. 40, D-01187 Dresden, Germany*

⁵*Department of Phys., Inst. of Theor. Physics, TU Dresden, D-1062 Dresden, Zellescher Weg 17, Germany*

⁶*Institute for Problems of Materials Science NASU, Krzhizhanovskogo 3, 03180 Kiev, Ukraine*

⁷*Donostia International Physics Center (DIPC), Paseo Manuel de Lardizabal 4,*

San Sebastian/Donostia, 20018 Basque Country, Spain

⁸*Department of Phys., Inst. of Theor. Physics, TU Dresden, Mommsenstraße, D-01069 Dresden, and Inst. for Theoretical Solid State Physics, IFW-Dresden, Helmholtzstraße 20, D-01069 Dresden, Germany*

(Dated: October 9, 2019)

We report inelastic neutron scattering experiments in $\text{Ca}_2\text{Y}_2\text{Cu}_5\text{O}_{10}$ and map out the full one magnon dispersion which extends up to a record value of 53 meV for frustrated ferromagnetic (FM) edge-sharing CuO_2 chain (FFESC) cuprates. A homogeneous spin-1/2 chain model with a FM nearest-neighbor (NN), an antiferromagnetic (AFM) next-nearest-neighbor (NNN) inchain, and two diagonal AFM interchain couplings (ICs) analyzed within linear spin-wave theory (LSWT) reproduces well the observed strong dispersion along the chains and a weak one perpendicularly. The ratio $\alpha = |J_{a2}/J_{a1}|$ of the FM NN and the AFM NNN couplings is found as ~ 0.23 , close to the critical point $\alpha_c = 1/4$ which separates ferromagnetically and antiferromagnetically correlated spiral magnetic ground states in single chains, whereas $\alpha_c > 0.25$ for coupled chains is considerably upshifted even for relatively weak IC. Although the measured dispersion can be described by homogeneous LSWT, the scattering intensity appears to be considerably reduced at ~ 11.5 and ~ 28 meV. The gap-like feature at 11.5 meV is attributed to magnon-phonon coupling whereas based on density matrix renormalization group simulations of the dynamical structure factor the gap at 28 meV is considered to stem partly from quantum effects due to the AFM IC. Another contribution to that gap is ascribed to the intrinsic superstructure from the distorting incommensurate pattern of CaY cationic chains adjacent to the CuO_2 ones. It gives rise to non-equivalent CuO_4 units and Cu-O-Cu bond angles Φ and a resulting distribution of all exchange integrals. The J 's fitted by homogeneous LSWT are regarded as average values. The record value of the FM NN integral $J_1 = 24$ meV among FFESC cuprates can be explained by a *non-universal* $\Phi (\neq 90^\circ)$ and Cu-O bond length dependent *anisotropic* mean direct FM Cu-O exchange $\bar{K}_{pd} \sim 120$ meV, similar to a value of 105 meV for Li_2CuO_2 , in accord with larger values for La_2CuO_4 and CuGeO_3 (~ 110 meV) reported by Braden *et al.* [Phys. Rev. B **54**, 1105 (1996)] phenomenologically. Enhanced K_{pd} values are also needed to compensate a significant AFM $J_{dd} \geq 6$ meV from the dd channel, generic for FFESC cuprates but ignored so far.

PACS numbers: 75.25.-j, 75.30.Kz, 75.50.Ee

I. INTRODUCTION

One-dimensional (1D) antiferromagnetic (AFM) spin (S) 1/2 systems have been studied intensively, since they exhibit exotic quantum effects. The spinon is a typical feature generic for the AFM Heisenberg chain. In contrast, 1D ferromagnetic (FM) systems do not show pronounced quantum effects since the FM state is an eigenstate of the spin Hamiltonian. However, frustrating couplings, such as a next-nearest neighbor (NNN) AFM J_2 and/or AFM interchain couplings (ICs), can cause a more interesting ground state [1]. In particular, they may

induce gaps of different nature for excited states, strongly dependent on the sign of the nearest-neighbor (NN) exchange J_1 : well-known for AFM J_1 for $0.241 \leq \alpha \lesssim 0.7$ in the context of the spin-Peierls problem [2] and recently found for FM J_1 at $\alpha > \alpha_c (= 1/4)$ due to quantum fluctuations [3], where the frustration α reads

$$\alpha = J_2 / |J_1| . \quad (1)$$

In $\text{Ca}_2\text{Y}_2\text{Cu}_5\text{O}_{10}$ (CYCO) and any other edge-sharing chain cuprates (see Sec. II and Fig. 1) described by the $S = 1/2$ J_1 - J_2 model, $J_2 > 0$ always holds due to the Cu-O-O-Cu superexchange. Then α^{-1} measures the coupling of two interpenetrating ferromagnetically interacting AFM Heisenberg chains, where the J_1 - J_2 chain is regarded as a topologically equivalent zigzag chain with different NN couplings. For FM J_1 , the ground state

* Present address: Department of Physics and Astronomy, Shanghai Jiao Tong University, Shanghai 200240, P. R. China

changes from a FM to an AFM spin-liquid with non-collinear spiral fluctuations for $\alpha > \alpha_c$ [1]. There are only few materials with long edge-sharing CuO_2 chains and relatively large J_1 - and J_2 -values near such a critical point. We mention three of them: (i) Li_2CuO_2 (LICO), with FM inchain order below its Néel temperature $T_N \approx 9$ K; (ii) $\text{Li}_2\text{ZrCuO}_4$, with a spiral ordering with $\alpha \approx 0.33$ (at $T < 7$ K), predicted in Ref. 4 and confirmed in Refs. 5 and 6 (see also [7]); (iii) further candidates near quantum criticality, where the insight gained for CYCO might be helpful to elucidate their exchange interactions and unusual magnetic states. Among them are $\text{La}_6\text{Ca}_8\text{Cu}_{24}\text{O}_{41}$ and derivatives which contain besides two-leg spin ladders (TLL) similar frustrated FM edge-sharing CuO_2 chains (FFESC).

A recent inelastic neutron scattering (INS) study for LICO [9–11] revealed a relatively large $J_1 = -19.7$ meV,

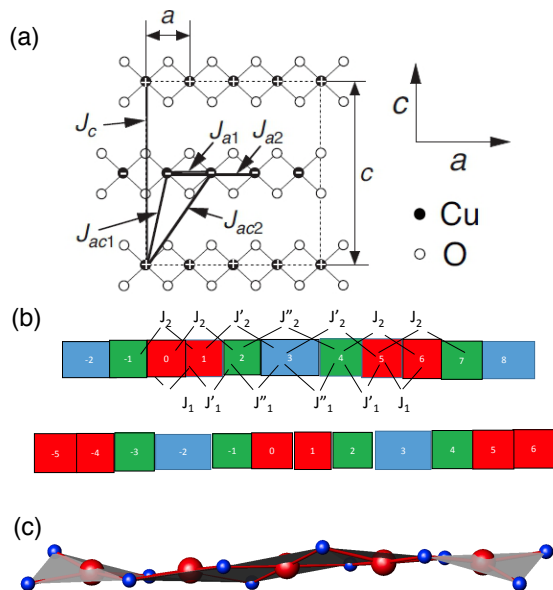


FIG. 1. (a) Schematic view of the CuO_2 spin chains in the ac plane of $\text{Ca}_2R_2\text{Cu}_5\text{O}_{10}$ ($R=\text{Y}$ and Nd) for an averaged idealized structure. Inchain couplings J_{a1} and J_{a2} as well as the two diagonal NN and NNN ICs J_{ac1} , J_{ac2} , and J_c are shown. The spin order in the ac plane is also depicted. Spins along $+b$ ($-b$) directions are shown with “+” (“-”), respectively. (b) A non-ideal Cu_5O_{10} chain due to its misfit with the adjacent cationic Ca_2R_2 ($R=\text{Nd}$ and Y) chains adopting symmetric distortions for simplicity. The 3 non-equivalent CuO_4 plaquettes of this case are depicted by red, green, and blue rectangles. Here a chain has 3 different boundaries (red-red, red-green, and red-blue pairs of bridging O) and three different Cu-O-Cu bond angles, giving rise to 3 different AFM contributions to each NN coupling (see Sec. V). At least 3 different NN and NNN couplings denoted by J_1 , J_1' , and J_1'' as well as J_2 , J_2' , and J_2'' [instead of 2 single J_{a1} and J_{a2} shown in (a)] appear. The general asymmetric chain has 5 non-equivalent plaquettes and a couple of 5 NN and NNN inchain couplings, respectively. (c) A distorted single chain according to the model by Thar *et al.* [8] (view along the c axis). Red (blue) spheres denote Cu (O) ions.

$\alpha = 0.332$, and a weak but nevertheless decisive AFM IC of 0.78 meV. Although $\alpha > \alpha_c$, a FM arrangement is realized in the chains due to specific AFM ICs. Within a refined linear spin-wave analysis employing the full magnon dispersion up to 53 meV and performing measurements along those scattering directions where the small IC can be separated from the large inchain one, we will show that J_1 of CYCO well exceeds the largest J_1 -values reported so far for LICO [9] and $\text{Li}_2\text{ZrCuO}_4$ [4, 5] among the FFESC family.

As shown in detail below, CYCO with a FM stacking of 2D Néel planes along the b axis is the “2D-analogue” of LICO. CYCO has the highest $T_N = 29.5$ K [12–14] and together with LICO the largest ordered magnetic moments among all FFESC. The critical point for the system of antiferromagnetically coupled mutually shifted NN chains by half a Cu-Cu distance in the chain direction (Fig. 1) is *upshifted* to $\alpha > 1/4$, reflecting a stabilization of the FM inchain ordering. On the other hand, the spin-wave dispersion for LICO shows a flat minimum at the magnetic zone center, which reflects also incommensurate correlations along the chains. Here weak AFM O-mediated ICs between adjacent chains are relevant too [9–11].

Since the large FM J_1 is the origin for a large magnon dispersion, its microscopic origin is of interest for the cuprate physics in general to be addressed in the framework of multiband Cu-O pd models. Then J_1 depends first of all on the direct FM exchange K_{pd} between two holes on NN Cu and O sites and on Hund’s exchange J_H of two holes in two different O $2p$ orbitals on the same O site which bridges twice two NN Cu sites. Although being key quantities, neither is precisely known. In particular, the $K_{pd} = 50$ meV suggested in Ref. 15 for LICO and CYCO and *all* other FFESC differs by more than 200% from the empirical value for CuGeO_3 [2] and even by 400% for the corner-sharing La_2CuO_4 , where K_{pd} and its weaker NN O-O counter part, K_{pp} , are known from advanced many-body calculations [16, 17]. We report on complementary quantum chemical (QC) and density functional theory (DFT) computations for LICO, derive also a significant K_{pd} -value and stress its key role for the FM J_1 and the magnon dispersion [9, 10]. We resolve a long-standing puzzle for seemingly AFM or small FM Curie-Weiss temperatures (Θ_{CW}) [13, 18] at odds with the inchain FM alignment of magnetic moments in the Néel-state using a high-temperature expansion (HTE) for the spin susceptibility $\chi(T)$ (Sec. V A). In the SM [7] we present a rich collection of cuprates with edge-sharing elements, provide further support for sizable FM NN couplings, and explain special reasons for weak or even AM values.

II. PREVIOUS AND NEW RESULTS IN CYCO

CYCO consists of edge-sharing CuO_2 chains [19], each $[\text{CuO}_2]^{-2}$ unit carries a spin $1/2$ [20]. The chains in the ac plane are shown in Fig. 1(a). CYCO exhibits an AFM

order below $T_N=29.5$ K. The spins align ferromagnetically along the a axis (chain direction) and b axis and antiferromagnetically along the c axis [12, 13]. The ordered magnetic moment is $0.9\mu_B$. The magnetic structure in the ac plane is shown in Fig. 1(a). CYCO shows commensurate and incommensurate orders of Ca and Y, which gives rise to a supercell with $5\times a$ and $4.11\times c$ in the simplest approximation [19]. In this supercell, there are 4 Ca/Y and 5 Cu positions along the chain. The alternating $\text{Ca}^{2+}/\text{Y}^{3+}$ chains cause sizable shifts of the O ions (Figs. 1b and 1c) at variance to chains with equivalent O sites [8]. However, it is unclear how much this superstructure (SS), affecting mostly the O sites, does modify the long-range magnetic order. The inchain spin arrangement is FM and no magnetic SS has been found so far. Hence, the static magnetic order seems to be hardly affected by the chain distortions, probably due to the few O spins.

The spin-Hamiltonian for CYCO may be written as

$$\hat{H} = \hat{H}_{ch} + \hat{H}_{IC} + \hat{H}_A, \quad (2)$$

where $\hat{H}_{ch}(\hat{H}_{IC})$ describes in(inter)-chain isotropic Heisenberg interactions of the form

$$\hat{H}_{ch} + \hat{H}_{IC} = \frac{1}{2} \sum_{\mathbf{R}, \mathbf{r}} J_{\mathbf{r}} \hat{\mathbf{S}}_{\mathbf{R}} \hat{\mathbf{S}}_{\mathbf{R}+\mathbf{r}}, \quad (3)$$

$J_{\mathbf{r}}$ being exchange interaction between a pair of copper spins $\hat{\mathbf{S}}_{\mathbf{R}}$ and $\hat{\mathbf{S}}_{\mathbf{R}+\mathbf{r}}$ in the same (for \hat{H}_{ch}) or in different (for \hat{H}_{IC}) chains; \hat{H}_A denotes uniaxial pseudodipolar

$$\text{anisotropic interactions: } \hat{H}_A = \frac{1}{2} \sum_{\mathbf{R}, \mathbf{r}} D_{\mathbf{r}} \hat{S}_{\mathbf{R}}^z \hat{S}_{\mathbf{R}+\mathbf{r}}^z. \quad (4)$$

In previous works [21–24], the INS results were interpreted assuming that all Cu sites are equivalent, i.e. ignoring a lattice modulation. The magnon dispersion curves were fitted by linear spin-wave theory (LSWT):

$$\begin{aligned} \omega_{\mathbf{q}} &= \sqrt{A_{\mathbf{q}}^2 - B_{\mathbf{q}}^2}, \quad \text{with} \quad (5) \\ A_{\mathbf{q}} &= J_{a1}(\cos q_a - 1) + J_{a2}(\cos 2q_a - 1) + J_b(\cos q_b - 1) \\ &\quad + J_c(\cos q_c - 1) + 2J_{ab}(\cos \frac{q_a}{2} \cos \frac{q_b}{2} - 1) \\ &\quad + 2(J_{ac1} + J_{ac2}) - D, \\ B_{\mathbf{q}} &= 2J_{ac1} \cos \frac{q_a}{2} \cos \frac{q_c}{2} + 2J_{ac2} \cos \frac{3q_a}{2} \cos \frac{q_c}{2}, \end{aligned}$$

where J_{a1} , J_{a2} are FM NN and AFM NNN in-chain interactions, J_{ac1} and J_{ac2} are NN and NNN ICs in ac plane (Fig. 1), J_b and J_c are interactions along the b and c directions, respectively; $\mathbf{q} = (q_a, q_b, q_c) = 2\pi(h, k, l)$ is the magnon momentum. Only an averaged value D of the anisotropy parameters $D_{\mathbf{r}_1}, D_{\mathbf{r}_2}$ enters the dispersion

$$D = \sum_{\mathbf{r}_1} D_{\mathbf{r}_1} - \sum_{\mathbf{r}_2} D_{\mathbf{r}_2}, \quad (6)$$

where the vectors $\mathbf{r}_1(\mathbf{r}_2)$ connect sites of the same (different) AFM sublattice.

Let us recall that a FM state is an eigenstate of $\hat{H}_{ch} + \hat{H}_A$ and magnons are its *exact* one-particle excitations. That is why the ordered moment in CYCO is close to $1\mu_B$ and LSWT provides adequate values of exchange parameters (cf. Sec. V C 1). The only source of quantum fluctuations in CYCO is the relatively weak \hat{H}_{IC} . It affects the magnon dynamics but does not change the overall shape of the LSWT dispersion, Eq. (5) (see Sec. V A).

In Ref. 21, the dispersion along high-symmetry directions starting from the zone center Γ was measured up to $W_E \sim 10$ meV. The full dispersion curves were available for the b and c directions $(0, k, 0)$ and $(0, 0, l)$, thus the IC parameters $J_b = 0.06$, $J_{ab} = 0.03$, $J_c = 0$, and $J_s = J_{ac1} + J_{ac2} \approx 2.24$ meV were established. On the contrary, only a small part of the dispersion was possible to be measured along the chain direction a . Inspection of Eq. (5) shows that the dispersion along the line $(h, 0, 0)$ is affected by the ICs. The influence of the tiny J_{ab} can be ignored but $J_{ac1,2}$ do substantially affect the dispersion at small \mathbf{q} . Moreover, the dispersion depends not only on the sum J_s , but also on the ratio J_{ac1}/J_{ac2} . That is why the fit of those measurements was ambiguous. Table I shows how the extracted inchain couplings became more and more accurate by including data up to higher energies.

New measurements along the lines $(h, 0, 1.25)$ and $(h, 0, 1.5)$ were performed in Ref. 24. The dispersion along the line $(h, 0, 1.5)$ ($q_c = 3\pi$) is independent of $J_{ac1,2}$, and its curvature near $h = 0$ is determined by α . It reveals a substantial value of J_{a2} and allows a new fit that includes also broad excitation data up to 25 meV. Both J_{a1} and J_{a2} (4th row of Table I) were found to be much stronger and consistent with theory. As mentioned above, for $\alpha > 1/4$, the ground state is an AFM spiral state. In our previous study [24] we found $\alpha \sim 0.19$, below the critical value of a single chain. In order to determine the overall profile of the magnon dispersion and refine also α , we performed INS experiments using a time-of-flight chopper spectrometer. This way, we probed the full dispersion that extends up to ~ 53 meV and α was refined as ~ 0.23 , closer to α_c .

As previously observed [21], the intensity of the magnons appears to be reduced at ~ 11.5 meV. In addition to this, we also found another gap-like behavior at ~ 28 meV. We refine the exchange parameters and discuss the origin of the gap-like behavior in the magnon dispersion. The gap at ~ 11.5 meV is related to the coupling with a weakly dispersive optical phonon. The gap-like feature at ~ 28 meV is ascribed to quantum effects due to the AFM ICs [21] and to the SS mentioned above.

III. EXPERIMENTAL METHOD

A CYCO single crystal was grown by the traveling solvent floating zone (TSFZ) method in air. The dimen-

TABLE I. The inchain couplings J_{a1} and J_{a2} from INS data analyzed within LSWT, the maximum energy (W_E) below which the INS data were fitted, and $\alpha = |J_{a2}/J_{a1}|$. Values in the first row represents theoretical predictions from Ref. 15.

year	J_{a1} (meV)	J_{a2} (meV)	W_E (meV)	α	Ref.
1998	-2.2	4.7	-	2.2	[15]
2001	-8	0.4	10	0.05	[21]
	-6.9	0.0	10	0	[21]
2012	-19.6	3.7	25	0.19	[24]
2019	-24	5.5	53	0.23	present work

sions of the rod shaped crystal was $\sim 6\Phi \times 25 \text{ mm}^3$. This crystal was already used in previous INS studies [21–24]. The present INS experiments were carried out on a hybrid neutron spectrometer HYSPEC [25] installed at the Spallation Neutron Source (SNS) and a triple-axis spectrometer HB-1 installed at the High Flux Isotope Reactor (HFIR) at Oak Ridge National Laboratory (ORNL). We utilized two incident energies of 27 and 60 meV on HYSPEC. Energy resolutions at the elastic position are ~ 1.3 and ~ 3.8 meV with $E_i = 27$ and 60 meV, respectively. Neutrons with a final energy of 13.5 meV were used, together with a horizontal collimator sequence of $48'-80'-S-80'-240'$ on HB-1. The energy resolution at the elastic position amounts to ~ 1.4 meV. Contamination from higher-order beams was effectively eliminated using pyrolytic graphite filters. The single crystal was oriented in the $(H, K, 0)$ scattering plane and mounted in a closed-cycle ^4He gas refrigerator on HYSPEC. On HB-1, the single crystal was oriented in the $(H, K, 0)$ and $(H, 0, L)$ scattering planes and mounted in a closed-cycle ^4He gas refrigerator. The visualization of the HYSPEC data were performed using the DAVE software [26].

IV. EXPERIMENTAL RESULTS & SPIN-WAVES

A. Interchain couplings (ICs)

As mentioned above, the previously studied dispersion along the $(0, 0, l)$ direction provides only the sum of ICs in the ac -plane $J_s = J_{ac1} + J_{ac2} \approx 2.24$ meV and the anisotropy parameter $D = -0.45$ meV [24]. As pointed out in Ref. 24, the weak ICs can be fitted more accurately from the dispersion relations at (h, k, l) with $h \neq 0$ and any k value, where the inchain couplings do not contribute. Hence, we probed the magnon at $(h, 0, l)$ with $h=0, 0.025, 0.005,$ and 0.1 at $T=5.5$ K on HB-1. Its dispersion is shown in Fig. 2. The LSWT analysis yields a much larger NNN IC on the two adjacent chains $J_{ac2}=2.26$ meV than the NN counter part $J_{ac1}=0.12$ meV (cf. the ratio $\tilde{J}_1/\tilde{J}_2 \sim 0.1$ in LICO [9]). The average anisotropic exchange parameter D in Eq. (6) was found as -0.21 meV.

Analyzing the unusual intensity suppression near 30 meV with the aid of density matrix renormaliza-

tion group calculations (see Sec. V A), we find that the ICs would most effectively suppress the intensity when $J_{ac1} \gg J_{ac2}$. This points to the imaginary part of the magnon self-energy $\Im\Sigma$, ignored in LSWT. It might cause this different behavior while $\Re\Sigma$, which governs the dispersion, is less sensitive to the ratio J_{ac1}/J_{ac2} .

An almost flat dispersion along the b axis is reproduced (Fig.2b) with the same coupling values as in our previous work [21, 23, 24]. The difference of the anisotropy parameter D_b from D was explained in Ref. 21 by a small deviation of the spin-Hamiltonian's anisotropy from uniaxial symmetry; the deviation does not visibly split the spin wave branches in the ac -plane and is not considered here. We mention the couplings as a useful reference for a realistic estimate of the analogous "face to face" interaction of CuO_4 plaquettes along the a axis in LICO in view of its role in the FM alignment of magnetic moments along the chains under debate [11, 27] and an order by disorder scenario [28] vs. the AFM IC mechanism based on shifted adjacent chains in Refs. [9, 29, 30]. To resolve this problem experiments around α_c would be helpful. In particular, an INS study under pressure and an anal-

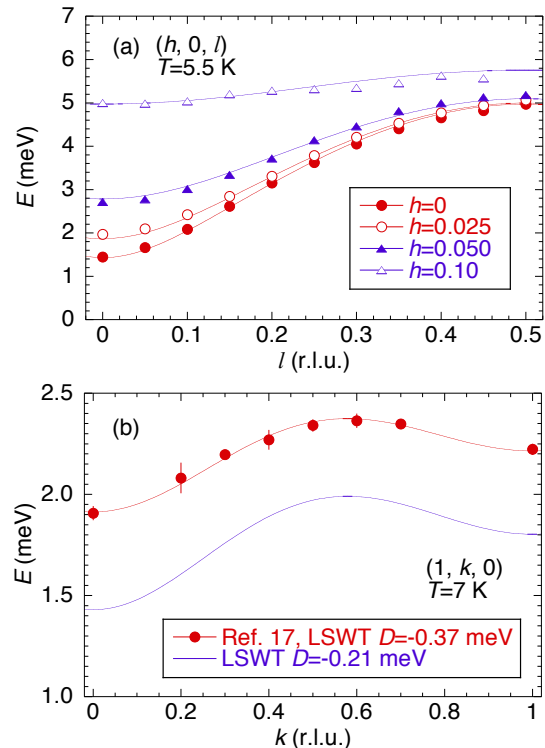


FIG. 2. (a) The weak magnon dispersion of CYCO perpendicular to the chain (a axis) direction within the ac plane $[(h, 0, l)$ with $h=0, 0.025, 0.005,$ and 0.1], measured at $T=5.5$ K with $E_f=13.5$ meV. Solid curves: the dispersions calculated using LSWT with the two skew ICs $J_{ac1}=0.12$, $J_{ac2}=2.26$, and the anisotropy parameter $D=-0.21$ meV. The error bars are smaller than the size of the symbols. (b) The dispersion along the b axis, which is well reproduced with $J_b=-0.0061$, $J_{ab}=-0.030$, and $D_b=-0.37$ meV.

ysis like ours would be interesting in view of the pressure study of LICO [31, 32], where above 6 GPa a phase transition to a monoclinic FM phase has been detected. Due to the larger IC coupling in CYCO higher pressures might be necessary for a similar transition. Hence, studies in $\text{La}_6\text{Ca}_8\text{Cu}_{24}\text{O}_{41}$ might be easier to perform although any analysis of the dispersive magnon modes could be difficult due to the presence of ladder spinons. Anyhow, pressure is a promising tool (see also the estimate of J_1 and α in Sec. E of SM [7]).

B. Inchain interactions

The analysis given above rests on the assumption of *flat homogeneous* CuO_2 chains, practically unaffected by the incommensurate structure of the adjacent cationic CaY chains, as described in Sec. II. The opposite is depicted in Fig. 1(c) for the simplest case when a symmetric quasi-period 5 SS is induced in the cuprate chain. A period 10 or 15 would give an even better approximation for the incommensurate SS induced by the strong Coulomb interaction between the differently charged cations and especially the closer O ions of the CuO_2 chains. The latter case might be close to an inhomogeneous "lock-in" structure containing "domains" of period 5 and period 10 units as well. Then the two mechanisms of gap production proposed here would be cooperative, resulting in a maximum experimentally observable effect. Since in a general period- m case the opening of $m - 1$ gaps is allowed, in the present case one is left with 4 gaps for a period-5 model while already 9 gaps for improved approximations of a period-10 (or even 14 gaps for a period-15) are allowed. The simplest lock-in structure "5+10" has 13 gaps. The replacement of the incommensurate SS by a quasi-commensurate one containing an *even* period component is essential because it allows the opening of a gap just at the wave vector of $1/4$ where the gap near 28 meV has been found. The magnitude of all gaps depends on the distributions of the local Φ and of the distances between NN bridging O ions and also on the twisting and/or other deformations away from the flat structure of ideal chains as in LICO. Also the dispersion is slightly affected by the opening of gaps if they are included in the fitting procedure (see Sec. V B and Sec. A in SM [7]). Due to the largely increasing number of corresponding couplings probably any distribution of gap amplitudes at the corresponding wave vectors generic for the adopted approximative commensurate SS could be fitted. In this context we do not exclude the possibility of a lock-in transition of the incommensurate cationic chain into a real long periodic commensurate $5m$ periodic-chain, where $m = 2, 3, 4, \dots$. Thus, any real progress by convincing fits should rest on a dialog examination of various local structural models compatible with the diffraction patterns from neutron and x-ray scattering. Improved detailed microstructure models in the real space for inhomogeneous long periodic CuO_2 chains have not yet been developed. The exam-

ination of such alternative microstructure models with increasing complexity is extremely tedious. Therefore, it is for a future study. Anyhow, we believe that the analysis of the gaps reported here is very important to find effective models with a reasonable number of parameters.

The unexpected lacking of Zhang-Rice excitons in a recent resonant inelastic x-ray scattering (RIXS) study [33], in sharp contrast to LICO and CuGeO_3 with "ideal" chains, is noteworthy. We suggest that the expected peak-like feature could not be resolved experimentally due to a relatively broad distribution (more than 0.5 eV) of different "local" excitation energies (at 4.5 eV in LICO) caused by the SS in CYCO. Further consequences of the composite symmetry of CYCO, such as suggested in Refs. 8, 34–36 or within the approaches proposed here, will be discussed elsewhere.

Figure 3 shows the INS spectra $S(Q, E)$ from our CYCO single crystal measured at 6 K. Figure 3(a) represents the low-energy excitations measured with $E_i=27$ meV. The intensity is averaged over the range of $1.8 \leq K \leq 3.2$ and $-0.1 \leq L \leq 0.1$. The magnon dispersion along K is almost flat and the band width is less than 0.2 meV [21]. Although the band width of the disper-

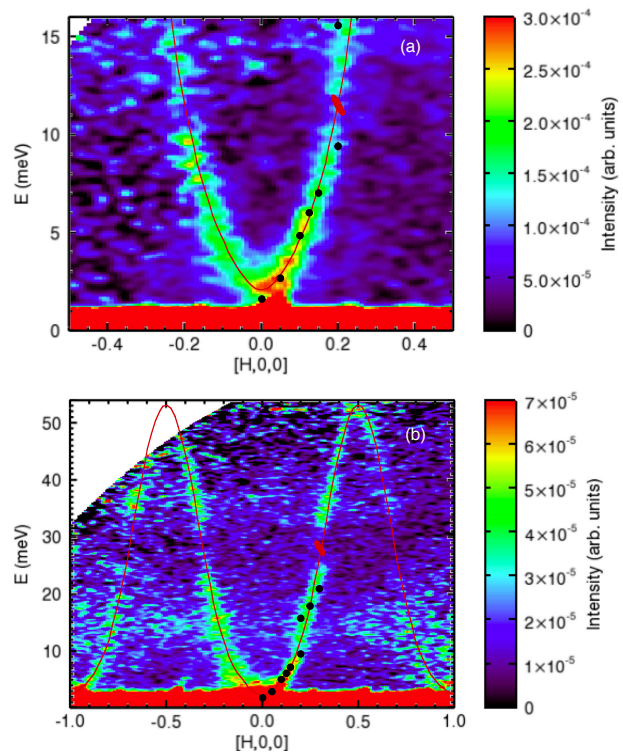


FIG. 3. Contour maps of the INS intensity $S(Q, E)$ for a CYCO single crystal measured at 6 K with $E_i=27$ meV (a) and 60 meV (b). Energy resolutions at the gap energies are estimated to be ~ 0.7 meV at 11.5 meV with 27 meV E_i (a) and ~ 2 meV at 28 meV with 60 meV E_i (b). The resolution volumes projected to the E - Q space are shown around the gap energies with red ellipses. Filled circles: data points reported in Refs. [21, 22]. Solid curves: the dispersion relation calculated using LSWT with $J_1=-24$, $J_2=5.5$, $J_{ac1}=0.12$, $J_{ac2}=2.26$, and $D=-0.21$ meV.

sion along L is about 3 meV, the dispersion in the range $-0.1 \leq L \leq 0.1$ is less than 0.5 meV [21]. Therefore, the broadening due to the integration should be small. On the other hand, the scattering intensity with $E_i=60$ meV was weak. In order to improve the statistics, the signal was integrated in a wide Q range. In Fig. 3(b), the intensity is averaged over $-0.2 \leq L \leq 0.2$, where the dispersion width is less than 1.5 meV, and entire K range measured. The range of K depends on the excitation energy, e.g., $0.5 \leq K \leq 5.5$ at 5 meV and $3.0 \leq K \leq 4.7$ at 51 meV. Therefore, the effective magnetic form factor gradually decreases with increasing energy and H value, which reduces the averaged intensity. However, the overall dispersion curve can be generated with reasonably good statistics by this method. Figure 3(b) clearly shows a single branch mode along H . The characteristic feature is that there are gap-like features at ~ 11.5 meV and ~ 28 meV, as shown in Fig. 3(a) and (b), respectively. The observed magnon dispersion has been analyzed with the help of LSWT (at $T = 0$). For this purpose we have used Eq. (5). We fixed the ICs determined in Sec. III A ($J_{ac1}=0.12$, $J_{ac2}=2.26$, and $D=-0.21$ meV). The small J_c was fixed at 0 meV [21] for simplicity, since the dispersion shown in Ref. 21 yields tiny values of -0.061 and 0.037 meV for the NN and NNN couplings, respectively. J_{a1} and J_{a2} were determined from the dispersion along H . J_{a1} affects the magnon band width and J_{a2} the dispersion shape in the low-energy region. We found that $J_{a1}=-24$ and $J_{a2}=5.5$ meV reproduce the overall dispersion, as shown in Figs. 3(a) and (b). The resulting

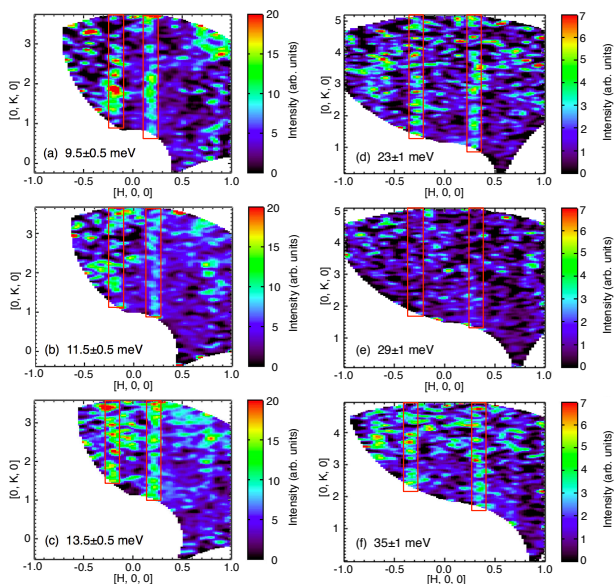


FIG. 4. Energy cuts of the INS intensity in the $(HK0)$ plane measured at 6 K. Spectra at 9.5 (a), 11.5 (b), and 13.5 meV (c), measured with $E_i=27$ meV and integrated in the range of $-0.1 \leq L \leq 0.1$. Spectra at 23 (d), 29 (e), and 35 meV (f), measured with $E_i=60$ meV and integrated in the range of $-0.2 \leq L \leq 0.2$. Red rectangles: the expected regions for line-shaped magnetic excitations along K .

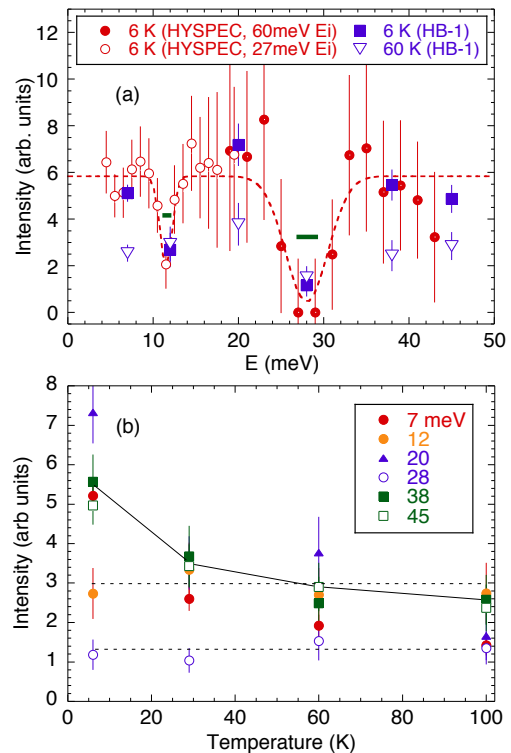


FIG. 5. Energy (a) and T (b) dependences of the integrated intensities from constant energy cuts and scans. Solid and broken lines: guides to the eye. The thick horizontal bars near 11.5 and 28 meV in (a) are estimated instrumental resolution.

$\alpha=0.23$ is close to the critical $\alpha_c=1/4$ (see also Sec. E in SM [7] for the non-criticality of coupled chains).

Noteworthy, the increase by a factor of 3 of $|J_{a1}|$ found over the years (see Table 1). Thereby the NNN inchain exchange $J_{a2} \equiv J_2$ has been strongly raised too, while α shows a more moderate increase. Possible disorder effects on the enhancement of J_2 in CYCO, $\text{Li}_2\text{ZrCuO}_4$, and LiCu_2O_2 are shown in Sec. I of SM [7]. The unusually small α -values in Table 1 reflect the previous non-optimal fitting due to the large number of involved couplings. This at first glance surprising result is now well understood. The increase of $|J_1| \equiv |J_{1a}|$ by ~ 100 K as compared to that from a still non-optimal fit [24] is very instructive. Good fits can be achieved only by probing the full dispersion, *i.e.* up to energies $E \geq 2|J_1|$, if the 3rd neighbor couplings ($J_3 \equiv J_{3a}$) are reasonably small [9].

C. Gap-like features

Figure 4 shows six energy cuts in the $(HK0)$ plane through $S(Q, E)$, measured with $E_i=27$ meV (a)-(c) and $E_i=60$ meV (d)-(f). Since the dispersion is almost flat along K , there are line-shaped dispersions along K , as indicated by red rectangles. Around the gap energies 11.5 and 29 meV, the intensity becomes weak throughout

the whole K range, indicating that the structure factor is modified considerably at these specific energies. In particular, the signal is very weak at 29 meV.

To show the intensity more quantitatively, the scattering intensity was plotted as a function of the excitation energy, as shown in Fig. 5(a). The intensity was obtained by fitting the constant energy cut profile with a Gaussian function. In this plot, the integration ranges are $-0.1 \leq L \leq 0.1$ and $1.5 \leq K \leq 2.5$ for 27 meV E_i data and $-0.2 \leq L \leq 0.2$ and $2.5 \leq K \leq 3.5$ for 60 meV E_i data. The intensities from the two sets of data are normalized using the data points around 20 meV. The correction of the inverse spin-wave velocity was made to convert from the Q integrated intensity to the energy integrated $S(Q, E)$, plotted in Fig. 5(a). The gap-like behavior is distinct at 11.5 and 28 meV. The dip is broader at 28 meV than at 11.5 meV, probably because of the combined effect of broader energy resolution (~ 2 meV) and wider integration range along L , with dispersion width of ~ 1.5 meV for the 60 meV E_i data. The broader energy resolution with 60 meV E_i also makes the gap at 11.5 meV smeared out [Fig. 3(b)], where the energy resolution is ~ 2.5 meV. Except the two dips, the intensity is almost constant throughout the whole energy range, which is expected for ferromagnets. One possibility to explain the gap behavior is the phonon-magnon coupling. Magnons can be interfered when a phonon mode is mixed. A magnon gap due to such an effect was actually reported in UO_2 [37–39], FeF_2 [40, 41], and $\text{La}_{1-x}\text{Ca}_x\text{MnO}_3$ [42].

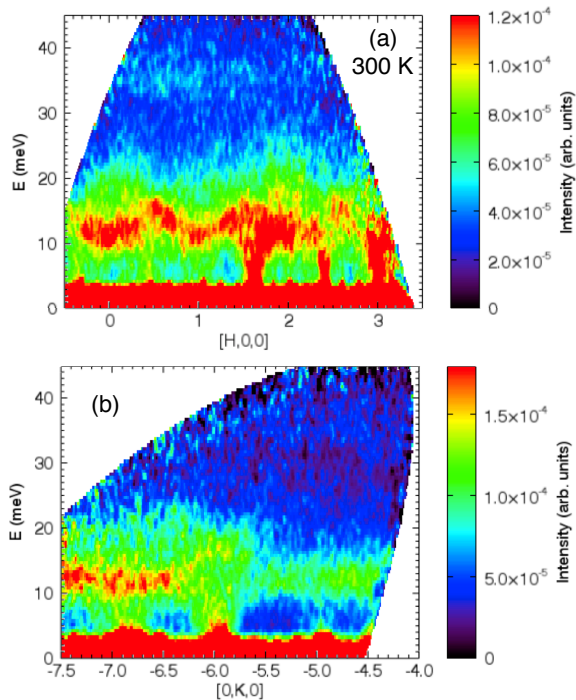


FIG. 6. Contour maps of the phonon dispersions along H (a) and K directions (b) measured at 300 K with $E_i=60$ meV. The intensities plotted in (a) and (b) are integrated in the range of $-6.5 \leq K \leq -4.5$ and $-0.5 \leq H \leq 0.5$, respectively.

A gap behavior in the magnon dispersion was also reported for magnetite Fe_3O_4 below the Verwey transition temperature (T), where charge ordering is expected [43]. The acoustic magnon mode shows a gap at 43 meV and $q=(0, 0, 1/2)$. The origin of the gap is still unknown, although both a charge-density wave and magnetoelastic coupling are considered as possible causes. We examined the phonon dispersions of CYCO carefully. A weakly modulating optical phonon mode along both H and K directions is observed around 11.5 meV, as shown in Fig. 6. This phonon can interfere with the magnon around 11.5 meV. If there exists strong magnon-phonon coupling, a bending of the dispersion curve is usually observed as well as an excitation gap [39]. No such bending was observed in the present measurements. As mentioned in Sec. III, the magnetic signal from the small magnetic moment ($S=1/2$) in CYCO is weak so that we need to integrate the signal in a wide range of Q region to clearly show the dispersion curve. This integration is likely to make the bending unclear since the optical phonon mode around 12 meV is slightly dispersive. In stark contrast, near 28 meV there is no phonon mode which would intersect the magnon dispersion (Fig. 6). Hence, the latter gap cannot be ascribed to phonon-magnon coupling. As shown above, the CuO_2 chains are distorted due to the misfit with the Ca-Y layer. Since the O distortions suggested in Ref. 8 are not so small, some changes of the dynamical structure factor and of the spin-wave dispersion might occur. Our LSWT calculations suggest nevertheless a weak change in the dispersion starting from a homogeneous chain but more pronounced changes in the intensity leading even to the opening of quasi-gaps have been found (see also Sec. A in SM [7] and below). Much more systematic studies of inhomogeneous models including also Dzyaloshinskii-Moriya (DM) couplings [allowed in that case] and experimental refinement of the structural model are desired to settle quantitatively this very complex problem. Similar studies for CYCO might be of interest too. As first insights we show in Sec. V B and in Sec. A of SM [7] the effect of various simple inhomogeneities. Since J_{a1} amounts to -24 meV (278 K), which is much larger than $T_N=29.5$ K, a steep magnon dispersion is still expected above T_N along the chain. It is also expected that the dominant IC $J_{ac2}(=2.26$ meV) becomes less effective above T_N . Therefore, the effect of the ICs can be elucidated by checking whether the gap-like behavior persists above T_N . Figure 7 displays constant- E spectra at 7, 12, 20, 28, 38, and 45 meV, measured at 6 and 60 K on HB-1. The magnetic excitations persist even at 60 K, although the peak width becomes broader. The change of intensity depends on energy. The T -dependence of the integrated intensities is shown in Fig. 5(b). Clearly, the intensities at 12 and 28 meV are T -independent. On the other hand, those at other energies decrease with increasing T . The integrated intensities at 6 and 60 K are shown as a function of energy in Fig. 5(b). The intensities at 6 K are consistent with those measured on HYSPEC. Since the intensities at 12

and 28 meV are unchanged and those at other energies are reduced, the gap-like behavior becomes less distinct at 60 K. Hence, the gap-like behavior at 28 meV is affected by the AFM ICs and is in fact a quantum effect specific for FM chains, as suggested above. The gap-like behavior at 11.5 meV may be due to magnon-phonon mixing, as mentioned above. Then, the magnon-phonon coupling strength might be also weakened at $T > T_N$.

In view of the recently found strong renormalization of the charge transfer energy Δ_{pd} in the RIXS spectra of LICO by high-frequency O derived modes at 74 meV [44] and near 70 meV for $\text{Ca}_{2+5x}\text{Y}_{2-5x}\text{Cu}_5\text{O}_{10}$ with $x=0, 0.3$, and 0.33 [45] (the latter two being hole (h)-doped derivatives of CYCO), the present observation for another active phonon at much lower energy is interesting and deserves to be analyzed also in the general context of electron-phonon coupling in strongly correlated systems. Here, INS brings a new low-energy scale not resolved in RIXS studies. Since there is no low-energy gap near 11 meV seen in the INS data of Ref. 9 for LICO, we suggest that it might be an optical phonon derived from the diatomic Ca/Y chain. Then a down shift of that phonon induced gap-like feature might be expected for the sister compound $\text{Ca}_2\text{Nd}_2\text{Cu}_5\text{O}_{10}$, having a slightly reduced $T_N = 24$ K [46], and even better with nonmagnetic isovalent substitutions of Y with Lu or Sc. The insertion of magnetic rare earth ions provides additional insight into the cuprate magnetism due to the interplay with the high-spin rare earth subsystem and the check

of intrinsic quantum effects. Substitution with Pr might also modify the magnetic structure of the chains through a decrease of the O hole numbers n_p due to the competing covalency with Pr $4f$ electrons, as it happens in $\text{PrBa}_2\text{Cu}_3\text{O}_{7-\delta}$ [47], with dramatic consequences for the corresponding pd exchange integrals [Eqs. (5,6) in Ref. [47]]. In particular, a strong decrease of J_1 might occur, if sizable O $2p$ -Pr $4f$ covalency is present. An ordering of the rare earth magnetic moments well above few K (typical for dipole-dipole couplings) in the Pr-based quasi-2D cuprates might explain details of the magnetic response in $\text{Ca}_2\text{Nd}_2\text{Cu}_5\text{O}_{10}$ [46]. A systematic study of the whole rare earth series would be interesting. To the best of our knowledge, $\text{Ca}_2R_2\text{Cu}_5\text{O}_{10}$ ($R=\text{Dy}$ and Gd) have been synthesized but their physical properties were not studied so far.

V. THEORY

In addressing the main experimental findings, this section consists of three parts. A and B are devoted to two different phenomenological simulations of the detected mid gap, while part C deals with microscopic aspects and consequences of the observed large magnon dispersion.

A. The mid gap-like feature as a quantum effect from diagonal AFM interchain coupling

To understand the gap-like behavior around 28 meV for flat chains, we have first calculated the dynamical spin structure which corresponds to the experimental INS affected also by the form factor. The former is defined as

$$S(q, E) = \sum_{\nu} |\langle \psi_{\nu} | S_q^{\pm} | \psi_0 \rangle|^2 \delta(E - E_{\nu} + E_0), \quad (7)$$

where S_q^{\pm} is the Fourier transform of the spin-flip operator S_i^{\pm} at site i while $|\psi_{\nu}\rangle$ and E_{ν} are the ν -th eigenstate and eigenenergy of the system, respectively ($\nu = 0$ corresponds to the ground state). Two-chain clusters (32×2 sites) were studied by using the Dynamical Density Matrix Renormalization Group (DDMRG) method [48]. Open boundary conditions were applied along the chain direction whereas periodic boundary conditions were applied perpendicularly to the chain axis. Then, for an effective two-chain model, ISs are taken to be $2J_{ac1}$ and $2J_{ac2}$ instead of J_{ac1} and J_{ac2} . The obtained spectra for some sets of ICs are shown in Fig. 8. The overall dispersion is well described by LSWT with Eqs. (2-6) and $J_{ac1} + J_{ac2} \approx 2.29$ meV [24]. Especially for $J_{ac1} = 2.29$ meV, $J_{ac2} = 0$, a gap-like behavior around $E = 30$ meV is clearly seen. This gap position is close to the INS-value of 28 meV. The gap-like feature near 28 meV can be understood as a splitting of the excitation levels at an intermediate momentum $q \sim \pi/2$, induced

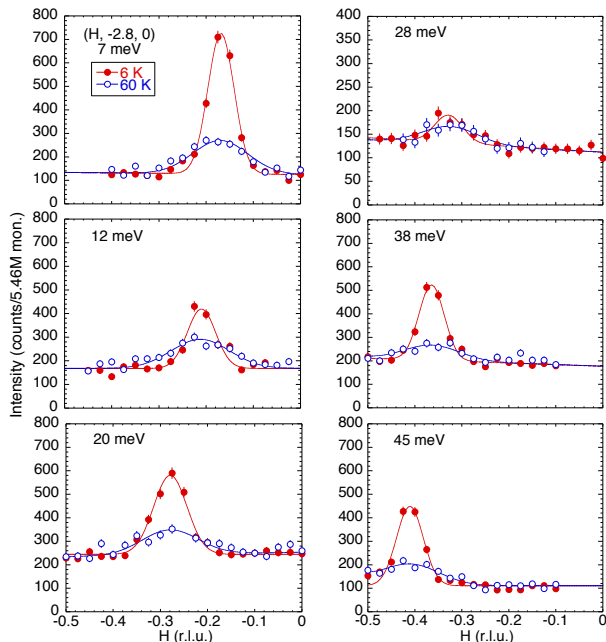


FIG. 7. Constant energy scans at $(H, -2.8, 0)$ measured at $E=7, 12, 20, 28, 38$, and 45 meV at $T=6$ and 60 K. Solid lines are the results of fits with a Gaussian function. r.l.u. represents reciprocal lattice units. To emphasize the peak structure, the vertical scale of the 28 meV data is different from the others.

by finite ICs. Let us qualitatively illustrate this by considering the spin configurations at $q = 2\pi/5$. For simplicity, we take two chains coupled by J_{ac1} and employ an Ising-like picture. A representative snapshot of the ground state $|\psi_0\rangle$ is schematically described in Fig. 9(a), where the spins are ferromagnetically aligned along the chain and antiferromagnetically between adjacent chains within the ac -plane. Roughly speaking, the operators $S_{q=2\pi/5}^\pm$ flip spins on every 5th site on each chain. Thus, spin configurations like **A** and **B** in Figs. 9(b) and (c) are created in the excited states $|\psi_\nu\rangle$ when S_q^\pm is applied to the ground state $|\psi_0\rangle$. Note that the energies differ between Figs. 9(b) and (c). The energy difference comes from interchain contributions which depend on the relative positions of the flipped spins. On the other hand, the intrachain contributions are the same. For Figs. 9(b) and (c) the interchain contributions per site are $E_{ac1}(\text{I}) = -\frac{2}{3}J_{ac1}$ and $E_{ac1}(\text{II}) = -\frac{1}{3}J_{ac1}$, respectively. This gives a splitting of the excited energy levels E_ν in Eq. (7). The ratio of the probability weights is 2:1 since it is proportional to the number of possible combinations of ICs. For arbitrary q we obtain $E_{ac1}(\text{I}) = (\frac{q}{\pi} - 1) J_{ac1}$ and $E_{ac1}(\text{II}) = (\frac{2q}{\pi} - 1) J_{ac1}$, weighted by $w(\text{I}) = \frac{q}{\pi}$ and $w(\text{II}) = 1 - \frac{q}{\pi}$, respectively. In Fig. 9(d) we plot E_{ac1} and

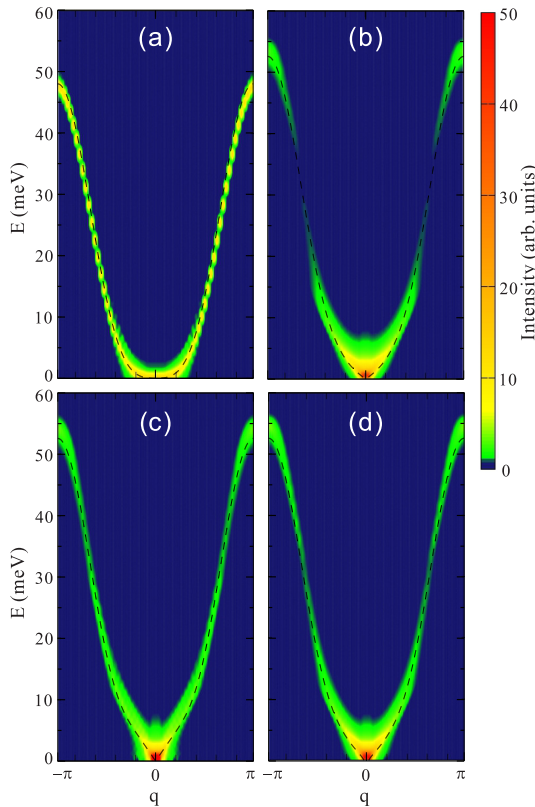


FIG. 8. DDMRG results of the dynamical structure factor $S(q, E)$ with $J_1 = -24$, $J_2 = 5.5$ meV for (a) $J_{ac1} = J_{ac2} = 0$ meV, (b) $J_{ac1} = 2.29$, $J_{ac2} = 0$ meV, (c) $J_{ac1} = 0$, $J_{ac2} = 2.29$ meV, and (d) $J_{ac1} = 1.537$, $J_{ac2} = 0.763$ meV. The dotted lines denote the magnon dispersions ω_q .

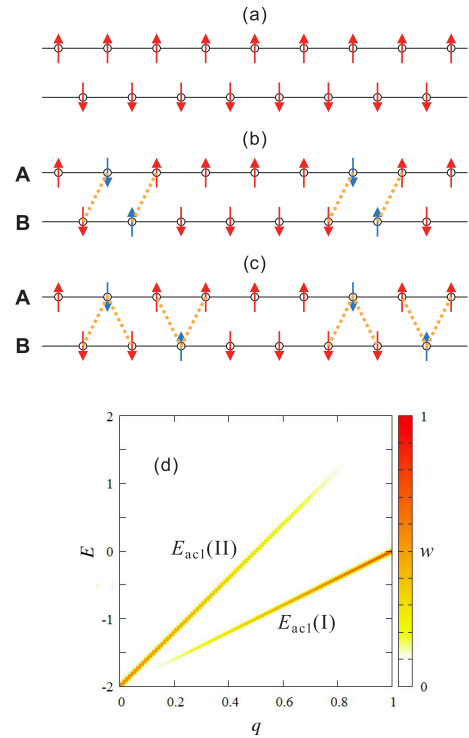


FIG. 9. Schematic spin configurations of (a) the ground state and (b)(c) excited states with $q = 2\pi/5$. Parallel spins are connected by dotted lines and the numbers of the parallel spin pairs are different between (b) and (c). (d) Energy contributions by IC J_{ac1} and their weights in the excited states. q is in a unit of π .

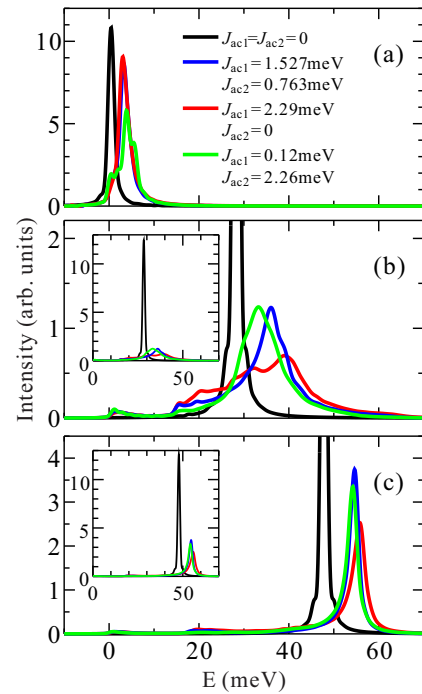


FIG. 10. DDMRG results of the dynamical correlation functions $S(q, E)$ at (a) $q = 0.15\pi$, (b) 0.67π , and (c) 0.97π . Insets display the entire range of the intensity.

w vs. q . The splitting is zero at $q = 0$ and increases with increasing q . Although the splitting is largest near $q = \pi$, it would be less represented in the spectral functions due to the polarized weights, i.e., $w(\text{I}) \gg w(\text{II})$. As a result, such a splitting is most visible around intermediate q . To confirm this, we plot the dynamical correlation functions $S(q, E)$ at $q = 0.15\pi$, 0.67π , and 0.97π for several sets of the ICs in Fig. 10. Without ICs ($J_{ac1} = J_{ac2} = 0$) no splitting is seen for any q [Fig. 8(a)]. But for finite ICs, the splitting is clearly confirmed at the intermediate momentum $q = 0.67\pi$ [Fig. 10(b)]. This feature is most obvious for $J_{ac1} = 2.29$ meV and $J_{ac2} = 0$ [Fig. 8(b)]. The splitting causes a continuum by quantum fluctuations and it appears as a broadening of the intensity in the spectrum. At lower ($q \approx 0$) and higher ($q \approx \pi$) momenta, the peak height is reduced by the ICs, but they are still sharp, only with a slight broadening [Figs. 10(a) and (c)]. The significant broadening at the intermediate momenta ($q \approx \pi/2$) provides a lack of q integrated intensities at intermediate energies E , which corresponds to the experimental dip of the Q integrated intensity. The broadening is less pronounced for other ICs, pointing to a gap-like behavior most pronounced for a larger J_{ac1}/J_{ac2} ratio. In fact, the gap-like feature is less obvious for $J_{ac2} > J_{ac1}$ [Figs. 8(c) and (d)].

B. Gaps from inhomogeneous CuO_2 chains

Here we briefly illustrate where gaps in the magnon curve can appear within the adopted period-10 scenario for the cationic Ca/Y chain system, ignoring thereby ICs for simplicity. Let us assume that the lattice modulation leads to small deviations from the ion positions in the flat homogeneous chain, i.e. $R + s \approx na$ “in average”. We consider a single chain where the structural modulations cause an alternation of the exchange couplings. The spin-Hamiltonian of a chain with a basis reads

$$\hat{H}_{ch} = \frac{1}{2} \sum_{R,s,r_s} \left[J_{r_s} \hat{\mathbf{S}}_{R+s} \hat{\mathbf{S}}_{R+s+r_s} + D_{r_s} \hat{S}_{R+s}^z \hat{S}_{R+s+r_s}^z \right], \quad (8)$$

$$\approx \sum_{R,s} \left[\varepsilon_{R+s} a_{R+s}^\dagger a_{R+s} + \frac{1}{2} \sum_{r_s} J_{r_s} a_{R+s}^\dagger a_{R+s+r_s} \right], \quad (9)$$

$$\varepsilon_s \equiv \frac{1}{2} \sum_{r_s} (J_{r_s} + D_{r_s}). \quad (10)$$

where R counts the cells and s the sites within the cell, r_s defines the neighbors coupled with the site s ; in Eq. (9), we expressed the spin-Hamiltonian in terms of spin deviation operators using the Holstein-Primakoff bosonization assuming a FM ground state of the chain.

We have calculated the structure factor in the large

Brillouin zone $-\pi/a < q \equiv 2\pi h < \pi/a$

$$S(q, \omega) \propto -\text{Im} \left(\left\langle \left\langle \hat{S}_q^x | \hat{S}_{-q}^x \right\rangle \right\rangle_\omega + \left\langle \left\langle \hat{S}_q^y | \hat{S}_{-q}^y \right\rangle \right\rangle_\omega \right) \quad (11)$$

$$\approx -\frac{1}{2} \text{Im} \left(\left\langle \left\langle a_q | a_q^\dagger \right\rangle \right\rangle_\omega + \left\langle \left\langle a_q | a_q^\dagger \right\rangle \right\rangle_{-\omega} \right),$$

$$\text{where } a_q = \frac{1}{\sqrt{Nn}} \sum_{R,s} e^{-iq(R+s)} a_{R+s} \equiv \frac{1}{\sqrt{n}} \sum_s e^{-iqs} a_{q,s},$$

where N is the number of cells, n is that of sites per cell.

In Fig. 11 we show how a two-fold SS of the J_1 -values (compatible with a period-10 SS) affects the intensity of the calculated LSWT dynamical spin structure factor $S(q, \omega)$. Notice the absence of shadow bands and the slightly changed dispersion visible in the height of the maxima (lowered here by ~ 5 meV) probably due to the omitted ICs. In order to “fit” the observed dispersion and the main gap near 28 meV, the remaining couplings have to be changed too. Thus, the SS does not only open gaps as expected, but it also changes the dispersion also far from the gap [49].

C. Theoretical aspects of large FM J_1 -values

Despite some exceptions, including CuGeO_3 (all due to large Φ and the presence of strong crystal fields), J_1 is usually FM (see Table I in SM [7]). $J_1 = -24$ meV in CYCO is remarkable. It exceeds J_1 of LICO (-19.6 ± 0.4 meV) and also that of $\text{Li}_2\text{ZrCuO}_4$ slightly (-23.5 meV) [4]. Since a highly dispersive magnon gives dynamical evidence for a strong FM NN J_1 , it deserves a phenomenological and microscopical analysis and verification by other data. We start with an analysis of the magnetic susceptibility $\chi(T)$ and then continue with

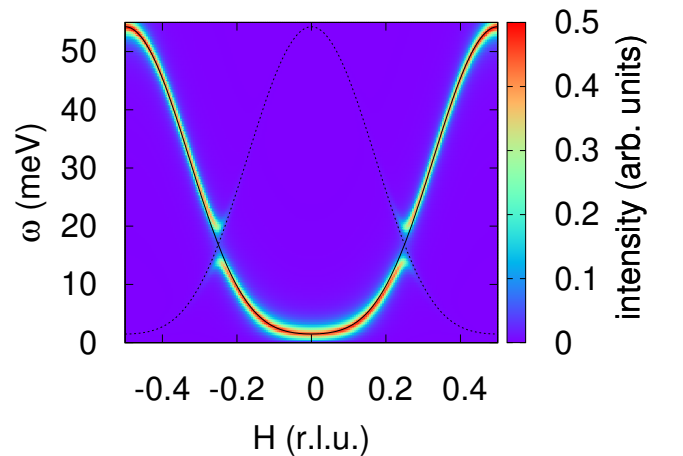


FIG. 11. (Color online) The dynamic structure factor $S(q, \omega)$ for the J_1 - J_1' - J_2 model. $J = -26.38$, $J_2 = 5.5$, $\delta = 3$, and $D = -1.5$ meV. Thin line: the two-fold supercell with $\delta = 0$ (see analogous features in Fig. S1 of SM [7] for the case of a five-fold supercell).

microscopic aspects of the closely related LICO with a simpler but similar averaged structure as CYCO. The validity of the large J_1 -regime is also confirmed by several DFT+ U calculations for LICO [9].

1. Consequences for the magnetic susceptibility

Ignoring the tiny FM couplings along the b axis, CYCO is a 2D Néel system with a relatively large FM Curie-Weiss (CW) temperature:

$$\Theta_{\text{CW}} \approx -\frac{1}{2} [J_{a1}(1 - \alpha) + z(J_{ac,1} + J_{ac,2})] \approx 80 \text{ K}, \quad (12)$$

where $2z$ measures the number of NN and NNN sites on the adjacent chains. Without the ICs one would arrive at $\Theta_{\text{CW}} \approx 107$ K. To show that the exchange values determined from our refined INS measurements are fully compatible with the $\chi(T)$ -data, we reproduce in Fig. 12 the data from Ref. 50. Similarly to our recent analysis of $\chi(T)$ for LICO [11], we have fitted the data in the range $240 < T < 300$ K with the expression

$$\chi(T) = \frac{5N_A g^2 \mu_B^2}{k_B} \chi_{10}(T), \quad \chi_{10}(T) = \sum_{n=1}^{10} \frac{c_n}{T^n}, \quad (13)$$

where $\chi_{10}(T)$ is the 10th-order HTE [51, 52]. N_A is the Avogadro number (one mole of CYCO contains $5N_A$ spins), μ_B is the Bohr magneton, and g is the gyromagnetic ratio. A small anisotropy of the couplings as well as the tiny inter-plane couplings ($J_b/k_B, J_{ab}/k_B < 1$ K) is unimportant for the $\chi(T)$ -analysis and was ignored here. Evidently, the HTE series, Eq. (13), fits well the data for $g_a \approx 2.04$, $g_b \approx 2.28$, $g_c \approx 2.02$ above $T \sim 240$ K. We recall that an ESR study on powder samples of CYCO reports $g_b \approx 2.31$ and $g_{\perp} \approx 2.03$ [53]. The [5,5] Padé approximation fits the curve down to $T \gtrsim T_N$. Fig. 12

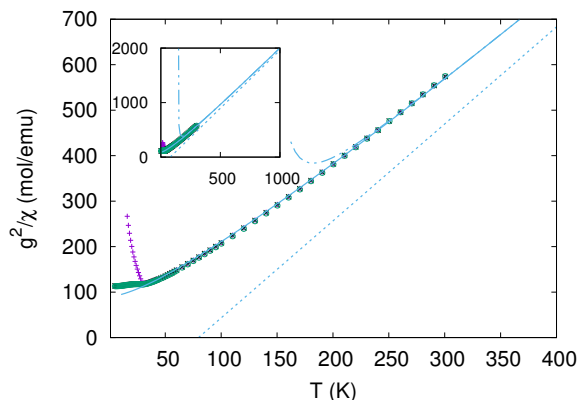


FIG. 12. The inverse spin susceptibility for a magnetic field along the a (\times), b ($+$), and c (\circ) axes of CYCO (from Ref. [50]). Dashed double-dotted line: fit by the 10th-order HTE Eq. (13); solid line: [5,5] Padé approximation. Short-dashed line: the exact CW asymptotic curve. Inset: Extended T -range up to 1000 K.

also shows the CW asymptotic curve, reached only at $T \gtrsim 1000$ K, as shown in the inset. From this comparison the strong IC in CYCO is evident, explaining the *absence* of criticality, which manifests itself in a strong up-shift of α_c (see SM [7]) and in the large moments seen in neutron diffraction in the quasi-2D Néel state below the high $T_N \approx 30$ K. In contrast, LICO, $\text{Ca}_2\text{Nd}_2\text{Cu}_5\text{O}_{10}$, and CuAs_2O_4 might be closer to the 1D α_c due to $\alpha > 1/4$ and a much weaker AFM IC, which is even there necessary to stabilize a FM alignment. For LICO the analogous AFM IC $J_{bc,1} + J_{bc,2}$ is only 9 K (0.8 meV) per bond, where the b axis is the chain direction.

To avoid such strange results found often in the literature from improper $\chi(T)$ fits (e.g. $\Theta_{\text{CW}}=2$ K [14] for CYCO), low- T INS (or RIXS) probing the magnon dispersion, combined with magnetization data up to the saturation field, allows to extract more reliable couplings. The former should be used to cross-check any exchange set derived from $\chi(T)$, if multiple J 's are involved. Noteworthy, for $\text{La}_6\text{Ca}_8\text{Cu}_{24}\text{O}_{41}$ [54] containing both *undoped* TLL and CuO_2 chains just like in CYCO but with a *smaller* Φ , a tiny $\Theta_{\text{CW}}=21\pm 1$ K has been reported [54] from linear fits of $1/\chi(T)$ data up to 300 K only. But from that $\Phi \approx 91.6^\circ$ K, according to Eqs. (14,16,18), even a *larger* FM J_1 is expected. Then, with a smaller AFM IC due to the low $T_N \approx 12.5$ K and a similar misfit from La^{3+} replacing Y^{3+} , as in CYCO, a much *larger* $\Theta_{\text{CW}} \sim 100 \gg 21$ K is requested. Another related issue is the incorrectly predicted critical h -doping when Θ_{CW} changes its sign, i.e., for weak h -doping a sizable magnon dispersion and hence $\Theta_{\text{CW}} > 0$ are still expected, at odds with the opposite sign provided so far in the literature from improperly fitted asymptotics. Our dispersion-law (with a generalization for frustration perpendicular to the AFM 2nd adjacent chain [55] as proposed for $\text{La}_5\text{Ca}_9\text{Cu}_{24}\text{O}_{41}$) allows to separate chains from ladders dominant above their spin gap [56].

Since frustrated FM systems are of general interest in the field of quantum magnetism and statistical physics [57–59], hopefully, our work will initiate further work. In particular, systematic studies of critical systems like CuAs_2O_4 with $\alpha \approx 0.27$ [60–62] will give insight into the role of quantum fluctuations (see Table I in SM [7]). In this context the study of other thermodynamic properties as the specific heat and thermal conductivity might be useful to check the coupling constants derived here. Other examples of weakly h -doped compounds [34, 63] will be addressed elsewhere.

2. QC and DFT analysis for LICO – comparison with Mizuno et al. [15]

The most notable theoretical finding of the present work with respect to an empirically large FM J_1 value is several microscopic FM intersite couplings behind the spin-chain model, obtained by QC and DFT-based analysis. Given the complex real structure of CYCO, we will

present theoretical studies for LICO since its structure is very close to the *averaged idealized* structure of CYCO. In fact, their C-O-Cu bond angles Φ differ by $\approx 0.1^\circ$, whereas the Cu-Cu distances $d_{\text{Cu-Cu}}$ by 0.04 Å and the Cu-O bond length $d_{\text{Cu-O}}$ by ≈ 0.025 Å only [35, 64]. We therefore believe that the NN results for LICO can be transferred to CYCO with an uncertainty of only a few percents. A semi-quantitative general analysis including several cuprates will be given elsewhere. Providing refined theoretical results for LICO very much simplifies the modeling and allows a critical check of the parameters *adopted* in Ref. 15 for LICO. It is convenient to decompose the total J_1 into a FM and an AFM contribution:

$$J_1 = J_1^{\text{FM}} + J_1^{\text{AFM}}, \quad \text{with} \quad (14)$$

$$J_1^{\text{FM}} \approx J_1(K_{pd}, K_{pp}) + J_1(J_H) - K_{dd} \quad \text{and} \quad (15)$$

$$J_1^{\text{AFM}} \approx J_\Phi + \frac{4t_{dd}^2}{U_d - V_{dd}}, \quad (16)$$

where K_{pd} , K_{pp} , and K_{dd} denote direct FM *intersite* Coulombic (Heisenberg) exchange integrals and J_H is the indirect *onsite* Hund's-rule coupling from each of the bridging O's. For the corresponding *pd*-Hamiltonian, see e.g. Refs. 15, 44, 65, and 66 and Fig. 13. The generalization including also the Cu-Cu intersite terms K_{dd} , V_{dd} , and the hopping t_{dd} (all ignored there) is straightforward. For enlarged K_{pd} and K_{pp} in the 2D geometry of La_2CuO_4 , see Refs. [16, 17].

Turning to the various FM sources in J_1^{FM} entering Eq.(15), we note that in general all fundamental FM exchange couplings are known by order of magnitude only: $1 \text{ meV} < K_{dd} \ll K_{pp} \ll K_{pd} \ll J_H < 1.5 \text{ eV}$. K_{pd} , K_{dd} , and K_{pp} are reported here for the first time for chain

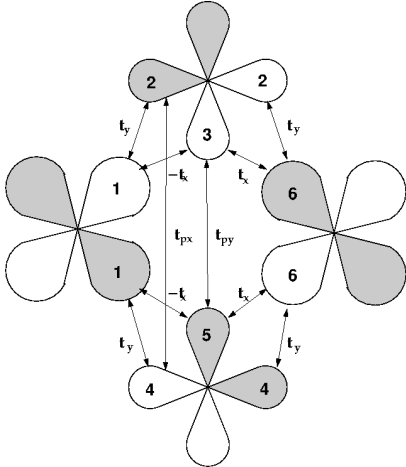


FIG. 13. *p* and *d* orbitals and transfer integrals of a CuO_2 -cluster treated exactly within a planar Cu $3d$ O $2p$ five-band Hubbard model: Cu $3d_{xy}$ 1 (left) and 6 (right); intermediate O $2p_{x,y}$ 2,3 (upper) 4,5 (lower). The chain is along the horizontal direction (*x* axis). For the sake of clarity the hopping t_{dd} between two Cu-sites along the *x* axis is not shown.

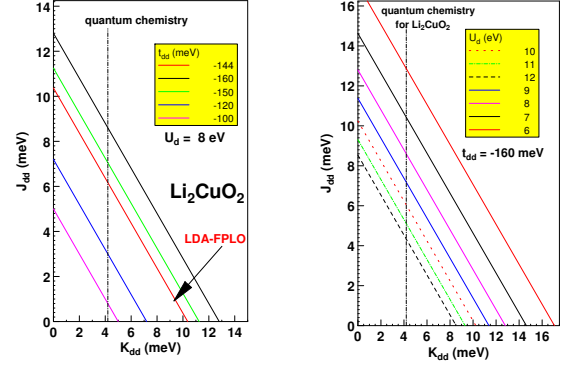


FIG. 14. Superexchange from the *dd* channel J_{dd} vs. the direct intersite FM exchange K_{dd} for various Direct Cu-Cu hoppings $|t_{dd}|$, e.g. $t_{dd} = -144$ (-160) meV by LDA (QC) mapping (both ignored in Ref. 15; for details, see Sec. C in SM [7]) (left) and adopted onsite Hubbard U_d values (right). Vertical d

ashed-dotted lines are the QC result for LICO.

cuprates. Refining the estimates given above, our QC result is $K_{dd} \approx 4.2 \text{ meV}$, indeed much smaller than various $K_{pp} < 20 \text{ meV}$, and $K_{p_x} \approx K_{p_y} \approx 105 \text{ meV}$ (for details see Sec. C in SM [7]). J_H somewhat exceeds the value of 600 meV adopted in Ref. 15. According to direct calculations and various empirical estimates, in particular, for related superoxides [67], a bit enhanced slightly screened J_H -value $\sim 0.7 \text{ eV}$ is even more realistic [68]. K_{pd} turns out to be the most important FM microscopic interaction for J_1 since a weak enhancement of a moderate J_H cannot explain the more than twice as large J_1 at fixed $K_{pd} = 50 \text{ meV}$ universally adopted by Mizuno *et al.* [15] (including also CYCO) who found $J_1 = 100 \text{ K}$ for LICO at odds with $|J_1| \geq 230 \text{ K}$ derived without fully probed by INS [9] magnon-dispersion leaving therefore some room for further refinements in future if the same sophisticated intensity analysis as in Sec. IV for CYCO could be applied there too.

Our DFT and QC analysis succeeded also in the determination of a remarkable direct *dd* transfer integral $|t_{dd}|$, 144 and 160 meV, respectively, due to the short NN Cu-Cu distance $d_{\text{Cu-Cu}} \approx 2.86 \text{ Å}$. A finite t_{dd} (ignored in Ref. 15) provides an *additional* AFM contribution if

$$|t_{dd}^c| > 0.5\sqrt{(U_d - V_{dd})K_{dd}}. \quad (17)$$

Typically t_{dd} is of the order of $+5 \text{ meV}$ (Fig. 14), yielding further arguments for a larger K_{pd} . With this AFM *dd* channel alone, $J_1 \approx 165 \text{ K}$ would be achieved when fixing K_{pd} . The precise value of U_d (actually unknown) affects strongly the efficiency of the *dd* AFM superexchange, as shown in Fig. 14, especially for FFESC cuprates with a short Cu-Cu distance. It markedly exceeds that for typical charge transfer insulators ($U_d \gg \Delta_{pd}$), where it is negligible due to the tiny t_{dd} . Also a realistic intersite Cu-Cu Coulomb interaction V_{dd} of 0.3 to 0.5 eV [69–72]

might be relevant (compared to Eqs. (23), (24), and (S24) and Sec. J in SM [7]). The dd channel is of interest for further theoretical studies since it gives a new Cu-Cu-O-Cu exchange path in addition to the known Cu-O-O-Cu one, with possible modifications of J_2 .

3. Comparison with other cuprates and general trends

Looking for an empirical support, we will compare our J_1 -values with those of other cuprates and provide thereby a critical analysis for the exclusive attempt to present a general description of edge-sharing chain cuprates and ladders performed 20 years ago [15], when almost no detailed microscopic studies were known. We will show that it is timely to reconsider not only LICO and CYCO since our criticism concerns the unjustified use of a systematically *underestimated*, *universal*, and *isotropic* direct FM Cu-O exchange $K_{pd} = 50$ meV [15] with serious consequences for the FM J_1 . It is in fact of general interest for all cuprates with edge-sharing elements, including infinite CuO_2 chains, ladders, coupled $\text{Cu}_n\text{O}_{n+2}$ ($n = 2, 3, 4 \dots$), and other finite edge-sharing CuO_4 units (see Table I of SM [7]). This provides the basic picture of the interactions in cuprates and the minimal stage with the 5-band Hubbard pd -model in terms of which their fundamental physical properties must be discussed.

The magnitude of the NN exchange is important for any quantum magnet, in particular, for cuprates with edge-sharing elements present in single and double (zigzag) chains, since it determines or strongly affects the role of frustration measured here by α in Eq. (1). As mentioned above, $\alpha \gg 1$ can be treated as an effective AFM system with slightly renormalized J_2 -values ignoring the finite α^{-1} -value at all. Unbiased QC and DFT studies allow insight into the magnitude of J_1 , despite some uncertainty due to certain correlation and spin-orbital effects ignored here. With this in mind, we select and comment on available data for various cuprates in Table I of SM [7]. Naturally, Φ near 90° , the Cu-Cu $d_{\text{Cu-Cu}}$ and the Cu-O distances within the generic CuO_4 plaquettes as well as the strength of the crystal field, strongly affected by the charge and position of the surrounding cations near the bridging O, are important physical ingredients.

Similar or even larger J_1 -values have been observed or predicted by theoretical studies [73–75] so far only in (i) ladder compounds (J_1 corresponding to the interladder couplings), (ii) double-corner-sharing (zigzag) chain compounds with predicted J_1 values of -28 to 55 meV, and (iii) alternating FM-AFM chain systems $\text{Li}_3\text{Cu}_2\text{SbO}_6$ [76] and $\text{Na}_3\text{Cu}_2\text{Sb}(\text{Te})\text{O}_6$ [73] with $J_1 = -23.56$ meV. $\text{Li}_3\text{Cu}_2\text{SbO}_6$ [76] and $\text{Na}_3\text{Cu}_2\text{SbO}_6$ [73, 77, 78], with similar AFM couplings but very different relatively large FM J_1 values, are particularly striking. In view of its large $\Phi = 95.27^\circ$, an AFM or very weak FM coupling would be expected according to Ref. 15. Hence, an enlarged FM interaction and/or a strongly suppressed AFM exchange

via the bridging O must be responsible for the resulting FM $J_1 = -17.8$ meV, twice of -8.6 meV estimated for $\Phi = 93.97^\circ$ (the case of LICO) [15]. The smaller value of -12.7 meV derived from INS data [78] is probably due to the too small limiting energy of 14.7 meV probed there, similarly as for CYCO previously. There the CuO_2 chains are distorted by a similar cationic misfit, as in CYCO, in the combined TLL and chain system $\text{La}_6\text{Ca}_8\text{Cu}_{24}\text{O}_{41}$. Due to the Φ closer to 90° also somewhat larger J_1 values are expected. Unfortunately, its chain magnon component is not yet fully understood, hampered by the dominant two-spinon contribution and the h -doping in some cases [79]. Our present J_1 -value strongly exceeds an earlier estimate of -2.15 meV for CYCO and that of -8.6 meV for LICO [15]. Furthermore, it is at odds with $\alpha = 2.2$ [15] and puts it close to α_c . The results from QC analysis for LICO show a markedly enlarged J_1 by 42% as compared with Ref. 15 but not enough when compared with the empirical and DFT-derived values with a still larger 130% enhancement. For the TLL SrCu_2O_3 a less dramatic but also enhanced value by about 15% was predicted which however is caused by the smaller Φ (see also Ref. 79). For $\Phi = 90^\circ$, generalizing an expression for J_2 by the account of a moderately enhanced direct FM pd intersite h -exchange K_{pd} , $\alpha \approx 3$ to 4 is estimated, as shown below. Then based on the empirical $J_2 \approx 166$ meV, $J_1 \approx -55$ to -41.5 meV can be estimated for SrCu_2O_3 as an upper bound and we would arrive at $J_1 \approx -38 \pm 1$ meV as a realistic estimate. Note that again it exceeds the value from Ref. [15], now by $\approx 25\%$ and $J_1^{\text{FM}} = -38$ meV like in LICO. Thus, one has enough reasons to doubt the results given there for various chains and ladders. Then one may ask: "What is the reason for the *material dependent* systematic underestimates given in Ref. [15]?" The numerous examples discussed above require a strong material dependence which is unlikely for J_H . But its efficiency is lowered for split O onsite energies due to strong crystal field effects. In addition the usual indirect superexchange J_Φ via the bridging O increases and one can easily arrive at small J_1 values ~ 80 - 100 K, as realized e.g. in linarite with a moderate $\Phi \approx 93^\circ$. Then K_{pd} remains the main microscopic source for FM J_1 values in cases as LICO since only a weak material dependence of J_H (governed mainly by U_p) is expected. The *two* interacting bridging O ions cause a slower convergency of standard perturbation theory, used previously to the effect of K_{pd} and J_H . Hence, exact diagonalizations on small clusters are used to study this point, as shown in Figs. 15 and 16.

4. Description in the five and single band Hubbard models

Now we will show semi-quantitatively that a realistic microscopic scenario for such large FM J_1 -values well exceeding -200 K can be proposed. Our arguments will be expressed in terms of the most natural and vivid multiband Cu $3d$ $O2p$ Hubbard model with five magnet-

ically active orbitals in the xy -plane containing ideally flat CuO_2 chains, namely, the single $\text{Cu } 3d_{xy}$ orbital and the two $\text{O } 2p_x$ and $2p_y$ orbitals for each of the two bridging O (Fig. 13), where x is the chain-axis (a axis in Fig. 1) and the y -axis corresponds to the crystallographic c

axis (see also SM [7]). Since this model contains already a large set of partly not precisely known interactions, we consider below also an effective single-band model with a reduced number of parameters. The first pd term of the AFM contribution according to standard 4th-order perturbation theory [80, 81] reads

$$\begin{aligned} J_\Phi &\approx \frac{4t_{p_x d}^2}{(\Delta_{p_x d} + V_{p_x d})^2} \left[\frac{2t_{p_x d}^2}{\Delta_{p_x d} + V_{p_x d}} + \frac{1}{U_d} \right] - \frac{4t_{p_y d}^2}{(\Delta_{p_y d} + V_{p_y d})^2} \left[\frac{2t_{p_y d}^2}{\Delta_{p_y d} + V_{p_y d}} + \frac{1}{U_d} \right], \\ &\approx \frac{4t_{pd}^2 \sin^2 \Phi/2}{(\Delta_{pd} + V_{pd})^2} \left[\frac{2t_{pd}^2 \sin^2 \Phi/2}{\Delta_{pd} + U_p} + \frac{1}{U_d} \right] - \frac{4t_{pd}^2 \cos^2 \Phi/2}{(\Delta_{pd} + V_{pd})^2} \left[\frac{2t_{pd}^2 \cos^2 \Phi/2}{\Delta_{pd} + U_p} + \frac{1}{U_d} \right], \\ &\approx -\frac{4t_{pd}^2}{(\Delta_{pd} + V_{pd})^2} \left[\frac{2t_{pd}^2}{\Delta_{pd} + U_p} + \frac{1}{U_d} \right] \cos \Phi, \end{aligned} \quad (18)$$

ignoring for shortness the O-O NN hopping terms (compare to Eqs. (S46) and (S47) in SM [7] for the case $\Phi = 180^\circ$, where the last Eq. is obeyed in the isotropic limit). It vanishes for $\Phi = 90^\circ$, if one ignores the slightly different O $2p_x$ and $2p_y$ onsite energies due to the weak crystal field [72]. In contrast, in cases of strong crystal fields or the presence of ligands, even at $\Phi = 90^\circ$ there is a significant AFM contribution that reduces the total value of J_1 . For the experimental value of Φ and by adopting the parameters of Ref. 15, i.e. ignoring first of all the intersite Coulomb interaction V_{pd} , one has $J_\Phi \approx 200$ K.

Since J_1^{AFM} depends markedly on Φ , the total J_1 may change its sign at Φ values far enough from 90° , which happens in fact in several cases different from LICO and CYCO (see Table I in SM [7]).

K_{pd} and J_H occur in reverse orders of the (t_{pd}/Δ_{pd}) -perturbation theory affecting their weight and n_p on the two O sites which interact by hoppings and FM K_{pp} . In the spirit of this approach for the five-band Hubbard model sketched in Refs. 81 and 82 for the case of edge-sharing plaquettes with two common O, Eq. (15) can be approximated by

$$J_1^{\text{FM}} \approx -K_{dd} - 8Z \left(\frac{t_{pd}}{\Delta_{pd}} \right)^2 K_{pd} - \frac{4Z^2 J_H}{(1 + U_{pp}/\Delta_{pd})} \left(\frac{t_{pd}}{\Delta_{pd}} \right)^4 \approx -K_{dd} - 4 \left(\frac{t_{pd}}{\Delta_{pd}} \right)^2 K_{pd} - \frac{J_H}{(1 + U_{pp}/\Delta_{pd})} \left(\frac{t_{pd}}{\Delta_{pd}} \right)^4. \quad (19)$$

where the renormalization factor $Z(t_{pp}^2/U_p, K_{pp}, \Delta_{pd}) < 1$ has been introduced. It contains higher-order corrections due to various O-O hoppings and direct FM couplings K_{pp} taken from our DFT and QC analysis.

For $\Delta_{pd} = 3.5$ eV, $Z \approx 0.48$. A quasi-linear law for J_1 , K_{pd} , and J_H , like in Eq. (19) (with slightly changed 2nd and 3rd coefficients due to additional interactions) holds, also beyond (t_{pd}/Δ_{pd}) -perturbation theory as confirmed by the exact treatment of $\text{Cu-O}_2\text{-Cu}$ dimers (see Fig. 16 and SM [7]) as well as for larger clusters with small finite size effects within the effective single-band Hubbard model. Then the estimated ratio ρ_{HK} of the FM on- and intersite contributions to J_1 reads [81]

$$\rho_{\text{HK}} = \frac{J_1^{\text{H}}}{J_1^{K_{pd}}} \approx \frac{J_1^{\text{H}}}{2K_{pd}(1 + (U_p - 2J_H)/\Delta_{pd})} \left(\frac{t_{pd}}{\Delta_{pd}} \right)^2, \quad (20)$$

where an often used approximation defines J_H :

$$J_H = 0.5(U_p - U_{pp}). \quad (21)$$

In case of ideal two-leg ladders, i.e. $\Phi = 90^\circ$ and $U_p = 4.4$ eV, Rice *et al.* [56] ignoring K_{pd} , derived a useful expression for the FM interladder coupling:

$$J_1^{\text{H}} = \frac{2t_{pd}^4}{\Delta_{pd}^2} \left[\frac{1}{E_T + 2\Delta_{pd}} - \frac{1}{E_S + 2\Delta_{pd}} \right], \quad (22)$$

where $E_T = 7.3$ eV ($E_S = 1.8$ eV) denote the energy of the Zhang-Rice triplet (singlet) state, respectively, for $t_{pd} = 1.3$ and $\Delta_{pd} = 3.3$ eV. Inserting these numbers into Eq. (22) one arrives at $J_1^{\text{H}} = 24.7$ meV and a frustration ratio of 6.7 using the experimental value $J_2 = J_{\text{leg}} = 166$ meV. The QC result can be confirmed if the direct FM coupling and the residual AFM couplings from $\Phi \neq 90^\circ$ and that from the dd channel are taken into account assuming equal leg and rung AFM exchange integrals. Experimentally, however, they differ slightly: $J_{\text{leg}}/J_{\text{rung}} \approx 1.1$ for SrCu_2O_3 , which is caused by different O $2p$ onsite energies. We ignore this small difference ~ 15 meV and use for the double-chain problem the experimental value of $J_{\text{leg}} = J_2$. From Eq. (22)

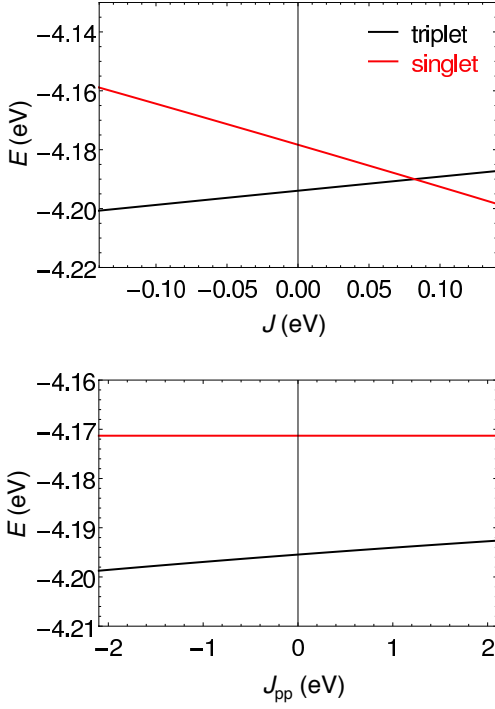


FIG. 15. Lowest singlet and triplet energies of a $\Phi = 90^\circ$ CuO_2Cu cluster as in Fig. 13 vs. the main FM exchanges for a set close to Ref. 15, where a $\text{O}_2\text{-CuO}_2\text{Cu-O}_2$ cluster was used. ($t_{p_xd} = t_{p_yd} = 0.7155$, $t_{dd} = 0$, $t_{p_x} = 0.17$, $t_{p_y} = 0.69$, $V_{pd} = V_{dd} = J_{dd} = 0$, $\Delta_{pd} = 3.2$, $E_{p_x} = 1.75$, $E_{p_y} = 1.45$, $U_d = 8.5$, $U_p = 4.1$, $K_{pd} = 0.05$, and $J_H = 0.6$; all in hole notation and in units of $t \equiv t_{pd} \approx 1$ eV) $J = -K_{pd}$ (**upper plot** for $J_H = 0.6$) and $J_{pp} = -J_H$ at $K_{pd} = 0.05$ (**lower plot**).

one estimates $-J_1^H \approx J_2/7 \approx 0.629$ eV. Using Eq. (20) one obtains $1/3$ for the set in Ref. [15] and $\approx 1/4$ for $K_{pd} \sim 100$ meV. Adopting nearly the same value for the ladder compound value as for LICO obtained here, one would arrive at $\alpha < 4$ to 5 in accord with a QC prediction for SrCu_2O_3 [83] (see also SM [7]). High-energy spectroscopy and more theoretical studies are desirable to put material specific upper limits on important U_d and J_H . Without the dd channel, the INS data [9] were described at $J_H = 0.6$ eV by already enlarged values $K_{pd} = 81$ and 96 meV, in accord with our optical conductivity, EELS, and RIXS spectra for LICO [66, 71, 84, 85]. Figs. 15 and 16 clearly show the larger sensitivity of the singlet-triplet separation to K_{pd} than to J_H , where only the triplet state is slightly affected. This confirms K_{pd} as the key FM source.

To summarize, a precise general microscopic assignment of the origin of the observed large J_1 -values is still difficult since K_{pd} , J_H , and the AFM J_{dd} are involved. But without doubt K_{pd} is the leading FM term. The short $d_{\text{Cu-Cu}}$ leads to a sizable direct intersite AFM superexchange, negligible in corner-sharing cuprates with $\approx \sqrt{2}$ larger $d_{\text{Cu-Cu}}$. The FM K_{pp} somewhat reduces the generic AFM J_2 . Cuprates are usually classified as charge transfer insulators, which is not strictly valid here

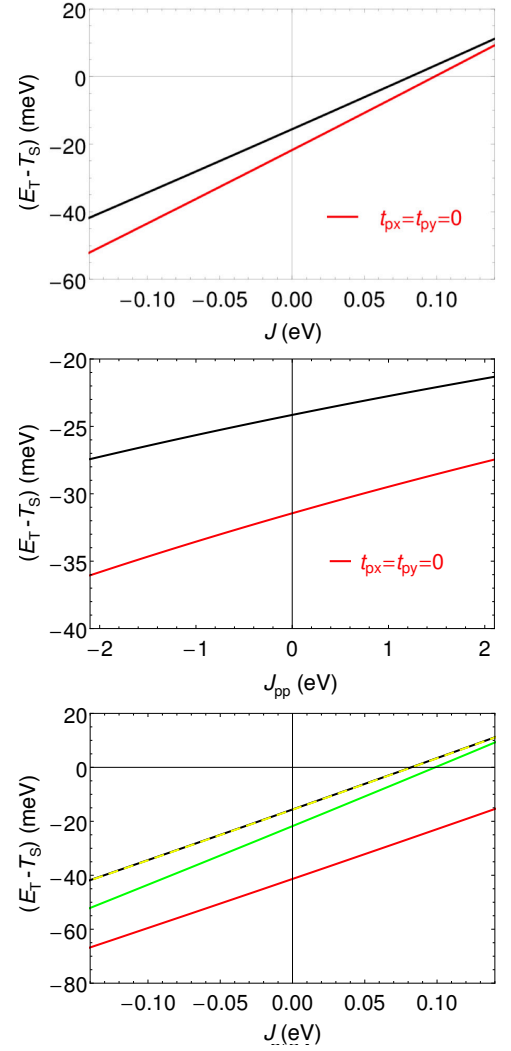


FIG. 16. The NN exchange $J_1 = E_T - E_S$ from exact diagonalizations similarly to Eq. (19). The suppression of the intersite interaction between the "upper" and lower O for $U_p = \infty$ (green curve) and $t_{p_y p_y} = t_{p_x p_x} = 0$ (red curve) as compared to the set described above (black curve). Dotted curve: including also the weak FM direct exchange K_{pp} ($K_{p_y p_y} = 18.4$, $K_{p_x p_y} = 13.4$, and $K_{p_x p_x} = 8.7$ meV).

since the J_1 is certainly affected by the additional superexchange governed by the Cu U_d and the hopping t_{dd} [Eqs. (13-15)] as in standard Mott insulators.

Within a much simpler effective single-band extended Hubbard model, larger clusters can be treated exactly. Here we include, in addition to the NN transfer integral $t \equiv t_1$, the Hubbard onsite repulsion U , and a NNN counterpart t_2 to the former, the NN and NNN intersite Coulomb interactions V_1 and V_2 , respectively, two external exchange couplings \tilde{J}_1 (to allow for a FM NN exchange) and \tilde{J}_2 to account for the corresponding FM contribution to J_2 arising from K_{pp} between O sites (see SM [7]). For a dimer, an exact analytical expression is

available [86] beyond the Hubbard-model:

$$J_1 = \frac{\sqrt{16t^2 + \tilde{U}^2} - \tilde{U}}{2} + \tilde{J}_1 \quad , \quad (23)$$

where $\tilde{U} = U - V + \frac{3}{4}\tilde{J}_1$. For $U \gg |t|, |\tilde{J}_1|$ in Eq. (23) simplifies to [used in Eqs. (14,15) for the *dd* channel]

$$J_1 \approx \frac{4t^2}{\tilde{U}} + \tilde{J}_1 \quad . \quad (24)$$

The 2nd, "external", term on the right hand side is FM and it overcompensates the first one, which represents the non-negligible AFM superexchange. The dimer model provides also a direct tool for materials like $\text{Li}_3\text{Cu}_2\text{SbO}_6$, $\text{Na}_3\text{Cu}_2\text{Sb}(\text{Te})\text{O}_6$, and other alternating FM-AFM chain compounds with a dominant FM NN exchange.

VI. SUMMARY

A large magnon dispersion up to 53 meV was observed in CYCO. It is caused mainly by a large extracted FM NN coupling $J_{a1} = -24$ meV exceeding that for LICO [9] and represents the highest value detected so far for any FFESC cuprate. From our experience with CYCO, a successful search of the *full* dispersion, up to ~ 45 meV would refine the J_1 and J_2 in LICO and $\text{Li}(\text{Na})\text{Cu}_2\text{O}_2$. The NNN AFM $J_{a2}=5.5$ meV puts CYCO near to criticality ($\alpha \sim 0.23$) for a 1D chain but not for strongly enough AFM coupled NN chains shifted by half a Cu-Cu distance. This chain structure causes an O mediated stable FM alignment of magnetic moments along the chain in a stacked structure of quasi-2D-Néel commensurate collinear magnetic ordering. From our analysis and microscopic arguments for systems with similar chains, we expect highly dispersive magnons for $\text{La}_6\text{Ca}_8\text{Cu}_{24}\text{O}_{41}$, $\text{Ca}_2\text{Nd}(\text{Gd})_2\text{Cu}_5\text{O}_{10}$, and $\text{SrCa}_{13}\text{Cu}_{24}\text{O}_{41}$ including the slightly *h*-doped systems. Then the available magnon dispersion-law should be helpful.

Gap-like features are observed at ~ 11.5 meV and ~ 28 meV. The smaller gap at 11.5 meV is ascribed to phonon-magnon coupling while the gap at 28 meV is ascribed to quantum effects due to the AFM IC as well as to the non-negligible inhomogeneous cuprate chain

structure caused by the misfit with the NN Ca/Y chains generic for the composite symmetry of its two subsystems in CYCO and in the cases mentioned above. Both effects are most cooperative for a lock-in SS consisting of $\text{Ca}_2\text{Y}_2\text{Cu}_5\text{O}_{10}$ and $\text{Ca}_4\text{Y}_4\text{Cu}_{10}\text{O}_{20}$ domains.

The large J_1 values in CYCO and LICO provide deep insight into the microscopic exchange pointing to a dominant direct FM interaction $K_{pd} \sim 105$ meV, more important than the indirect O $2p_x p_y$ exchange mediated by the Hund's coupling J_H . Noteworthy, we found that the usually ignored direct Cu-Cu superexchange may somewhat reduce the effect of FM couplings. J_H and U_d should be studied systematically [68], especially in view of smaller empirical values of $J_H \leq 0.6$ eV reported for superoxides [67]. Although the issue of a large FM J_1 -value is now almost unraveled, we are still left with a new question: given such natural $K_{pd} \sim 100$ meV, what is the reason for the markedly *lower* values for linarite and some FFESC materials? Presumably, ligand effects lowering the efficiency of J_H and raising the O mediated superexchange. Thus, seemingly well understood "classical" systems, studied already for many years, are still sources of surprises, deserved to be studied in more detail to elucidate the interactions behind the exchanges described by various spin-Hamiltonians and their interplay with structural details.

ACKNOWLEDGMENTS

We used resources at the High Flux Isotope Reactor and Spallation Neutron Source, DOE Office of Science User Facilities operated by the Oak Ridge National Laboratory. Support by the SFB 1143 of the DFG is acknowledged (SN). We thank U. Nitzsche for technical assistance and S. Johnston, D. Miloslavlevic, A. Tsirlin, O. Janson, J. Málek, R. Klingeler, W.E.A. Lorenz, T. Schmitt, C. Monney, J. van den Brink, U. Röbber, A.S. Moskvina, D. Khomskii, A.M. Oles, G. Sawatzky, K. Wohlfeld, A. Yaresko, G. Roth, and J. Thar for discussions. Special thanks to GR and JT for providing figures of the CuO_2 chains in CYCO according to their structure model as well as to DT, AT, OJ, SL, and UN for providing unpublished theoretical results included partly in Table I of SM [7]. We also thank J. Richter and A. Hauser for help with their HTE package code used here.

-
- [1] R. Bursill, G. A. Gehring, D. J. J. Farnell, J. B. Parkinson, T. Xiang, and C. Zeng, *Journal of Physics: Condensed Matter* **7**, 8605 (1995).
 - [2] M. Braden, G. Wilkendorf, J. Lorenzana, M. Aïn, G. J. McIntyre, M. Behruzi, G. Heger, G. Dhalenne, and A. Revcolevschi, *Phys. Rev. B* **54**, 1105 (1996).
 - [3] C. E. Agrapidis, S.-L. Drechsler, J. van den Brink, and S. Nishimoto, *Phys. Rev. B* **95**, 220404(R) (2017), and *Sci.Post Phys.* **6**, 019 (2019).
 - [4] S.-L. Drechsler, O. Volkova, A. N. Vasiliev, N. Tristan, J. Richter, M. Schmitt, H. Rosner, J. Málek, R. Klingeler, A. A. Zvyagin, and B. Büchner, *Phys. Rev. Lett.* **98**, 077202 (2007).
 - [5] J. Sirker, *Phys. Rev. B* **81**, 014419 (2010).
 - [6] Y. Tarui, Y. Kobatashi, and M. Sato, *J. Phys. Soc. Jpn.* **77**, 043703 (2008).
 - [7] Supplementary material.
 - [8] J. Thar, R. Müller, S. Mattauch, B. Büchner,

- and G. Roth, Acta Cryst. **A62**, s185 (2006), s. also: J. Thar "Präparation und Charakterisierung von $(\text{Ca}_{1-x}\text{Y}_x)_4\text{Cu}_5\text{O}_{10}$ ($0 < x < 0.5$)", Diplomerwork, Inst. f. Kristallogr., RWTH Aachen. Figs. 6.1, 6.7, 6.8, 6.10.
- [9] W. E. A. Lorenz, R. O. Kuzian, S.-L. Drechsler, W.-D. Stein, N. Wizen, G. Behr, J. Málek, U. Nitzsche, H. Rosner, A. Hiess, W. Schmidt, R. Klingeler, M. Loewenhaupt, and B. Büchner, Europhys. Lett. **88**, 37002 (2009).
- [10] W. E. A. Lorenz, *On the Spin-Dynamics of the Quasi-One-Dimensional, Frustrated Quantum Magnet Li_2CuO_2 Studies by means of Inelastic Neutron Scattering and Thermodynamic Methods*, PhD dissertation, TU Dresden (2011), <http://d-nb.info/1067190074/34>.
- [11] R. O. Kuzian, R. Klingeler, W. E. A. Lorenz, N. Wizen, S. Nishimoto, U. Nitzsche, H. Rosner, D. Milosavljevic, L. Hozoi, R. Yadav, J. Richter, A. Hauser, J. Geck, R. Hayn, V. Yushankhai, L. Siurakshina, C. Monney, T. Schmitt, J. Málek, G. Roth, J. Thar, T. Ito, H. Yamaguchi, M. Matsuda, S. Johnston, and S.-L. Drechsler, New J. of Phys. **20**, 058001 (2018), in their late Corrigenda and the Reply by Shu *et al.*, *ibid.*, 059501 and 058002, respectively. Some incorrect statements still do remain to be discussed elsewhere [see also R. O. Kuzian *et al.*, arXiv 1708.06335v2 (2018)].
- [12] M. Matsuda, K. Ohoyama, and M. Ohashi, Journal of the Physical Society of Japan **68**, 269 (1999).
- [13] H. F. Fong, B. Keimer, J. W. Lynn, A. Hayashi, and R. J. Cava, Phys. Rev. B **59**, 6873 (1999).
- [14] V. Kargl and P. Böni and A. Mirmelstein and B. Roessli and D. Sheptyakov, Physica B: Cond. Matter **359**, 1255 (2005).
- [15] Y. Mizuno, T. Tohyama, S. Maekawa, T. Osafune, N. Motoyama, H. Eisaki, and S. Uchida, Phys. Rev. B **57**, 5326 (1998).
- [16] M. S. Hybertsen, E. B. Stechel, M. Schlüter, and D. R. Jennison, Phys. Rev. B **41**, 11068 (1992).
- [17] M. S. Hybertsen, E. B. Stechel, W. M. C. Foulkes, and M. Schlüter, Phys. Rev. B **45**, 10032 (1992).
- [18] V. S. Kargl, *Magnetic properties of low dimensional spin systems*, PhD-dissertation, TU Munich (2006).
- [19] P. K. Davies, E. Caignol, and T. King, Journal of the American Ceramic Society **74**, 569 (1991).
- [20] Due to the hybridization between the Cu $3d_{xz}$ and the bridging O $2p_z$ and $2p_x$ orbitals, the spin 1/2 is distributed between these 3 orbitals with a dominant Cu $3d$ weight $n_d \approx 0.78$ in accord with the observation of a finite O moment of 22 ± 4 % [87] Within the error bars the same ratio has been found earlier for the ordered moments also by neutron diffraction in the CuO_2 chains of $\text{La}_{14-x}\text{Ca}_x\text{CuO}_{24}\text{O}_{41}$ [88]. This ratio of the O and Cu occupation numbers is generic for FFES CuO_2 chain systems. In the formal limit $n_d \rightarrow 1$ CYCO and LICU would be *unfrustrated* AFM or FM simple quasi-1D pure Mott-insulators with a weak AFM or FM NN exchange integral J_{dd} of few meV and a weak magnon dispersion $\sim 2J_{dd}$ ().
- [21] M. Matsuda, H. Yamaguchi, T. Ito, C. H. Lee, K. Oka, Y. Mizuno, T. Tohyama, S. Maekawa, and K. Kakurai, Phys. Rev. B **63**, 180403 (2001).
- [22] M. Matsuda, K. Kakurai, M. Yethiraj, and K. Oka, J. Phys. Soc. Jpn. **74**, 1578 (2005).
- [23] M. Matsuda, K. Kakurai, S. Kurogi, K. Kudo, Y. Koike, H. Yamaguchi, T. Ito, and K. Oka, Phys. Rev. B **71**, 104414 (2005).
- [24] R. O. Kuzian, S. Nishimoto, S.-L. Drechsler, J. Málek, S. Johnston, J. van den Brink, M. Schmitt, H. Rosner, M. Matsuda, K. Oka, H. Yamaguchi, and T. Ito, Phys. Rev. Lett. **109**, 117207 (2012).
- [25] B. Winn, U. Filges, V. Ovidiu Garlea, M. Graves-Brook, M. Hagen, C. Jiang, M. Kenzelmann, L. Passell, S. M. Shapiro, X. Tong, and I. Zalitznyak, in *European Physical Journal Web of Conferences*, Vol. 83 (2015) p. 03017.
- [26] R. T. Azuah, L. R. Kneller, Y. Qiu, P. L. W. Tregenna-Piggott, C. M. Brown, J. R. D. Copley, and R. M. Dimeo, J. Res. Natl. Inst. Stand. Technol. , 341 (2009).
- [27] G. J. Shu, J. C. Tian, C. K. Lin, M. Hayashi, S. C. Liou, *et al.*, New J. of Phys. **19**, 023026 (2017).
- [28] H. J. Xiang, C. Lee, and M. H. Whangbo, Phys. Rev. B **76**, 220411(R) (2007).
- [29] S. Nishimoto, S.-L. Drechsler, R. O. Kuzian, J. van den Brink, J. Richter, W. E. A. Lorenz, Y. Skourski, R. Klingeler, and B. Büchner, Phys. Rev. Lett. **107**, 097201 (2011).
- [30] S. Nishimoto, S.-L. Drechsler, R. Kuzian, J. Richter, and J. van den Brink, Phys. Rev. B **92**, 214415 (2015).
- [31] S. You, Z. Li, L. Yang, C. Dong, L. Chen, C. Jin, J. Hu, G. Shen, and H. Mao, J. Solid State Chem. **182**, 3085 (2009).
- [32] Z. Li, Y. S. Tse, S. You, C. Q. Jin, and T. Iitaka, J. Solid State Chem. **182**, 3085 (2009).
- [33] T. Schmitt and C. Monney, (2017), private commun.
- [34] H. Yamaguchi, K. Oka, and T. Ito, Physica C: Superconductivity **320**, 167 (1999).
- [35] Y. Gotoh, I. Yamaguchi, S. Takeya, H. Fujihisa, K. Honda, T. Ito, K. Oka, and H. Yamaguchi, J. Alloys and Comp. **408**, 1226 (2006).
- [36] N. Wizen, *Hochdruckkristallzüchtung von ausgewählten Oxiden*, PhD-dissertation, TU Dresden (2009).
- [37] R. A. Cowley and G. Dolling, Phys. Rev. **167**, 464 (1968).
- [38] R. Caciuffo, G. Amoretti, P. Santini, G. H. Lander, J. Kulda, and P. d. V. Du Plessis, Phys. Rev. B **59**, 13892 (1999).
- [39] R. Caciuffo, P. Santini, S. Carretta, G. Amoretti, A. Hiess, N. Magnani, L.-P. Regnault, and G. H. Lander, Phys. Rev. B **84**, 104409 (2011).
- [40] B. Rainford, J. Houmann, and H. Guggenheim, in *Neutron Inelastic Scattering 1972* (International Atomic Energy Agency, Vienna, Austria, 1972) p. 655.
- [41] S. W. Lovesey, J. Phys. C: Solid State Phys. **5**, 2769 (1972).
- [42] M. Hennion and F. Moussa, New J. of Phys. **7**, 84 (2005).
- [43] R. J. McQueeney, M. Yethiraj, W. Montfrooij, J. S. Gardner, P. Metcalf, and J. M. Honig, Phys. Rev. B **73**, 174409 (2006).
- [44] S. Johnston, C. Monney, V. Bisogni, K.-J. Zhou, R. Kraus, G. Behr, V. N. Strocov, J. Málek, S.-L. Drechsler, J. Geck, T. Schmitt, and J. van den Brink, Nature Commun. **7**, 10563 (2016).
- [45] W. S. Lee, S. Johnston, B. Moritz, J. Lee, M. Yi, K. J. Zhou, T. Schmitt, L. Patthey, V. Strocov, K. Kudo, Y. Koike, J. van den Brink, T. P. Devereaux, and Z. X. Shen, Phys. Rev. Lett. **110**, 265502 (2013).
- [46] N. Wizen, N. Leps, G. Behr, R. Klingeler, B. Büchner, and W. Löser, J. Cryst. Growth **401**, 596 (2014).
- [47] R. Fehrenbacher and T. M. Rice, Phys. Rev. Lett. **70**,

- 3471 (1993).
- [48] E. Jeckelmann, Phys. Rev. B **66**, 045114 (2002).
- [49] We mention formally the third scenario for $\delta > -J_1$. It reminds an alternating FM-AFM type case of weakly AFM coupled FM dimers, i.e. alternating pairs of CuO_4 units with $\Phi \approx \pi/2$ and big $\Phi \gtrsim 100^\circ$ with a sign change. Then the small gap is like that for a Haldane $S = 1$ chain with weak AFM coupling of spins 1 FM dimers with a large local gap, i.e. singlet excitations from triplet "ground states". Here, we deal with *two* magnon branches and a smaller dispersion of each as that observed above. The opposite case with AFM dimers and weaker FM couplings has been recently proposed for $\text{BaCu}_2\text{V}_2\text{O}_8$ [7, 89]. But it is unclear whether this model could describe also the observed smooth dispersion in a broad energy range up to 53 meV as shown clearly already by the two scenarios considered above. Hence, we regard the FM-AFM chain scenario as less likely relevant for CYCO than the other ones. ().
- [50] K. Kudo, S. Kurogi, Y. Koike, T. Nishizaki, and N. Kobayashi, Phys. Rev. B **71**, 104413 (2005).
- [51] A. Lohmann, H.-J. Schmidt, and J. Richter, Phys. Rev. B **89**, 014415 (2014).
- [52] For the 10th-order HTE see the HTE10 package from <http://www.uni-magdeburg.de/jschulen/HTE10/>.
- [53] S. Okubo, K. Kawakami, M. Yoshida, and H. Ohta, physica status solidi (c) **3**, 2828 (2006).
- [54] S. A. Carter, B. Batlogg, R. J. Cava, J. J. Krajewski, W. F. Peck Jr., and T. M. Rice, Phys. Rev. Lett. **77**, 1378 (1996).
- [55] M. Matsuda, K. Kakurai, J. E. Lorenzo, L. P. Regnault, A. Hiess, and G. Shirane, Phys. Rev. B **68**, 060406(R) (2003).
- [56] T. M. Rice, B. Gopalan, and M. Sigrist, Europhys. Lett. **23**, 445 (1993).
- [57] P. Müller, J. Richter, and D. Ihle, Phys. Rev. B **95**, 134407 (2017).
- [58] M. Härtel, J. Richter, D. Ihle, and S.-L. Drechsler, Phys. Rev. B **78**, 174412 (2008).
- [59] Y. Iqbal, P. Ghosh, R. Narayanan, B. Kumar, J. Reuther, and R. Thomale, Phys. Rev. B **94**, 224403 (2016).
- [60] K. Caslin, R. K. Kremer, F. S. Razavi, A. Schulz, A. Muñoz, F. Pertlik, J. Liu, M.-H. Whangbo, and J. M. Law, Phys. Rev. B **89**, 014412 (2014).
- [61] K. Caslin, R. K. Kremer, F. S. Razavi, M. Hanfland, K. Syassen, E. E. Gordon, and M.-H. Whangbo, Phys. Rev. B **93**, 022301 (2016).
- [62] K. Caslin, *Investigations of Frustrated Quasi-One-Dimensional Quantum Spin-Chain Materials*, PhD-dissertation, Brock University (2015).
- [63] A. Hayashi, B. Batlogg, and R. J. Cava, Phys. Rev. B **58**, 2678 (1998).
- [64] F. Sapina, J. Rodriguez-Carvajal, M. Sanchis, R. Ibáñez, A. Beltrán, and A. Beltrán, Solid State Comm. **74**, 779 (1990).
- [65] J. Málek, S.-L. Drechsler, U. Nitzsche, H. Rosner, and H. Eschrig, Phys. Rev. B **78**, 060508 (2008).
- [66] C. Monney, V. Bisogni, K.-J. Zhou, R. Kraus, V. N. Strocov, G. Behr, J. Málek, R. Kuzian, S.-L. Drechsler, S. Johnston, A. Revcolevschi, B. Büchner, H. M. Rønnow, J. van den Brink, J. Geck, and T. Schmitt, Phys. Rev. Lett. **110**, 087403 (2013).
- [67] I. Solovyev, Z. Pchelkina, and V. Mazurenko, CrystEngCom **16**, 522 (2014).
- [68] J.M. Tomczak, private communication; and S.-L. Drechsler *et al.*, in preparation (2019).
- [69] In a recent RIXS-study for $\text{Sr}_{14}\text{Cu}_{24}\text{O}_{41}$ a significant related intersite Coulomb interaction $V_{pd} = 1.5$ eV had to be adopted [70] in accord with the theoretical recommendation for quasi-1D systems $V_{pd} \approx U_{dd}/5$ [90]. Similarly, to describe the optical conductivity and EELS data as well as the J_1 -value for Li_2CuO_2 , $V_{pd} = 0.95$ eV and $V_{dd} = V_{pp} = 0.2$ eV have been used [71, 85]. ().
- [70] A. Higashiya, S. Imada, T. Murakawa, H. Fujiwara, S. Kasai, A. Sekiyama, S. Sugai, K. Okada, M. Yabashi, K. Tamasaku, T. Ishikawa, and H. Eisaki, New J. Phys. **10**, 05033 (2008).
- [71] S.-L. Drechsler, J. Málek, R. Kuzian, S. Nishimoto, U. Nitzsche, W. Lorenz, R. Klingeler, B. Büchner, and M. Knupfer, Physica C **470**, Suppl. **1**, S84 (2010).
- [72] R. Neudert, H. Rosner, S.-L. Drechsler, M. Kielwein, M. Sing, Z. Hu, M. Knupfer, M. S. Golden, J. Fink, N. Nücker, M. Merz, S. Schuppler, N. Motoyama, H. Eisaki, S. Uchida, M. Domke, and G. Kaindl, Phys. Rev. B **60**, 13413 (1999).
- [73] M. Schmitt, O. Janson, S. Golbs, M. Schmidt, W. Schnelle, J. Richter, and H. Rosner, Phys. Rev. B **89**, 174403 (2014).
- [74] E. Bordas, C. de Graef, R. Caballol, and C. J. Calzado, Phys. Rev. B **71**, 045108 (2005).
- [75] C. J. Calzado, J. F. Sanz, and J. P. Malrieu, The Journal of Chemical Physics **112**, 5158 (2000).
- [76] C. Koo, E. Zvereva, I. Zhukaev, M. Richter, M. Stratan, A. Vasiliev, V. Nalbandyan, and R. Klingeler, J. Phys. Soc. Jpn. **85**, 084702 (2016).
- [77] Y. Miura, R. Hirai, Y. Kobayashi, and M. Sato, J. Phys. Soc. Jpn. **75**, 084702 (2006).
- [78] Y. Miura, Y. Yasui, M. Moyoshi, M. Sato, and J. Kukurai, J. Phys. Soc. Jpn. **77**, 104709 (2008).
- [79] Another relevant case is that of ferromagnetically coupled corner-sharing double (zigzag) chains as in SrCuO_2 and various ferromagnetically coupled ladder systems with a huge NNN AFM coupling $J_2 \gg -J_1$ which dominates their high- T magnetic and dynamical response, hindering the extraction of J_1 . An analysis of the FM J_1 value like that given here below has not yet been performed. The reported relatively large $J_1 \approx -30.8$ meV for SrCu_2O_3 was mainly caused in the simulations [15] by a more than three times smaller competing J_Φ via the bridging O as compared to LICU and CYCO [see Eq. (16)]. ().
- [80] S. Tornow, O. Entin-Wohlman, and A. Aharony, Phys. Rev. B **60**, 10206 (1999).
- [81] W. Geertsma and D. Khomskii, Phys. Rev. B **54**, 3011 (1996).
- [82] Notice the multiplication by a factor of -2 due to the different definitions of the spin-Hamiltonians. ().
- [83] E. Bordas, C. de Graef, R. Cabasllol, and C. J. Colzado, Theor. Chim. Acc. **116**, 535 (2006).
- [84] S.-L. Drechsler, J. Málek, W. E. A. Lorenz, R. O. Kuzian, R. Klingeler, S. Nishimoto, U. Nitzsche, M. Knupfer, N. Wizen, G. Behr, H. Rosner, H. Eschrig, and B. Büchner, J. of Phys.: Conf. Ser. **200**, 012028 (2010).
- [85] In cluster studies [44, 65, 66, 71, 84] within the 5-band extended Hubbard model with up to 6 CuO_4

- units, omitting V_{dd} but with $V_{pd} = 0.95$ eV and an already enhanced $K_{pd} = 95$ meV, an enlarged J_1 -value ≈ -19.8 meV was obtained [see also Eq. (23)] within the effective single-band Hubbard-type model for CuO₂ plaquette]. ().
- [86] R. Schumann, (2019), *et al.* in preparation.
- [87] M. Matsuda, K. Kakurai, H. Yamaguchi, T. Ito, C. Lee, and K. Oka, *Applied Physics A* **74**, s637 (2002).
- [88] M. Matsuda, K. M. Kojima, Y. J. Uemura, J. L. Zarestky, K. Nakajima, K. Kakurai, T. Yokoo, S. M. Shapiro, and G. Shirane, *Phys. Rev. B* **57**, 11467 (1998).
- [89] E. S. Klyushina, A. T. M. N. Islam, J. T. Park, E. A. Goremychkin, E. Wheeler, B. Klemke, and B. Lake, *Phys. Rev. B* **98**, 104413 (2018).
- [90] K. Okada and A. Kotani, *J. Phys. Soc. Jpn.* **66**, 341 (1997).
- [91] T. Helgaker, P. Jorgensen, and J. Oslen, *Molecular Electronic-Structure Theory* (Wiley, Chichester, 2000).
- [92] N. B. Balabanov and K. A. Peterson, *J. Chem. Phys.* **123**, 064107 (2005).
- [93] T. H. Dunning Jr., *The Journal of Chemical Physics* **90**, 1007 (1989).
- [94] R. Dovesi, C. Ermondi, E. Ferrero, C. Pisani, and C. Roetti, *Phys. Rev. B* **29**, 3591 (1984).
- [95] J. Sanz and J. Malrieu, *J. Phys. Chem.* **97**, 99 (1993).
- [96] H.-J. Werner, P.J. Knowles, *et al.*, *Wiley Interdisciplinary Reviews: Computational Molecular Science* **2**, 242 (2012).
- [97] K. Koepnik and H. Eschrig, *Phys. Rev. B* **59**, 1743 (1999).
- [98] I. Opahle, K. Koepnik, and H. Eschrig, *Phys. Rev. B* **60**, 14035 (1999).
- [99] J. P. Perdew, K. Burke, and M. Ernzerhof, *Phys. Rev. Lett.* **77**, 3865 (1996).
- [100] W. A. Harrison, *Electronic Structure and the Properties of Solids* (Freeman, San Francisco, 1980).
- [101] M. Matsuda, K. Katsumata, T. Yokoo, S. M. Shapiro, and G. Shirane, *Phys. Rev. B* **54**, 15626(R) (1996).
- [102] F. Heidrich-Meisner, A. Honecker, and T. Vekua, *Phys. Rev. B* **74**, 020403(R) (2006).
- [103] H. T. Lu, Y. J. Wang, S. Qin, and T. Xiang, *Phys. Rev. B* **74**, 134425 (2006).
- [104] H.-J. Schmidt, A. Lohmann, and J. Richter, *Phys. Rev. B* **84**, 104443 (2011).
- [105] H.-J. Schmidt, J. Schnack, and M. Luban, *Phys. Rev. B* **64**, 224415 (2001).
- [106] S.E. Dutton, M. Kumar, M. Mourigal, Z.S. Soos, J.-J. Wen, C.L. Broholm, N. H. Andersen, Q. Huang, M. Zbiri, R. Toft-Petersen, and R. J. Cava, *Phys. Rev. Lett.* **108**, 187206 (2011).
- [107] M. Bosiočić, F. Bert, S. E. Dutton, R. J. Cava, P. J. Baker, M. Požek, and P. Mendels, *Phys. Rev. B* **96**, 224424 (2017).
- [108] H.-J. Grafe, S. Nishimoto, M. Jakovleva, E. Vavilova, L. Spillecke, A. Alfonsov, M.-I. Sturza, S. Wurmehl, H. Nojiri, H. Rosner, J. Richter, U. K. Rößler, S.-L. Drechsler, V. Kataev and B. Büchner, *Sci. Rep.* **7**, 6729 (2017).
- [109] K. Nawa, Y. Okamoto, A. Matsuo, K. Kindo, Y. Kitahara, S. Yoshida, S. Ikeda, S. Hara, T. Sakurai, S. Okubo, H. Ohta, and Z. Hiroi, *J. Phys. Soc. Jpn.* **83**, 103702 (2014).
- [110] O. Janson, A. A. Tsirlin, M. Schmitt, and H. Rosner, *Phys. Rev. B* **82**, 014424 (2010).
- [111] H. Rosner, *Electron. Struct. and Exchange Integrals of Low-Dimensional Cuprates*, PhD-dissertation, TU Dresden (1999).
- [112] Y. Kim, R. J. Birgeneau, F. C. Chou, M. Greven, M.A. Kastner, Y.S. Lee, B.O. Wells, A. Aharony, O. Entin-Wohlman, I. Ya. Korenblit, A. B. Harris, R. W. Erwin, and G. Shirane, *Phys. Rev. B* **64**, 024435 (2001).
- [113] P. Babkevich, N.E. Shaik, D. Lançon, A. Kikkawa, and M. Enderle, and R. A. Ewings, H. C. Walker, D. T. Adroja, P. Manuel, D. D. Khalyavin, Y. Taguchi, Y. Tokura, M. Soda, T. Masuda, and H. M. Rønnow, *Phys. Rev. B* **96**, 014410 (2017).
- [114] S. Fatale, C.G. Fatuzzo, P. Babkevich, N.E. Shaik, J. Pelliciani, X. Lu, D.E. McNally, T. Schmitt, A. Kikkawa, Y. Taguchi, Y. Tokura, B. Normand, H. M. Rønnow, and M. Grioni, *Phys. Rev. B* **96**, 115149 (2017).
- [115] A. N. Yaresko, A. Y. Perlov, R. Hayn, and H. Rosner, *Phys. Rev. B* **65**, 115111 (2002).
- [116] V. Y. Yushankhai and R. Hayn, *Europhys. Lett.* **47**, 116 (1999).
- [117] M. Schmitt, *Microscopic Description of magnetic model compounds*, PhD-dissertation, TU Dresden (2011).
- [118] Y. Yasui, N. Igawa, and K. Kakurai, *JPS Conf. Proc.* **8**, 034012 (2015).
- [119] S. Nishimoto, S.-L. Drechsler, R.O. Kuzian, J. Richter, J. Málek, M. Schmitt, J. van den Brink, and H. Rosner, *Europhys. Lett.* **98**, 37007 (2012).
- [120] S. J. Hibble, J. Köhler, A. Simon, and S. Paiser, *J. Solid State Chem.* **88**, 534 (1990).
- [121] A.A. Gippius, E.N. Morozova, A.S. Moskvina, A.V. Zalesky, A.A. Bush, M. Baenitz, H. Rosner, and S.-L. Drechsler, *Phys. Rev. B* **70**, 020406(R) (2004).
- [122] L. Capogna, and M. Reehuis, A. Maliuk, R.K. Kremer, B. Ouladdiaf, M. Jansen, and B. Keimer, *Phys. Rev. B* **82**, 014407 (2010).
- [123] M. Schäpers, H. Rosner, S.-L. Drechsler, S. Süllow, R. Vogel, B. Büchner, and A. U. B. Wolter, *Phys. Rev. B* **90**, 224417 (2014).
- [124] K. C. Rule, B. Willenberg, and M. Schäpers, A. U. B. Wolter, B. Büchner, S.-L. Drechsler, G. Ehlers, D. A. Tennant, R. A. Mole, J. S. Gardner, S. Süllow, and S. Nishimoto, *Phys. Rev. B* **95**, 024430 (2017).
- [125] I. A. Zaliznyak, H. Woo, T. G. Perring, C. L. Broholm, C. D. Frost, and H. Takagi, *Phys. Rev. Lett.* **93**, 087202 (2004).
- [126] K. Sparta, A. Löffler, C. Gross, W. Aβmus, and G. Roth, *Z. Kristallogr.* **221**, 782 (2006).
- [127] K. Ruck, M. Wolf, M. Ruck, D. Eckert, G. Krabbes, and K. H. Müller, *Mat. Res. Bull.* **36**, 1995 (2001).
- [128] V. Bisogni, S. Kourtis, C. Monney, K. Zhou, R. Kraus, C. Sekar, V. Strocov, B. Büchner, J. van den Brink, L. Braicovich, T. Schmitt, M. Daghofer, and J. Geck, *Phys. Rev. Lett.* **112**, 147401 (2013).
- [129] G. Deng, D. Yu, R. Mole, E. Pomjakushina, K. Conder, M. Kenzelmann, S. Yano, C.-W. Wang, K. C. Rule, J. S. Gardner, H. Luo, S. Li, C. Ulrich, P. Imperia, W. Ren, S. Cao, and G. J. McIntyre *Phys. Rev. B* **98**, 184411 (2018).
- [130] S. Lebernegg, A. Tsirlin, O. Janson, and H. Rosner, *Phys. Rev. B* **88**, 224406 (2013).
- [131] J. Holmlund, C.S. Knee, J. Andreasson, M. Granath, A.P. Livinčuk and L. Börjesson, *Phys. Rev. B* **79**, 085109 (2009).

SUPPLEMENTARY PART TO

”Highly dispersive magnons with spin-gap like features in the $s = 1/2$ frustrated ferromagnetic chain compound $\text{Ca}_2\text{Y}_2\text{Cu}_5\text{O}_{10}$ detected by inelastic neutron scattering”

by

M. Matsuda, J. Ma, V.O. Garlea, T. Ito, H. Yamaguchi, K. Oka, S.-L. Drechsler, R. Yadav, L. Hozoi, H. Rosner, R. Schumann, R.O. Kuzian, S. Nishimoto

A. Dynamical structure factor and gaps in the magnon dispersion for inhomogeneous cuprate chains

Here we provide details of the calculation of the dynamical structure factor $S(\omega, q)$ for the 1D spin-Hamiltonian given by Eq. (5) in the MT in terms of Green’s functions G (GF) and provide the results for the simplest case where within the period 5 approximation for the Ca-Y cationic chain system opens gaps in the magnon curve in addition to FIG. 11 in the MT for the case of a doubling of the CuO_2 chain compatible with a period 10 superstructure for CYCO. The commutator two-time retarded GF for the operators \hat{X} and \hat{Y} is defined as

$$\langle\langle \hat{X} | \hat{Y} \rangle\rangle \equiv -i \int_{t'}^{\infty} dt e^{i\omega(t-t')} \langle [\hat{X}(t), \hat{Y}(t')] \rangle,$$

where the expectation value $\langle \dots \rangle$ denotes the ground state average, the time dependence of an operator $\hat{X}(t)$ is given by $\hat{X}(t) = e^{it\hat{H}} \hat{X} e^{-it\hat{H}}$. It is convenient to introduce the notations

$$G_q \equiv \langle\langle a_q | a_q^\dagger \rangle\rangle_\omega \quad \text{and} \quad G_{q,s} \equiv \langle\langle a_{q,s} | a_q^\dagger \rangle\rangle_\omega. \quad (\text{S1})$$

Here we consider the $J_1 - J'_1 - J_2$ model We have $n = 2$, $s = a, 2a$ and introduce $\varepsilon_a = -\frac{1}{2}(J_1^z + J_1^{z'}) - J_2^z = \varepsilon_{2a} \equiv \varepsilon$ The equations of motion for the GF are

$$(\omega - \varepsilon - J_2 \cos 2qa) G_{q,a} = \frac{e^{iqa}}{\sqrt{2}} + \frac{1}{2} (J_1 e^{-2iqa} + J'_1) G_{q,2a}, \quad (\text{S2})$$

$$(\omega - \varepsilon - J_2 \cos 2qa) G_{q,2a} = \frac{e^{2iqa}}{\sqrt{2}} + \frac{1}{2} (J_1 e^{2iqa} + J'_1) G_{q,a}. \quad (\text{S3})$$

$$\text{Introducing the notations} \quad J_1 \equiv J + \delta, \quad J'_1 \equiv J - \delta, \quad \text{and} \quad \varepsilon \equiv -J - J_2 - D, \quad (\text{S4})$$

$$\text{we obtain} \quad G_q = \frac{e^{-iqa}}{\sqrt{2}} G_{q,a} + \frac{e^{-2iqa}}{\sqrt{2}} G_{q,2a} = \frac{1}{\omega - \varepsilon - J_2 \cos 2qa - J \cos qa - \frac{\delta^2 \sin^2 qa}{\omega - \varepsilon - J_2 \cos 2qa + J \cos qa}}. \quad (\text{S5})$$

FIG. 11 in the MT shows the structure factor for this case. For the 1D model depicted in FIG. 1b in the MT with $n = 5$ we have a system of 5 linear Eqs. for $G_{q,s}$ solved numerically. The result is shown in FIG. S1 for the parameters:

$$J'_1 = J, \quad J_1 = J + 2\delta, \quad J''_1 = J - \delta, \quad (\text{S5}') \quad J'_2 = I, \quad J_2 = I + \gamma, \quad J''_2 = I - 2\gamma \quad (s5'').$$

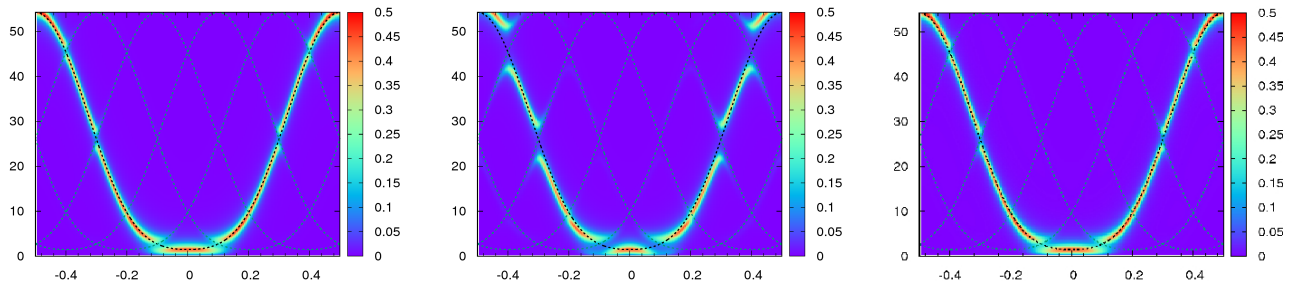


FIG. S1. The structure factor for a lattice with a period 5 and the coupling constants of the spin Hamiltonian shown in FIG. 1 of the MT with the relations between the parameters from Eqs. (S5') and (S5''), $J = -26.38$, $J_2 = 5.5$, $D = -1.5$ meV. **Left:** $\delta = \gamma = 2$; **Middle:** $\delta = 5$, $\gamma = 2$ **Right:** $\delta = 0$, $\gamma = 2$. Thin lines: the spectrum for the 5-fold supercell with $\delta = \gamma = 0$.

B. FM and AFM contributions to the NN and NNN exchange within single and 5-band Hubbard models

Here we sketch the derivation of the isotropic part of the 1D spin-Hamiltonian given by Eqs. (1-5) in the MT within the simplest approach of an effective generalized extended single band-Hubbard model (ESBHM) at half filling and as well as we present a general rigorous analytical solution of the $\Phi = 90^\circ$ problem generic for FFESC within the multi-band $O2pCu3d$ model [1]. The former includes 4 terms: kinetic contributions given by the NN and NNN hoppings with the transfer integrals $t \equiv t_1 \equiv t$ and t_2 , resp., the onsite and NN, NNN intersite Coulomb repulsions U , V_1 and V_2 , resp., and the corresponding external intersite exchange integrals \tilde{J}_1 and \tilde{J}_2 introduced to allow for FM NN-spin spin couplings and sizable AFM NNN exchange couplings, resp., missing in the simple Hubbard model.

$$H = \sum_{i,\sigma} t \left(c_{i+1}^\dagger c_i + h.c. \right) + t_2 \left(c_{i+2}^\dagger c_i + h.c. \right) + U n_{i,\uparrow} n_{i,\downarrow} + V_1 n_{i+1} n_i + V_2 n_{i+2} n_i + \tilde{J}_1 c_{i+1,\uparrow}^\dagger c_{i,\uparrow} c_{i+1,\downarrow}^\dagger c_{i,\downarrow} + \tilde{J}_2 c_{i+2,\uparrow}^\dagger c_{i,\uparrow} c_{i+2,\downarrow}^\dagger c_{i,\downarrow} \quad (S6)$$

where n_i is the density operator. With respect to edge-sharing CuO_2 chain compounds and LICU in particular, the ESBHM parameters obey the following hierarchy of inequalities generic for strong coupling (strong correlations):

$$U > 3V_1, V_1 \geq 5V_2, V_2 \geq 2t_1 \sim 2t_2, t \gg |\tilde{J}_1| \gg \tilde{J}_2, \quad (S7)$$

which allows one to expand tedious expressions. Noteworthy, relative small interactions as the NN intersite Coulomb interaction V_2 might cause visible effects. [s. e.g. FIG. 13 of the MT and Eq. (S13).] For the trimers and dimers the ESBHM [Eq. (S6)] can be exactly diagonalized even in an analytic form for any parameters. To start with the dimer, we deal with 16 eigenstates in the ESBHM. Among them there are a singlet (S) and 1 triplet (T), state, i.e. in total 4 spin states relevant here. The energy of the triplet and singlet states are respectively given by

$$E_T = \tilde{J}_1/4 + V_1, \quad E_S = -0.5 \left(\sqrt{16t^2 + \tilde{U}^2} - \tilde{U} \right) + V_1 - 3\tilde{J}_1/4, \quad \text{with} \quad \tilde{U}_d = U - V_1 + 3\tilde{J}_1/4. \quad (S8)$$

For a FM $\tilde{J}_1 < 0$ the ground state (GS) is formed by the triplet and for an AFM \tilde{J}_1 by the singlet state. The difference of the eigenenergies yields the NN exchange integral J_1 of the corresponding spin-Hamiltonian. Thus, we have *exactly*

$$J_1 - \tilde{J}_1 = 0.5 \left(\sqrt{16t^2 + \tilde{U}^2} - \tilde{U} \right) \approx 4t^2/\tilde{U}. \quad (S9)$$

The latter Eq. is valid for $U \gg t$ relevant here and for moderate $V_1 \ll U$ values, in particular for $V_1 = 0$ adopted in Ref. 2. Eq. (S9) can be expanded for small t/\tilde{U}_d . For $\tilde{J}_1 = 0, V_1 = 0$ one has $J_1 = 0.5(\sqrt{16t^2 + \tilde{U}^2} - \tilde{U})$. At strong coupling it yields the AFM superexchange $4t^2/U$ of the Hubbard model. Turning to the asymmetric dimer with 2 holes on 3 orbitals: 1 Cu and 2 planar O orbitals, we note that there is an exact very tedious analytical solution for *any* ESBHM parameter values available [1]. That spin model has $2^3 = 8$ states, among them: a quadruplet with the energy E_Q and total spin $S = 3/2$ as well as 2 doublets with energies E_{D_1}, E_{D_2} , and spin $S = 1/2$. These energies provide the mapping Eqs. for the exchange parameters we are looking for:

$$E_Q = J_1/2 + J_2/4, \quad E_{D_1} = -3J_2/4, \quad E_{D_2} = -J_1 + J_2/4. \quad \text{As a result we have} \quad (S10)$$

$$J_1 = 2(E_Q - E_{D_2})/3 \text{ and } J_2 = -J_1/2 + E_Q - E_{D_1}. \text{The quadruplet energy in terms of the ESBHM reads} \quad (S11)$$

$$E_Q = 2V_1 + V_2 + \tilde{J}_1/2 + \tilde{J}_2/4 \quad \text{Then Eqs. (S10 -S12) can be rewritten as:} \quad (S12)$$

$$J_1 = \tilde{J}_1 - 2\varepsilon/3J_2 = \tilde{J}_2 + (\varepsilon - \epsilon)/3, \text{ where } E_{D_1} = \epsilon + 2V + V_2 - 3\tilde{J}_1/4. \quad (S13)$$

The exact analytical expressions for the ESBHM are very cumbersome to be given here. The shifted eigenvalues ε and ϵ have been introduced to find approximations for the 2 corresponding ones of the doublet states at strong coupling.

The energies of the doublets D_1 and D_2 are given by the lowest eigenvalues of their two 4×4 matrices, respectively:

$$\hat{D}_1 = \begin{pmatrix} -\frac{3}{4}\tilde{J}_2 + 2V + V_2 & t & -2t_2 & t \\ t & U + V_2 - t_2 & t & 0 \\ -2t_2 & t & U + 2V & -t \\ t & 0 & -t & U + 2V + t_2 \end{pmatrix}, \quad (\text{S14})$$

$$\hat{D}_2 = \begin{pmatrix} -\tilde{J}_1 + \frac{1}{4}\tilde{J}_2 + 2V + V_2 & \sqrt{3}t & 0 & -\sqrt{3}t \\ \sqrt{3}t & U + V_2 + t_2 & t & 0 \\ 0 & t & U + 2V & -t \\ -\sqrt{3}t & 0 & -t & U + 2V - t_2 \end{pmatrix}. \quad (\text{S15})$$

Both Eqs. can be rewritten to get analytic expressions in *any* order of the perturbation theory by an iterative procedure:

i.e. the eigenvalue problem of Eq. (S14) can be rewritten as $J_1 - \tilde{J}_1 = -\frac{2}{3}\varepsilon = \frac{2t^2 \left[\frac{1}{z_1 - \varepsilon} + \frac{1}{z_3 - \varepsilon} \right]}{1 + \frac{t^2}{z_2 - \varepsilon} \left[\frac{1}{z_1 - \varepsilon} - \frac{1}{z_3 - \varepsilon} \right]}$. (S16)

$$\varepsilon = -\frac{3t^2 \left[\frac{1}{z_1 - \varepsilon} + \frac{1}{z_3 - \varepsilon} \right]}{1 + \frac{t^2}{z_2 - \varepsilon} \left[\frac{1}{z_1 - \varepsilon} - \frac{1}{z_3 - \varepsilon} \right]}, \text{ or more explicitly } \varepsilon^{(n+1)} = -\frac{3t^2 \left[\frac{1}{z_1 - \varepsilon^{(n)}} + \frac{1}{z_3 - \varepsilon^{(n)}} \right]}{1 + \frac{t^2}{z_2 - \varepsilon^{(n)}} \left[\frac{1}{z_1 - \varepsilon^{(n)}} - \frac{1}{z_3 - \varepsilon^{(n)}} \right]}, \quad (\text{S17})$$

where $Z_1 = \tilde{U}_2 - (2V - V_2) + t_2 + \tilde{J}_1 - \tilde{J}_2$, $Z_2 = \tilde{U}_2 + \tilde{J}_1 - \tilde{J}_2$, $Z_3 = \tilde{U}_2 - t_2 + \tilde{J}_1 - \tilde{J}_2$.

The exact solution is reproduced for $n \rightarrow \infty$. Anyhow, at strong coupling, 1 or 2 iterations are sufficient for an insight. Our recursion formula provides analytical expressions in any even order of the perturbation theory in terms of $(t/U)^{2n}$, $n = 0, 1, 2, \dots$. Notice the asymmetry between the t and t_2 expansions, the latter contains also *odd* terms of t_2/U . Iterating Eq. (17), we have in 0^{th} and 1^{st} order $\varepsilon^{(0)} = 0$ or $J_1 = J_1^{(0)} = \tilde{J}_1$, resp., according to Eq. (S16) and

introducing $U_J = U_2 + \tilde{J}_1 - \tilde{J}_2 = U - V_2 + \tilde{J}_1 - \tilde{J}_2/4$, $U_2 = U - V_2 + 3\tilde{J}_2/4$, in the next step we arrive at (S18)

$$J_1^{(1)} - \tilde{J}_1 = 2t^2 \frac{\frac{1}{Z_1} + \frac{1}{Z_3}}{1 + \frac{t^2}{Z_2} \left[\frac{1}{Z_1} - \frac{1}{Z_3} \right]} = \frac{4t^2}{U_1} \left[1 + \frac{1}{2} \left(\frac{v_1}{1 - v_1} + \frac{v_2}{1 - v_2} \right) \right] \left[1 + \frac{t^2}{(U_1 - V_2)U_1} \left(\frac{v_1}{1 - v_1} - \frac{v_2}{1 - v_2} \right) \right]^{-1}, \quad (\text{S19})$$

where $U_1 = U + \tilde{J}_1 - \tilde{J}_2/4$, $v_1 = (2V - t_2)/U_1$, and $v_2 = (V_2 + t_2)/U_1$. (S20)

After the 2nd iteration step one arrives at a similar expression, where the large $U_1 \gg J_1 - \tilde{J}_1$ is slightly renormalized:

$$\tilde{U}_1 = U_1 + 3 \left(J_1^{(1)} - \tilde{J}_1 \right) / 2 \quad \text{or} \quad \tilde{U}_1^{(n+1)} = U_1 + 3 \left(J_1^{(n)} / 2 - \tilde{J}_1 \right). \quad (\text{S21})$$

Thus, the recursion results in a fast converging renormalization of U_1 . The recursion for E_{D_1} , i.e. ϵ reads

$$\epsilon = -\frac{4t^2 \frac{1}{\tilde{U}_{22-\epsilon}} + t^2 \left[\frac{1}{\tilde{U}_{11-\epsilon}} + \frac{1}{\tilde{U}_{33-\epsilon}} + 4t_2 \frac{1}{\tilde{U}_{22-\epsilon}} \left(\frac{1}{\tilde{U}_{11-\epsilon}} - \frac{1}{\tilde{U}_{33-\epsilon}} \right) \right] - 4t^4 \frac{1}{(\tilde{U}_{11-\epsilon})(\tilde{U}_{22-\epsilon})(\tilde{U}_{33-\epsilon})}}{1 - t^2 \frac{1}{\tilde{U}_{22-\epsilon}} \left[\frac{1}{\tilde{U}_{11-\epsilon}} + \frac{1}{\tilde{U}_{33-\epsilon}} \right]}, \quad (\text{S22})$$

where $U_{11} = U - 2V - t_2 + 3\tilde{J}_2/4$, $U_{22} \equiv U_2 = U - V_2 + 3\tilde{J}_2/4$, and $U_{33} = U - V_2 + t_2 + 3\tilde{J}_2/4$. (S23)

Note the dominant AFM term triggered by t_2 and the weak FM 4th order term corresponding to Néel fluctuation with \parallel NNN spins. The 2nd order term vanishes for $V = t_2 = 0$ due to the compensation with a 2nd order term from

$\varepsilon/3$. Since $\tilde{U}_2 \gg -\varepsilon$, an iteration procedure applied to Eq. (S22) converges fastly. Then for J_2 we arrive at

$$J_2^{(1)} - \tilde{J}_2 = \frac{4t_2^2}{\tilde{U}_{22} - \varepsilon^{(0)}} + t^2 \left[\frac{1}{U_{11} - \varepsilon^{(0)}} + \frac{1}{U_{33} - \varepsilon^{(0)}} + t_2 \frac{4}{U_{22} - \varepsilon^{(0)}} \left(\frac{1}{U_{11} - \varepsilon^{(0)}} - \frac{1}{U_{33} - \varepsilon^{(0)}} \right) \right] +$$

$$-t^2 \left[\frac{1}{\tilde{U}_2 + t_2 - 2(V - V_2) + \tilde{J}_1 - \tilde{J}_2} + \frac{1}{\tilde{U}_2 - t_2 + \tilde{J}_1 - \tilde{J}_2} \right]$$

$$\approx \frac{4t_2^2}{U_{22}} + t_2 \frac{4t^2}{U_{11}U_{22}U_{33}} (2V - V_2) + t^2 (2t_2 + \tilde{J}_1 - \tilde{J}_2) [1/(U_{11}Z_1) + 1/(U_{33}Z_3)], \quad (\text{S24})$$

$$\varepsilon^{(0)} = -0.5 \left(\sqrt{U_{22}^2 + 16t_2^2} - U_{22} \right) \approx -4t_2^2/U_{22}. \quad (\text{S25})$$

For $t \equiv t_1 = 0$, i.e. if for $\Phi = 90^\circ$ one ignores the different onsite energies and t_{dd} or due to an accidental compensation of the dd and the pd channels. Then the central spin is magnetically coupled only by the external couplings \tilde{J}_1 and we arrive at a dimer-like formula for J_2 replacing V_1 by V_2 [s. Eq. (S9).], i.e. V_1 drops out:

$$J_1^{(0)} = \tilde{J}_1 \quad \text{and} \quad J_2^{(0)} - \tilde{J}_2 = 8t_2^2 / \left(\sqrt{16t_2^2 + U_2^2} + U_2 \right) \approx 4t_2^2 / (U_2 + 4t_2^2/U_2) \approx 4t_2^2/U_2. \quad (\text{S26})$$

Turning to $J_2^{(1)}$ and $J_2^{(2)}$, we note the appearance of 3 FM contributions at most. The 4th order term $-4t^4/(U_{11}U_2U_{33})$ is independent of \tilde{J}_1 . It is indeed small, although it can be significantly enhanced as compared with the simple Hubbard model [s. FIG. S3] \sim by the factor $U_2/(1 - 2V + V_2 - t_2)$ for strong intersite Coulomb repulsions. The FM terms induced by the auxiliary FM couplings as well as for $t_2 < 0$ and for $2t_2 < \tilde{J}_2 - \tilde{J}_1$ occur already in the 2nd order of t/U . Neglecting the 2nd term $\frac{4t_2^2}{U_2} \approx 6.4$ meV in the last denominator of Eq. (S26) introduces a small error for $J_2^{(0)} - \tilde{J}_2 \sim 1.6 \cdot 10^{-3}$, only. Anyhow, ignoring the weak \tilde{J}_2 using $U_2 \approx 4$ eV and $t = 80$ meV we would arrive at $J_2^{(0)} = 6.39$ meV in accord with the INS data. Taking into account a further slight enhancement by the 2nd order effect from the finite t there is some room for a small FM J_2 -value of the order of $0.1\tilde{J}_1$. Thereby a non-negligible intersite Coulomb repulsion might be helpful according to Eq. (S26). Without more sophisticated microscopical studies we will ignore a sizable FM contribution to J_2 in accord with our QQC K_{pp} and adopt hereafter $\tilde{J}_2 \approx 0$.

Now we may follow the weak evolution of J_1 with increasing cluster size as well as provide a first estimate for J_2 , too. First, in the simple Hubbard model extended by \tilde{J}_1 , only, we arrive at:

$$J_1^{(0)} = \tilde{J}_1, \quad J_1^{(1)} - \tilde{J}_1 = \frac{4t^2}{U + \tilde{J}_1}, \quad J_1^{(2)} - \tilde{J}_1 = \frac{4t^2}{U + \tilde{J}_1 + 6t^2 \frac{1}{U + \tilde{J}_1}}, \quad J_1^{(2)} - \tilde{J}_1 = \frac{4t^2}{U + \tilde{J}_1 + 6t^2 \frac{1}{U + \tilde{J}_1 + 6t^2 \frac{1}{(U + \tilde{J}_1)}}}. \quad (\text{S27})$$

Thus, the AFM contribution to J_1 is only very slightly enhanced: ongoing from the dimer to the trimer

$$\frac{J_{1,\text{trimer}} - \tilde{J}_1}{J_{1,\text{dimer}} - \tilde{J}_1} = \frac{1 + \frac{3}{4} \frac{\tilde{J}_1}{U}}{1 + \frac{\tilde{J}_1}{U}} \approx 1 - \frac{\tilde{J}_1}{4U} \approx 1.002. \quad (\text{S28})$$

adopting $\tilde{J}_1 \sim -25$ meV from the INS data and $U \approx 4$ eV in 2nd order and 1.0028 in 4th order of t/U , respectively. Similar very small changes occur for larger clusters. Hence, a simple dimer-trimer approach is justified.

Next, switching on t_2 and \tilde{J}_2 we arrive also at a very small change of $J_1 \sim 4 \times 10^{-4}$ or $t_2 = 80$ meV and $U \approx 4$ eV:

$$J_1^{(1)} - \tilde{J}_1 = \frac{4t^2}{U_1} \left[1 + \frac{t_2^2}{U_1^2 - t_2^2} \right]. \quad (\text{S29})$$

Finally, we will consider the more interesting and important case of finite NN and NNN intersite Coulomb repulsions V and V_2 . We restrict ourselves to the lowest order expansion in the strong coupling limit $|t|/U \sim 2.5 \times 10^{-2} \ll 1$ relevant here. The AFM contribution to both exchanges are monotonously increasing functions of V and V_2 . For small $V \ll U$ it can be linearized. For $t_2 > 0$ as considered here there is an absolute enhancement for $V > 0.5t_2$ (ignoring the weak V_2 which further reduces this critical value). Then one arrives in 2nd order of t/U at

$$J_1^{(1)} - \tilde{J}_1 = \frac{4t^2}{U_1} \left[1 + \frac{1}{2} \left(\frac{v_1}{1 - v_1} + \frac{v_2}{1 - v_2} \right) \right]. \quad (\text{S30})$$

At variance with the cases considered above, a relative strong intersite Coulomb interaction $V \sim U/4 \sim 1$ eV, i.e. $v_1 \sim 0.5$, can in principle considerably enlarge the AFM contribution to J_1 (See FIGs. S2 and S3.) and this way also add a non-negligible FM contribution via $-J_1$ to J_2 according to Eq. (S16) which is only partially compensated by its

own induced AFM contribution. This increase leads to an enhancement of the phenomenological FM \tilde{J}_1 -value which roughly scales with K_{pd} . The influence for realistic $V_2 \approx t_2 \sim 160$ meV by the 2nd factor in Eq. (S34) is very weak. The increase in the trimer stems from the different energy denominators $\approx U - 2V$ vs. $U - V$ in the dimer case with one bond, only. Notice that this V -dependence cannot be described in terms of a small V/U expansion, instead the analytic expression with the correct account of the denominator $\sim U - 2V$ in Eq. (S30) is essential.

Notice that in both small superexchange terms $\propto t^2$ of Eqs. S17 and S18, the small terms V_2 and \tilde{J}_2 might be ignored. Indeed, for the former one estimates $V_2/V_1 \sim 0.5/\varepsilon_\infty \sim 1/6 \div 1/7$, where $\varepsilon_\infty \approx 3 \div 3.5$ is the dielectric constant. For the latter value we estimate $-\tilde{J}_2/\tilde{J}_1 < K_{pp}/K_{pd} \sim 1/10 \div 1/5$. Notice that in both expressions the 2nd order higher terms in t may compete (slightly reduce) with the dominant first FM term and with the NNN hopping t_2 induced AFM superexchange (second term). In particular, the occurrence of the dominant AFM contribution from t_2 (i.e. the O-O derived transfer integral is decisive for the frustration in the edge-sharing CuO_2 chains, i.e. J_2 is always AFM in nature. In FIG. S3 the influence of the NN and NNN intersite Coulomb interactions V_1 and V_2 on the NN AFM superexchange $\propto t^2$ is depicted. Notice the pronounced nonlinear dependence caused by the formal divergence of the expression in brackets at $V_1 = (U + V_2 + \tilde{J}_1 - \tilde{J}_2/4)/2$. [For the FFES CuO_2 chain systems under consideration $V_1/U \lesssim 1/4$ is expected which is still not too close to that point of artificial divergency justifying the lowest order in the expansion used in Eq. (S24).] Notice the dominant influence of a small but finite V_2 for the FM superexchange contribution to J_2 in the present lower order approximation. Finally, we turn to the case of 2 holes and $\Phi = 90^\circ$. It is usually considered in low orders of the perturbation theory in terms of t_{pd}/Δ [4, 5] which however exhibits in the presence of K_{pd} , intersite Coulomb interaction W and especially t_{pp} a slow convergency behavior. Hence, we present here an exact analytic expression taking fully into account the first 3 interactions and postpone the third interaction relevant for the intra-plaquette O-O hopping for a future study. Thus, we deal with a 4-site (orbital) problem with two Cu $3d_{xy}$ sites and one O-site with two orbitals in between. Within the planar case we have the following parameters: the two onsite repulsions $U_d > U_p$, the onsite interorbital repulsion U_{pp} affecting the Hund's rule coupling J_H according to Eq. (21) in the MT, the intersite repulsion $W = V_{pd}$, the direct FM exchange K_{pd} and the hopping t_{pd} . The O and Cu onsite energies $\Delta = \varepsilon_p - \varepsilon_d$ were measured as $\pm\Delta/2$, respectively. Then the GS is

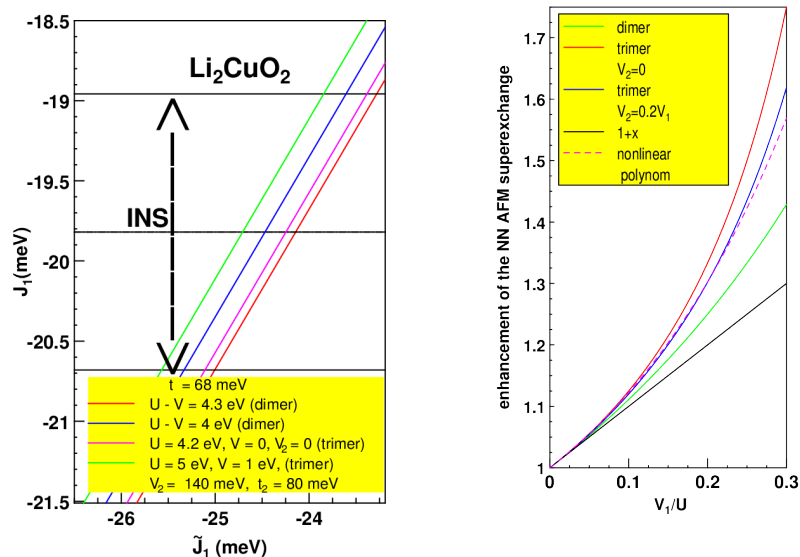


FIG. S2. **Left:** The empirical NN exchange J_1 from the INS [3] LSWT analysis including the experimental error bars vs. various possible phenomenological FM contributions \tilde{J}_1 of the extended one-band Hubbard model (E1BH). **Right:** relative enhancement of the AFM contribution to J_1 as a function of the NN intersite Coulomb repulsion $V = V_1$ for a trimer and a dimer cluster as well as the NNN V_2 for a trimer within the E1BH-model based on Eq. (S24).

given by the lowest eigenvalue from the triplet matrix:

$$\hat{T}_{GS} = \begin{pmatrix} W - \frac{1}{4}K_{pd} & \sqrt{2}t & \sqrt{2}t \\ \sqrt{2}t & \Delta - \frac{1}{4}J_H & 0 \\ \sqrt{2}t & 0 & -\Delta \end{pmatrix}, \quad (S31)$$

$$\hat{S}_2 = \begin{pmatrix} W + \frac{3}{4}K_{pd} & \sqrt{2}t & \sqrt{2}t \\ \sqrt{2}t & \Delta + \frac{3}{4}J_H & 0 \\ \sqrt{2}t & 0 & -\Delta \end{pmatrix}, \quad (S32)$$

For simplicity we show here the eigenvalues ignoring the intersite interaction W . Then the triplet energy reads

$$E_T = \frac{1}{12} \left[K_{pd} + J_H - 2\sqrt{(J_H - K_{pd})^2 - K_{pd}J_H - 12J_H\Delta + 48\Delta^2 + 192t_{pd}^2} \cos \left[\frac{1}{3} \arccos(\phi_T) \right] \right],$$

$$\phi_T = \frac{(J_H - K_{pd})(72\Delta^2 - K_{pd}^2 + K_{pd}J_H + 2J_H^2 - 36J_H\Delta - 288t_{pd}^2)}{2 \left((J_H - K_{pd})^2 + K_{pd}J_H + 12J_H\Delta + 48\Delta^2 + 192t_{pd}^2 \right)^{3/2}} \quad (S33)$$

The corresponding expression for the lowest singlet state is given by

$$E_S = \frac{1}{4} \left[K_{pd} + J_H - 2\sqrt{(J_H - K_{pd})^2 - K_{pd}J_H - 12J_H\Delta + 48\Delta^2 + 192t_{pd}^2} \cos \left[\frac{1}{3} \arccos(\phi_S) \right] \right],$$

$$\phi_S = \frac{3\sqrt{3}(J_H - K_{pd})(-16\Delta^2 - K_{pd}^2 + K_{pd}J_H + 2J_H^2 - 36J_H\Delta - 32t_{pd}^2)}{2 \left((J_H - K_{pd})^2 + K_{pd}J_H + 12J_H\Delta + 48\Delta^2 + 64t_{pd}^2 \right)^{3/2}} \quad (S34)$$

Ignoring the intra-plaquette O-O transfer t_{pp} and the weak direct FM exchange K_{pp} , the FM NN exchange is given by twice the singlet-triplet energy difference. [s. the remark after Eq. (S9) for a dimer here simply generalized by the factor 2 due to the account of 2 exchange paths via the 2 noninteracting O.] $J_1 = -2(E_S - E_T)$. Anyhow, their exchange governed mainly by t_{pp} and U_p , has been taken fully into account in our solutions shown in FIG. 16 of the MT. These hoppings were taken from *modified* Slater-Koster integrals. based on atomic wave functions in Refs. 2 and 6. However, in a real ionic solid their absolute values and the ratio are affected by the crystal field. In this context we mention that $t_{p_y} = 0.59$ eV in Refs. 1 and 3, whereas it is ≈ 1 eV in our DFT-calculations. The Cu-O transfer integrals are a bit closer differing by about 20%, only. In view of these uncertainties it is often useful to determine the main hoppings from fitting experimental optical, EELS and RIXS spectra. As a result we arrived in the past at intermediate values close to those of the DFT. The expressions given below illustrate the complex interplay of

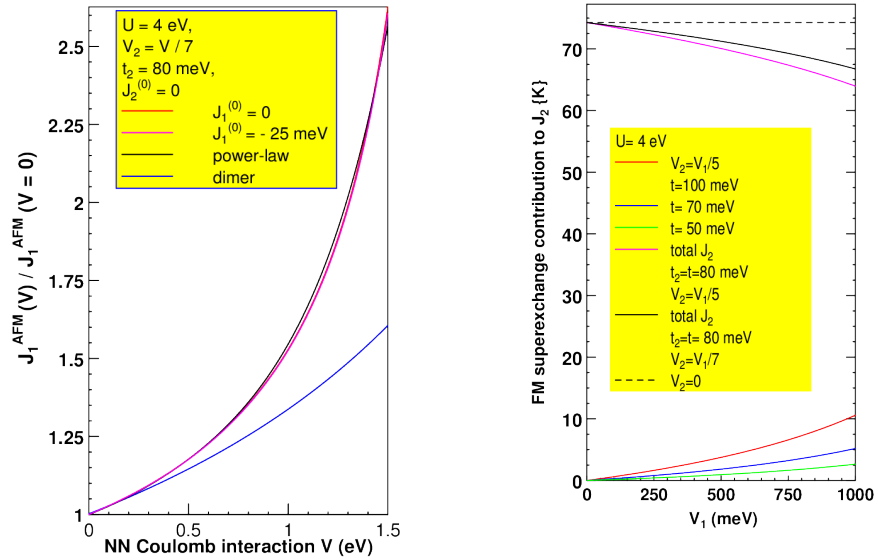


FIG. S3. Left: relative enhancement of the AFM contribution to J_1 vs. the intersite Coulomb interactions $V = V_1$ ((NN) and V_2 (NNN)). Right: enhancement of the FM contribution to J_2 (lower curves) and total J_2 (upper curves) up to the constant shift due to a finite FM \tilde{J}_2 (from K_{pp}) vs. V_1 and two typical values of V_2 adopting various dielectric screenings.

various Hamiltonian parameters hidden by the simple quasi-linear behaviors. Thus, expanding Eqs. (S33) and (S34) in powers of K_{pd}/t_{pd} , we get in first order

$$J_1 = -K_{pd} \frac{t_{pd}^2}{\Delta^2 + t_{pd}^2} + \frac{1}{32} K_{pd}^2 \frac{t_{pd}^2}{(\Delta^2 + t_{pd}^2)^{3/2}} \left[1 + \frac{3\Delta^2}{\Delta^2 + t_{pd}^2} \right] +$$

$$-\frac{1}{8} J_H \left(1 - \frac{8\Delta}{\sqrt{\Delta^2 + t_{pd}^2}} + \frac{7\Delta^2}{\Delta^2 + t_{pd}^2} + K_{pd} \frac{t_{pd}^2 + 4\Delta(\Delta - \sqrt{\Delta^2 + t_{pd}^2})}{2(\Delta^2 + t_{pd}^2)^{3/2}} \right) + \frac{5}{148} J_H^2 \frac{t_{pd}^2}{(t_{pd}^2 + \Delta^2)^{5/2}}. \quad (\text{S35})$$

For $(t_{pd}/\Delta)^2$ the 3rd term yields a small 2nd order dependence $\sim -\frac{1}{16} J_H \frac{t_{pd}^2}{\Delta^2}$ but ≈ -9.3 meV, only, adopting $|t_{pd}| = 0.5\Delta$. Thus, for $J_H = 0.6$ eV and $K_{pd} = 0.1$ eV the Hund's rule term yields $\approx 1/3$ of J_1^{FM} , i.e. it is still significant but not dominant. Note that its contribution is further reduced inspecting the 2nd order term which yields a tiny AFM contribution $\sim J_H^2 t_{pd}^2 / \Delta^5$. Also the 2nd order quadratic term in K_{pd} is negligible. Thus, the quasi-linear dependence of J_1 on the two main FM interactions employed in the MT has been verified. The corresponding plots (s. Fig. S4) are shown for the set used in Ref. [2] and for a doubled K_{pd} , i.e. \approx to $J/t_{pd} = -0.05, -0.1$, respectively. From Figs. S4 and 16 in the MT it is clear that J_H contributes less than $\sim 25\%$ to 30% to the singlet-triplet separation, i.e. to J_1^{FM} entering Eq. (14) of the MT.

C. Quantum chemistry and DFT calculations: computational details

Among the various pieces of information we used for the analysis of the different contributions to the effective magnetic couplings is the strength of direct exchange between spins belonging to NN Cu^{2+} ions. The strength of this direct exchange on two edge-sharing plaquettes was determined on the basis of *ab initio* Hartree-Fock calculations [7]. Given the complicated incommensurate lattice structure of CYCO [8], we employed however the simpler lattice

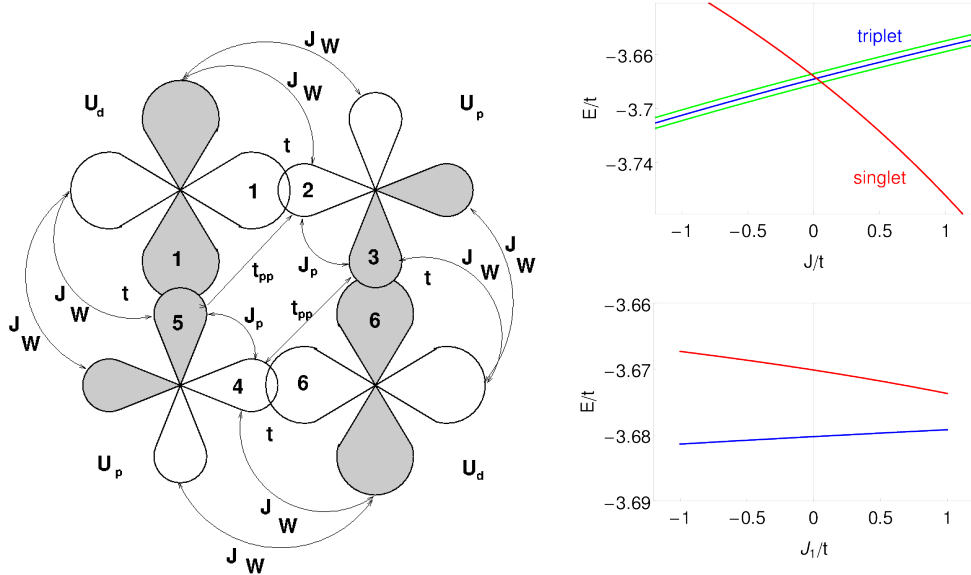


FIG. S4. **Left:** Orbitals and transfer integrals of a CuO_2Cu -cluster treated exactly in the planar $\text{Cu } 3d \text{ O } 2p$ 5-band Hubbard model: $\text{Cu } 3d_{xy}$ 1 (left) and 6 (right); intermediate $\text{O } 2p_{x,y}$ 2,3 (upper) 3,4 (lower). Here at variance to FIG. 13 in the MT a representation of the $\text{O } 2p$ states \parallel and \perp to the Cu-O bonds has been chosen and the chain axis is taken along the descending diagonal. For the 3 exchange couplings the notations $J = -K_{pd}$, $J_p = -J_H$, $J_{dd} = -K_{dd}$ have been used. W is the intersite (Cu-O) Coulomb interaction. The interorbital Coulomb repulsion at $\text{O } U_{pp}$ is included via J_H and Eq. (21) in the MT. **Right:** The lowest triplet and singlet states as a function of K_{pd} ($J \leq 0$). **Upper:** without intersite Cu-O Coulomb interaction $W = 0$ and finite $V_{pd} = 0.8t_{pd}$ (lower) for $\Delta = 3.2$ and weak $J_H = 0.5t_{pd}$ and $J = -K_{pd} = 0.1$. In both cases $U_d = 8$, $U_p = 4$, and $\Delta_{pd} = 3.3$ in units of t . To show the lifting of the 3-fold degenerated triplet state an external magnetic field (green lines) with $h = 0.002$ was applied. (For $g=2$ this corresponds to 17.3 T.) The dd -channel is switched off (i.e. $t_{dd} = J_{dd} = K_{dd} = V_{dd} = 0$).

configuration of the closely related LICU [9]. The material model consists in this case of two NN magnetic centers (Cu^{2+} sites), the six O ligands coordinating these two Cu ions, and the nearby sixteen Li atoms. The plaquette plane coincides with the xy plane, with the x axis pointing along the chain. The remaining part of the crystalline lattice was modeled as a finite array of point charges fitted to reproduce the ionic Madelung field in the cluster region. All-electron basis sets of quadruple-zeta quality were used for Cu [10] while basis sets of quintuple-zeta quality were applied for the two bridging O's [11]. For the non-bridging O ligands and for the Li ions, basis functions of triple-zeta [11] and single-zeta quality [12] were used, respectively. The direct FM Cu-Cu exchange integral $K_{dd} = -4.1$ meV was determined from the splitting between the singlet and triplet states associated with the d^9-d^9 electron configuration as obtained from a restricted open-shell Hartree-Fock (ROHF) calculation [7, 13]. Further, to gain some insight as concerns the magnitude of direct hopping between two NN Cu sites (t_{dd}), we considered the same two-plaquette cluster described above but removed one electron (giving a d^9-d^8 configuration for the NN Cu ions). Orbitals as obtained in the ground-state N -electron calculation, with no further optimization, were used to this end. The hopping between NN Cu sites was then computed as half of the energy separation between ROHF states having the d_{xy} electron either in the two-site molecular-like orbital (MO) of gerade symmetry or in the MO of ungerade symmetry [13, 14]. The resulting hopping is -174 meV. Similarly, -160 meV is obtained from the splitting of the bonding and antibonding Cu d_{xy} MO's in the GS N -electron configuration. The computations were performed using the quantum chemistry (QC) package MOLPRO [15]. A more detailed QC analysis of exchange mechanisms in Li_2CuO_2 , beyond the present results for the direct dd exchange (K_{dd}) and for the t_{dd} hopping integral, will be provided elsewhere.

We additionally performed calculations within the local density approximation (LDA) and the general gradient approximation (GGA), using the full-potential local orbital FPLO code [16–18], version fplo14.00-49. For the exchange-correlation potential, the LDA and GGA parametrizations of Perdew-Wang [19] and Perdew-Burke-Ernzerhof [20] were chosen, respectively. Both exchange-correlation potentials yield essentially the same band structure. To obtain precise band-structure information, the final calculations were carried out on a well converged mesh of 1920 k -points ($16 \times 12 \times 10$ mesh). The LICU crystal structure of Ref. [9] was used. The tb-hoppings and the respective on-site energies were evaluated on the basis of Wannier functions (WF's). The single-band model implies a single Cu-centered $3d_{xy}$ WF. For the pd -model, a minimal 5-band construction (Cu $3d_{xy}$, O $2p_x$, $2p_y$) and an 11-band model (all Cu and O orbitals) were derived (with xy for the plaquette plane and x for the chain direction). A 12 k -point mesh was used for the WF fit (while the WF grid subdivision was $30 \times 30 \times 30$ in the `=.wundef` file). We obtained for the effective single-band approximation small NN and NNN transfer integrals $t \equiv t_1 = 0.068$ eV and $t_2 = 0.080$ eV. Within the multiband pd -model we computed Cu-site energies $\varepsilon_d = -2.42$ eV (in electron (*el*)-notation) and a level splitting of 194 meV for the relevant O $2p$ orbitals, with $\varepsilon_{p_x} = -3.986$ and $\varepsilon_{p_y} = -3.792$ eV. Larger hopping integrals $t_{pd_{Ox}} = 0.933$, $t_{pd_{Oy}} = 0.8129$, $t_{p_x p_x} = 0.7676$ eV were found for the multiband model, with $t_{p_y p_y} = -0.084$ eV and $t_{p_y p_y} = 1.035$ eV (compare with 0.69 eV in the Slater-Koster type parametrization [21] used in Ref. 2 and denoted as t_{p_y} in Fig. 13 of the MT of the intra plaquette transfer integral between the lower and the upper O as discussed elsewhere). A transfer integral $t_{dd} = -143.8$ meV was computed, similarly to the ROHF estimates given above. With respect to the pd and dd channels, we note that a straightforward extraction from DFT band structure analyzed in terms of a single-band extended TB-model by fitting its antibonding Cu-O band is somewhat dangerous due to the *linear* interference with the indirect pd kinematic contributions. In contrast the superexchange (SE) one looks for depends mainly on *even* powers of each component resulting in a *larger* SE. Anyhow, a separation of the indirect pd channel from the dd one is also necessary to estimate correctly the effective $U_{\text{eff}} \approx \Delta_{pd} + V_{pd}$ which enters the pd channel, only. Similarly, the different contributions from the two $p_x d$ and $p_y d$ channels must be also separated since it strongly affects the FM J_H on J_1 from the two bridging O considered below (s. Fig. 16 in the MT). These problems are almost gone using a multi-band WF-function analysis or an orbital specific basis as we did here.

D. No criticality and sizable quantum fluctuations for chains with strong diagonal AFM interchain couplings

Here we demonstrate the significant up-shift of the quasi-classical critical point (CCP) between a quasi-2D Néel state with collinear FM chain ordering and a quasi-2D-spiral state with a non-collinear ordering [22, 23] for the quasi-2D model of AFM interacting chains adopted in the MT illustrated by two simple examples. Thereby we have changed only one of the main inchain interaction parameters and leave the other 4 parameters fixed (s. FIG. S1.) In case of reducing the AFM IC despite some flattening of the dispersion there are no qualitative changes showing the absence of criticality. In general, allowing the change of all parameters, one might arrive at a critical point yielding smaller α -values being closer to that of single chains with $\alpha_c = 1/4$. But the systematical study of such a "critical" surface in the 5D parameter space is very time consuming and even difficult to present the large manifold of critical points in a vivid manner. Model studies of reduced Hamiltonians e.g. for equal IC in the isotropic case $D = 0$ in a 3D parameter space is under progress. Here, we focus on the interplay of α vs. AFM IC. Fixing J_1 and J_2 but adding a weak FM as derived above NNN-IC J_b , in the formal limit $J_{ac,1}, J_{ac,2} \rightarrow 0$ one is left with two interpenetrating FM coupled

sublattices and the resulting ordering would be determined by a *quantum* "order by disorder" problem. A quantum critical point (QCP) would occur, only, if the resulting GS would be a FM state at variance with the AFM Néel GS of FM aligned chains. This situation differs from that for LICU where the uniform FM inchain ordering is induced solely by the weak AFM IC with shifted adjacent chains (s. Fig. 1 of the MT) Then a 3D-criticality would be reached for a slightly weakened IC by about 4 K (in total 32 K summing up all NNN) a critical point to the ordered spiral states is achieved. Analogously, for fixed IC at 9.2 K a critical point is achieved at an upshifted value of $\alpha = 0.39$, only, to be compared with the measured 0.332 [3].

The recently reported pressure dependence of the lattice structure and the stability of the orthorhombic phase below ≈ 6 GPa, only, for LICU [24] is of great interest, because it is accompanied at first by an increase of Φ up to 97° which causes a decrease of $-J_1$ and an increase of J_2 resulting in an increase of α at almost unchanged AFM IC according to DFT+ U calculations by U. Nitzsche [25] (s. also the Tab. I). Then, according to these findings an *incommensurate* spiral state is expected in a *classical conventional* scenario at intermediate pressure before a transition to a monoclinic phase with smaller Φ -and expected strongly increased (decreased) $-J_1$ (J_2), resp., which explains naturally the reentrant transition to a commensurate state with FM aligned moments along the chains called "accidental" by the authors [26], provided the AFM IC remains relatively weak as suggested by the reported lattice structure and especially if, $\alpha < 1/4$ in that novel monoclinic phase as suggested by the experimental much closer Φ to $\pi/2$ than in the orthorhombic phase. The absence of critical fluctuations in CYCO and Li_2CuO_2 at *ambient* pressure are seen in the thermodynamic properties, in particular, in the large ordered magnetic moments which are ascribed also to a significant easy-axis anisotropy for the latter. Hence, a high-pressure study of the ordered magnetic moment for CYCO and LICU as well is highly desirable to elucidate the stability of the commensurate chain Néel phases. The stability of the induced FM inchain ordering can be revealed by dynamical measurements as the INS considered here. With the AFM IC properly taken into account there is a critical point nearby which separates a commensurate and collinear Néel phase with unusual FM ordering along the chain direction from a non-collinear spiral state. Thus, near that critical point at *finite* pressure for *weak* diagonal AFM IC between shifted chains there is now indeed room for an interesting "order from disorder" specific quantum mechanism proposed for LICU [27] originally already for the case of ambient pressure. There, however, it seems to be ruled out experimentally by the mentioned thermodynamic data and the success of the LSWT. In contrast, in the critical region more sophisticated many-body effects for the magnons as renormalizations of the large dispersion and damping effects frequently discussed in the literature might be however expected. The somewhat smaller IC extracted from the LSWT analysis in LICU (9 K (0.8 meV) vs. 13 or 11 K) from the LSDA+ U calculations might be already considered as a related physical effect. Then the question arises to what extent the expected incommensurate spiral phase shrinks or it is removed by such quantum order by disorder effects forming a modulated FM state [28]?. In this context one might speculate that the observed, but not yet understood, incommensurate phase in the related slightly *h*-doped $\text{La}_5\text{Ca}_9\text{Cu}_{24}\text{O}_{41}$ [29] might be governed by a related mechanism, since a weaker IC is suggested (i) by the lowered $T_N = 10.5$ K as compared with the undoped parent compound $\text{La}_6\text{Ca}_8\text{Cu}_{24}\text{O}_{41}$ ($T_N = 12.2$ K) both are apparently already much less stable than CYCO with the highest $T_N \approx 29.5$ for all FFESC-systems. (ii) The inspection of the $\chi(T)$ shown in Ref. 28 (which is determined by the frustrated CuO_2 chains due to the large two-leg ladder gap) of the undoped parent compound $\text{La}_6\text{Ca}_8\text{Cu}_{24}\text{O}_{41}$ with a maximum position near 20 K pointing to a *larger* 1D frustration ratio than in CYCO: $\alpha > 0.3$ to 0.4. Adopting $\alpha = 1/3$ or 0.4, one estimates for that peak position (0.04 to 0.06) $|J_1|$ [30–32], resp., which yields $-J_1 \approx 43$ to 28 meV according to a full diagonalization of a large cluster with $N = 24$ sites or by the transfer-matrix

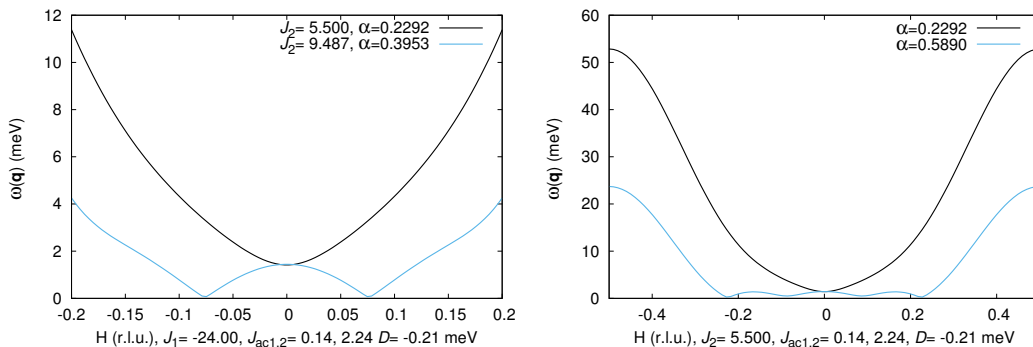


FIG. S5. Dispersion for hypothetical systems with changed inchain couplings in order to reach the spiral critical point. (Left): for changing J_2 , only, leaving all other three exchange interactions and the anisotropy parameter D fixed; (Right): the same for J_1 . Notice the occurrence of four minima pointing to two competing distorted phases.

renormalization group technique. Thus, an empirical J_1 value $\sim 36 \pm 6$ meV might be estimated. But having in mind also the corresponding J_2 -value, and our geometrical experience with various CuO_4 plaquettes and the involved Φ [33], a smaller interval, say $-J_1 = 30 \pm 2$ meV seems to be more reasonable. (s. also the discussions in Chapt. I with respect to $\text{Li}_2\text{ZrCuO}_4$ and LICU). Anyhow, the estimated $|J_1|$ exceeds the values of CYCO and LICU. Our empirical estimate is certainly again well above the prediction of 18.5 meV [2] (s. Tab. I). [34] Then, reanalyzing these data, the main inchain exchanges can be estimated from already measured thermodynamic quantities and the vicinity to an at first glance expected spiral GS could be checked. However, the observed unusual for a spin-1/2 Heisenberg model *collinear* and *modulated* FM ordering along the chains is probably caused by a special spin anisotropy which prevents the non-collinear spiral ordering. The slightly *h*-doped $\text{La}_5\text{Ca}_9\text{Cu}_{24}\text{O}_{41}$ [29] seems to be a real candidate for quantum criticality whose frustrated CuO_2 chain might be described with stronger inchain couplings and modified weak ICs opposite to earlier attempts. The latter might be determined from the known Neel temperatures or from the two gaps expected in this system, too, which depend sensitively on the IC, provided the scattering intensity from the ladder excitations could be separated from the chain ones. Our large dispersive magnon for CYCO should be a good starting point with some modifications to allow a very soft local behavior near the wave vector corresponding to the spiral critical point in chain direction and natural enhanced damping effects expected in that region. Anyhow, we strongly believe that the large inchain exchange integrals for CYCO are much less affected by such remnant quantum fluctuations and the derived large J_1 -values for both CYCO and LICU from the observed large dispersions do remain valid. In contrast, LICU and probably also $\text{Ca}_2\text{Nd}_2\text{Cu}_5\text{O}_{10}$ and CuAs_2O_4 might be closer to the inchain spiral α_c due to slightly larger α -values and a significantly weaker AFM IC which is even there necessary to stabilize the observed modulated FM alignment of the magnetic moments along the chains.

E. Aspects of the phonon mode responsible for the low-energy gap-like feature near 11 meV

To get qualitative insight into the origin and the nature of the phonon mode responsible for the first gap-like feature observed near 11 meV at the wave vector $H=0.2$, we suggest that it should be an optical mode due to the weak observed dispersion. We assume that it is derived from the cationic chains with alternating Ca^{2+} and Y^{3+} ions. Having in mind also the sister compound $\text{Ca}_2\text{Nd}_2\text{Cu}_5\text{O}_{10}$, we are confronted with a two-atomic chain model with rather different masses M_2 . We will measure them in units of the Ca -mass M_1 . This mass ratio amounts for the general system $\text{Ca}_2\text{R}_2\text{Cu}_5\text{O}_{10}$ including the isovalent substitutions for Y by R = Sc, Y, Nd, and Lu 1.113, 2.21, 3.99 and 4.37, resp. Then in a toy model approach with a single force constant K_1 one has the following phonon dispersion-law

$$\omega_{\text{ph}} = \sqrt{\frac{K_1 \left[M_1 + M_2 + \sqrt{M_1^2 + M_2^2 + 2M_1M_2 \cos(ka^*)} \right]}{M_1M_2}}, \quad (\text{S36})$$

where a^* is the Ca-R distance related to the Cu-Cu one a of the spin chain a as $a^* = 1.25a$. Then the attributed experimental crossing point with the magnon appears near $H=0.2$ (s. FIG. 2 in the MT) which corresponds to $\pi/2a^*$. The calculated dispersion of ω_{ph} from Eq. (S36) is shown in FIG. S6 (**left**). Since the observed dispersion is smaller, one might expect that at least NNN neighbor and also further more distant neighbors might be responsible for the requested flattening of the dispersion. In view of their ionic character slowly decaying contributions from long-range ionic forces in addition to the hard-core NN ones resulting from the finite ionic radii are indeed expected. Then due to the different involved charges larger NNN Y-Y interaction as compared to the NNN Ca-Ca counter parts should be realized. Within a pure point-charge Coulomb picture their ratio should be universally 9/4. The absolute values can be estimated from the screened ionic couplings $K_{2,\text{YY}} = 9e^2/(4\epsilon a^{*2})$ for the Y-Y case and similarly as $2e/(3\epsilon a^2)$ for the 3rd neighbor Y-Ca elastic coupling, where $\epsilon \approx 3.5$ denotes the dielectric constant like in LICU [2, 35]. In a realistic picture also various skew couplings all scaled by the inverse square of the corresponding distances on the adjacent and further distant chains are expected to contribute as well as the ionic interactions with O and Cu. Since the latter elongations modify the Δ_{pd} , a weak coupling to the magnon via the modulation of J_1 and J_2 is expected in accord with the weak mixing mentioned in Sec. III. A quantitative consideration of the latter is tedious and beyond of the scope of the present paper. Finally, in case of magnetic rare earth elements R=Nd in $\text{Ca}_2\text{Nd}_2\text{Cu}_5\text{O}_{10}$ [36, 37] an ordering of these f -moments at few K well below the observed high $T_N \approx 24$ K of the Cu derived spin-1/2 moments is expected. In fact, the $\chi(T)$ data exhibit a broad peak near 15 K in a field of 1 Tesla \parallel to the b -axis and a broadened feature around 8 K \parallel to \mathbf{c} [37] pointing to a 2nd magnetic transition below this upper limit, i.e. near 10 K which is too high for a simple weak dipole-dipole coupling. In the high- T_c cuprates only in the case of $\text{PrBa}_2\text{Cu}_3\text{O}_6$ a magnetic transition at ≈ 16 K much higher than in all others rare earth substituted cases has been found. We speculate that here already for the case of Nd, the O-holes have some covalence with the Nd $4f$ -electrons.

Anyhow, the elongated R-ions of that phonon will interact also via the elastic NNN coupling $K_{2,\text{RR}}$ and affect the O-ions bearing charge and a magnetic moment. The much heavier Nd mass is expected to downshift the phonon

mode, even stronger than shown in FIG. S6 (**Left**) also due to a somewhat weaker NN $K_{1Ca,R}$ force constant from the smaller ionic radius of Nd^{3+} as compared to Y^{3+} . The "hybridization" with the acoustic Cu-O mode might strengthen the flattening of the optical phonon mode. Anyhow, a detailed study of this phonon mode and its interplay with magnetism might provide much more insight into the magnetism of the two magnetic subsystems and their interplay.

F. Details of the $\chi(T)$ fit using the 10th order high- T expansion for the magnetic susceptibility

We use the method and the program packages from Refs. 38–40 for the 10th-order high- T expansion (HTE) of $\chi(T)$ for a general spin-model with up to 4 different exchange parameters J_1, J_2, J_3, J_4 . The spin model for CYCO reads

$$\hat{H} = \frac{1}{2} \sum_{\mathbf{R}, \mathbf{r}} J_{\mathbf{r}} \hat{\mathbf{S}}_{\mathbf{R}} \hat{\mathbf{S}}_{\mathbf{R}+\mathbf{r}}, \quad (\text{S37})$$

depicted in FIG. 1 of the MT, we take $J_1 = J_{1a}/k_B \approx -278.5$ K, $J_2 = J_{2a}/k_B \approx 63.82$ K, $J_3 = J_{ac1}/k_B \approx 1.38$ K, $J_4 = J_{ac2}/k_B \approx 26.24$ K. The input for the HTE package is the definition file where all bonds within a cluster or a $2L \times L \times L$ ($L=10$) super-cell of a periodic Heisenberg lattice are enumerated with the indication of a corresponding value of the exchange interaction. We use an originally developed C++ program, for the generation of the definition file. The HTE program provides *exact analytic* expressions for 10 coefficients of the HTE

$$\frac{k_B}{5N_A g^2 \mu_B^2} \chi(T) = \sum_{n=1}^{\infty} \frac{c_n}{T^n} \quad (\text{S38})$$

and computes the Padé (PA) approximants, ratios of two polynomials: $\chi(T) \approx [m, n] = P_m(T)/P_n(T)$. The PA extend the region of validity of the HTE [39]. The analytic expressions for the first 5 coefficients c_n for the model (S37) are

$$c_1 = +1/4, \quad (\text{S39})$$

$$c_2 = -(1/8)(J_1 + J_2 + 2J_3 + 2J_4), \quad (\text{S40})$$

$$c_3 = (1/8)(J_1 J_2 + 2J_1 J_3 + 2J_1 J_4 + 2J_2 J_3 + 2J_2 J_4 + J_3^2 + 4J_3 J_4 + J_4^2), \quad (\text{S41})$$

$$c_4 = 4 \left[(J_1^3 + J_2^3)/24 + J_1 J_2 (J_1 - 4J_2)/32 - (J_1^2 + 6J_1 J_2 + 8J_3 J_4 + J_2^2)(J_3 + J_4)/4 - 11J_1 J_3^2/16 - 19(J_1 + J_2)J_3 J_4/8 - ((J_1 + J_2)J_4^2 + J_2 J_3^2) - (J_3^3 + J_4^3)/6 \right] \quad (\text{S42})$$

$$c_5 = 5J_1^4/1536 - 23J_1^3 J_2/768 + J_1^2 J_2^2/512 - J_1 J_2^3/96 + (7/64)J_1^2 J_2 (J_3 + J_4) + 5J_2^4/1536 + 3/16 J_1 J_2^2 J_3 + 25/256 J_1^2 J_3^2 + 3J_1 J_2^2 J_4/16 + (5/32)(J_1^2 J_4^2 + J_2^2 J_3^2) + 23J_1^2 J_3 J_4/128 + 13J_1 J_2 J_3^2/32 - (1/48)(J_2^2 J_4 + J_1^3 J_4 + J_2^2 J_3 + J_1^3 J_3) + 33J_1 J_2 J_3 J_4/32 + 19J_1 J_3^3/384 + 31J_1 J_2 J_4^2/64 + 33J_2^2 J_3 J_4/128 + 89J_1 J_2^2 J_4/128 + J_2 J_3^3/6 + 5J_2^2 J_4^2/32 + (109/128)J_3 J_4 (J_1 J_4 + J_2 J_3 + J_2 J_4) + 13(J_3^4 + J_4^4)/768 + 49J_3^3 J_4/192 + J_4^3 (J_1 + J_2)/6 + 51J_2^2 J_4^2/64 + J_3 J_4^3/3 \quad (\text{S43})$$

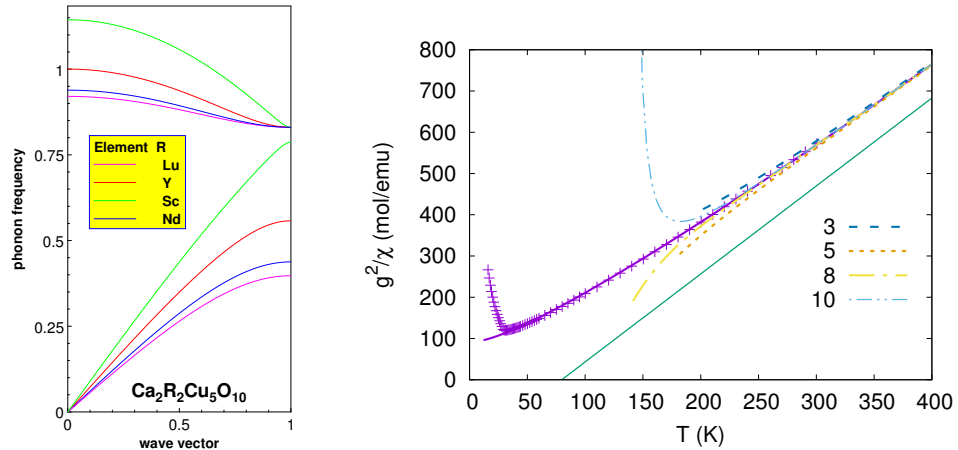


FIG. S6. **Left:** Phonon dispersion for various elements R in the alternating cationic $\text{Ca}^{2+}\text{-R}^{3+}$ chain within the NN coupling approximation given by the force constant K_1 normalized to the case of Y at the Γ -point in the BZ for the optical phonon mode. The wave vector k is given in units of π/a^* , where a^* denotes the R-Ca distance and R is a trivalent element. In these units the experimental crossing point with the magnon amounts 0.5. **Right:** Symbols: the inverse spin susceptibility for the magnetic field along b (+) axis of CYCO, Ref. [41]. Dashed lines 3,5,8,10 of the 3th, 5th, 8th and 10th HTE orders, thick solid line: the [5,5] Padé approximant for the 10th order, thin solid line: the exact Curie-Weiss asymptotic.

The coefficients c_n , $n > 1$ are functions of the exchange parameters J_i given by Eqs. (S40-S43). Their explicit form depends on the geometry of the bonds encoded in the input definition file. Only the *single* parameter g was varied during the fit for each direction of the magnetic field. FIG. S6 **Right** shows the curves of the HTE series for various orders and the [5,5] Padé approximant for the 10th order that fits the data even down to T_N as shown also in Fig. 12 of the MT. The CW-asymptotics is given by the *2nd* order of the HTE series

$$\frac{k_B}{5N_A g^2 \mu_B^2} \chi_{\text{CW}}(T) = \frac{c_1}{T - \Theta_{\text{CW}}}, \quad \text{and} \quad \Theta_{\text{CW}} = \frac{c_2}{c_1} \approx +80 \text{ K}. \quad (\text{S44})$$

Inserting the expressions (S39),(S40) into Eq. (S44) gives Eq. (21) of the MT. It is an *exact* relation, which coincides with the mean-field result. [s. Eq. (27) of Sect. IV.B in Ref. 42.] Θ_{CW} is determined by the dominant inchain exchange (J_1 , J_2 in case of our chains), while the 3D GS and especially T_N do depend on the small IC, too.

G. Curie-Weiss temperature and saturation field – a comparison with CuSb_2O_4 and $\text{NaCuMoO}_4(\text{OH})$

The difficulty to apply a HTE can be circumvented applying a strong magnetic field (up to saturation at H_s where all AFM couplings are suppressed) at very low T . In the isotropic limit [s. Eq. (S21) in the Suppl. Mat. of Refs. 43,44] there is a convenient and accurate relation valid approximately at low- T

$$g\mu_B H_s + 2J_b + 4\Theta_{\text{CW}} = 2|J_1|(1 - \alpha). \quad (\text{S45})$$

For CYCO H_s slightly exceeds 70 Tesla [41] whereas our predicted value Θ_{CW} for CYCO is much larger than the experimental values of 39 K and 26.3 K for two other frustrated quasi-1D systems: CuAs_2O_4 [45] and CuSb_2O_4 [46] with a predominant FM J_1 coupling. CuAs_2O_4 exhibits probably a FM ordering below $T_C = 7.6$ K near the critical point and the point also to a weak AFM IC whereas CuSb_2O_4 shows a *helical* ordering below $T_N = 1.8$ K pointing to a larger α . The propagation vector $\tau = (0, 0, 0.3962)(\phi = 71^\circ)$ points to a pitch between neighboring Cu moments intermediate between linarite (0.186, $\phi = 33.48^\circ$) and LiVCuO_4 ($\phi = 83.6^\circ$) and at first glance to a decreased $|J_1|$ caused by the larger Φ changing from $\Phi = 91.5^\circ$ to $\Phi = 94.5^\circ$. Slight deviations from a perfect FM interchain ordering point to the presence of weak AFM frustrating IC in addition to stronger FM ones. Ignoring that weak IC and adopting $\alpha = 1/4$ for simplicity (close to 0.244 proposed by the author), one arrives from Eq. (S45) with $H_s = 0$ generic for a FM at $T = 0$ at $J_1 = 104 \pm 2.5$ K, only, in accord with the result of their DFT-calculations slightly above a large $U \approx 9$ eV (i.e. 8 eV in their notation of $U_{\text{eff}} = U - J_{\text{Cu}}$) and a $J_2 = 26$ K (2.24 meV) [108.7 K and 27.5 K, resp.]. The effective J_2 is somewhat reduced by the twisting of non-ideal Cu_2O_4 unites and it is also smaller than our value for CYCO of ≈ 64 K. In view of the discussion given in the MT and the actual Φ close to $\pi/2$, the small value of J_1 is surprising. It points to a sizable AFM contribution of the *dd*-channel in some conflict with a large U_d but it is supported by the shorter Cu-Cu distance as compared to CYCO and Li_2CuO_2 (see Tab. I). Using the experimental $H_s \approx 14$ T, $g = -2.1$ from EPR and $\Theta_{\text{CW}} = 26.3$ K for the Sb sister $\text{CuSb}_2\text{CuO}_4$, ignoring for simplicity possible nematicity, one arrives in the one-magnon picture at $-J_1 = 124.95$ K (10.77 meV) and $J_2 = 62.5$ K (5.15 meV) adopting their proposed $\alpha = 0.5$ compatible with their DFT result but now near $U_{\text{eff}} = 6$ eV [117 K and 63.8 K, respectively] Within this picture increasing Φ , surprisingly $-J_1$ is slightly *increased* whereas J_2 is twice as large as in the As sister compound. The inspection of the structural data of CuSb_2O_4 with two different Cu-O-bond lengths points to a more general $J_1, J_1 - J_2$ model with *alternating* FM NN couplings J_1 and $-J_1$ at least, similarly to the spin and nematic liquid system LiCuSbO_4 [47] above 125 mK [48] with a subsequent 3D ordering below and with -160 K and -90 K, respectively, and $J_2 = 24$ K according to our DFT-results [49].

Another example of interest is $\text{NaCuMoO}_4(\text{OH})$ [50] [a candidate for multipolar physics]. Its $H_s \approx 26$ T. But at variance with the cases considered above, it exhibits a small *negative* $\Theta_{\text{CW}} = -5$ K. Using again Eq. (S45) and the experimental $g = 2.18$, one arrives at $|J_1| = J_2 + 9$ K which a bit differs from the values $J_1 = 51$ K and $J_2 = 36$ K derived from their fits of $\chi(T)$ -data. Using instead somewhat closer values such as $J_1 = -48$ K (-4.12 meV) and $J_2 = 39$ K (3.36 meV) self-consistency can be achieved. The latter value is \sim usually obtained by DFT+ U calculations but the former is at first glance anomalously small. The very different Φ for the two non-equivalent O(1) and O(4) suggests that the small total $J_1 = J_{1,\text{O}(1)} + J_{1,\text{O}(4)} - J_{\text{O}(1),\text{O}(4)}$ is the sum of two opposite contributions connected with each of this non-equivalent O and the AFM higher order interaction between them discussed in the MT and illustrated in Fig. 14 therein. Thereby each of them is expected \approx one half of a normal FM contribution like in LICU for the former from $\Phi_{\text{O}(1)} = 91.97^\circ$ and an AFM $\sim 1/2$ of that in CuGeO_3 . The still larger $\Phi_{\text{O}(4)} = 103.65^\circ$ nearly "compensates" the weaker splitting effect caused by the more moderate crystal field expected in $\text{NaCuMoO}_4(\text{OH})$. Thus, we estimate $J_1 \sim -0.5 \cdot 22 \text{ meV} + 0.5 \cdot 14 \text{ meV} = -4 \text{ meV}$ in accord with Eq. (S45) yielding -4.15 meV.

H. FM NN-couplings or contributions in some cuprates with edge-sharing elements

In Tab. I we collect available data of the FM NN exchange coupling in frustrated CuO_2 chain and ladder compounds as well as in alternating chain FM-AFM and FM-FM systems with the aim (i) that the cases already considered in Ref. 2 show a systematic underestimation which we ascribed in the MT to an underestimated direct Cu-O FM exchange K_{pd} and to stress its *nonuniversality*, (ii) to demonstrate that the sign change of J_1 happens often at larger $\Phi > 95^\circ$ than suggested in Ref. 2, and (iii) find candidates where the so far ignored AFM dd -channel might essentially contribute to small or even tiny J_1 in view of moderate Φ . The list of materials is by no means complete. Anomalous small or even AFM NN J_1 values might be realized only for special reasons not considered in Ref. 2, e.g., in the case of green diopside[51] where the NN-coupling in the dimer Cu_2O_6 double plaquettes amounts about 3 meV, only, or being even AFM as in the case of *malachite* $\text{Cu}_2(\text{OH})_2\text{CO}_3$ representing alternating AFM-AFM chains due to the buckled non-ideal corner-sharing (with $\Phi \approx 122^\circ$) of the connected double dimer-plaquettes.

To illustrate higher orders of the perturbation theory, we reconsider here the results for the exchange between non-equivalent Cu-A and B-sites in $\text{Ba}(\text{Sr})_2\text{Cu}_3\text{O}_4\text{Cl}_2$ [52] up to 6th order in an 11-band pd model and use them to estimate the FM exchange from the recent INS [53, 54] and RIXS [55] data. The FM J_{AB} results from the edge-sharing between the and Cu_B subsystems. We start with the large (small) AFM exchanges J_{AA} (J_{BB}), respectively:

$$J_{AA} = \frac{4t_{pd}^2}{(\Delta_A + V_{pd})^2} \left(\frac{2t_{pd}^2}{\Delta_A + U_p} + \frac{t_{pd}^2}{U_d} - K_{pd} + \frac{K_{pd}^2}{\Delta_A + V_{pd}} \right). \quad (\text{S46})$$

With $K_{pd}=0.2$ eV, $V_{pd}=1.2$ eV in accord with the MT, and standard $t_{pd}=1.3$ eV, $U_d=9$ eV, and $U_p=4$ eV as well as $\Delta_A=3.2$ eV ones, we arrive at $J_{AA}=163$ meV in accord with $J_{AA}=169$ meV from INS [54] and $J_{AA}=165$ meV (RIXS [55]). They are reproduced exactly for fixed other parameters at $K_{pd} = 180$ meV and 192 meV, respectively, and $U_{\text{eff}} \approx \Delta_A + V_{pd} = 4.4$ eV, and Raman data and that of 130 meV estimated in Ref. 53. if $K_{pd} = 0.22$ eV and $\Delta_A = 3.5$ eV are adopted. Also the effective hoppings in the used there 1-band Hubbard model $|t_{AA} \approx t_{pd}^2/(\Delta_a + V_{pd}) = 0.497$ eV comes out close, as compared with 0.475 eV [55]. Thus, the experimental $J_{AA} \approx 165$ meV is reproduced for $K_{pd} \approx 0.2$ eV like 0.2 ± 0.02 eV from QCC for La_2CuO_4 [56, 57]. It amounts $\approx 400\%$ of the K_{pd} from Ref. 2. For $K_{pd}=0$, we would have $J_{AA} \approx 174$ meV which is 5% too large. Now, turning to J_{BB} , we have

$$J_{BB} = \frac{8t_{pd,B}^2 t_{\pi\pi}^2}{\Delta_B^2} \left[\frac{1}{(\Delta_B + V_{pd})^2} \left(\frac{t_{pd,B}^2}{U_d} - K_{pd} \right) + t_{pd,B}^2 \left(\frac{1}{2\Delta_B + U_p} + \frac{1}{\Delta_B} \right) \left(\frac{1}{\Delta_B + V_{pd}} + \frac{1}{\Delta_B} \right)^2 \right], \quad (\text{S47})$$

$$\text{The FM contribution to } J_{AB} \text{ reads: } J_{AB} = - \frac{8t_{pd}^2 t_{pd,B}^2 K_{pd}}{(\Delta_A + \Delta_B + V_{pd})^2} \left(1 - \frac{K_{pd}}{\Delta_{AB} + V_{pd}} \right) \left(\frac{1}{\Delta_A} + \frac{1}{\Delta_B} \right)^2, \quad (\text{S48})$$

where $\Delta_A = \varepsilon_p - \varepsilon_d$, $\Delta_B = \varepsilon_\pi - \varepsilon_d$, $\Delta_{AB} = \varepsilon_p - \varepsilon_{p,B}$. Ignoring small O on-site energy differences and using $t_{pd,B} \approx 0.5t_{pd}$ [52], we have $J_{AA} \gg J_{BB}$ in accord with experiment. The FM $J_{AB} \approx -20$ meV agrees with the LSDA from [58] where a spiral GS was supposed for $\text{Ba}_2\text{Cu}_3\text{O}_4\text{Cl}_2$ but exceeds the LSWT values twice, pointing to many-body effects near a QCP between AFM and spiral orderings with a pitch $\phi_p \approx \pi/2$ due to the frustrated Cu_B -spins embedded into a strongly coupled AFM lattice of the Cu_A spins. This frustration is independent on $\text{sign}(J_{AB})$ but here sizably FM for plaquettes with $\Phi \approx \pi/2$. Our estimate with $K_{pd} \sim 0.1$ eV well exceeds ≈ -6.6 meV, for a moderate J_H , only, [59].

I. Enlarged NNN J_2 -values and related disorder effects in the sister compounds $\text{Li}_2\text{ZrCuO}_4$ and LiCu_2O_2

Both systems have attracted attention already 15 years ago. Nevertheless open questions do still exist partly due to missing single crystals and unclear Li (split) positions for the former and Li and Cu^{2+} disorder in the latter. Despite the large FM J_1 problem for both compounds also the enhanced empirical J_2 values probably caused by not yet clearly understood site substitutional disorder effects, too. Such effects might play some role for the unusually enhanced J_2 values for CYCO, $\text{La}_6\text{Ca}_8\text{Cu}_{24}\text{O}_{41}$ and their weakly h -doped derivatives. Within the first analysis of $\chi(T)$ (with $g = 2$ and $\chi_0 = 0$ taken for simplicity to show the generic behavior of the thermodynamic properties with decreasing α -values near criticality) and specific heat data analyzed within a 1D J_1 - J_2 model point to $\alpha \approx 0.3$ and large values: $J_1 = -23.53$ meV, $J_2 = 7.06$ meV [60] has been fully reproduced in Ref. 32. Its author noticed also, that adopting $g = 2.2$, $\chi_0 = 0$, and $\alpha = 0.4$ instead yields also a "reasonable" fit of $\chi(T)$ but now with puzzling much smaller $J_1 = -6.46$ meV and $J_2 = 2.585$ meV. Both fits differ slightly in the vicinity of the maximum of $\chi(T)$ (s. the inset in Fig. 12 of Ref. 32). Since these values are in conflict with our microscopic analysis in the MT and in Chapt. H, we argue that *intermediate* values of $g \approx 2.1$ and $\alpha \approx 0.35$ in accord with $\alpha = 0.33$ reported by Y. Tarui *et al.* [61] from a simulation of an adopted antiphase ordering of spirals in the simulation of their might resolve both the fitting problem and provide also more realistic intermediate J_1 and J_2 -values closer to the disordered DFT-description [62] with 17 meV and 4.5 (5.6 meV for $\alpha = 0.33$) (s. Tab. I). The latter is close to 5.5 meV extracted in the MT for

CYCO. It might provide a disorder scenario for that relatively large value. Then the record value of J_1 for FFESC is given now by CYCO with 24 meV. But even higher values are expected for $\text{La}_6\text{Ca}_8\text{Cu}_{24}\text{O}_{41}$ with 28-29 meV (s. Chapt. D) where disorder and/or damping effects are larger, leading to $J_2 \approx 11$ meV.

Returning to $\text{Li}_2\text{CuZrO}_4$, we note that the authors of a recent neutron diffraction study doubted these nearly critical α -values and suggest instead an *in-phase* spiral ordering [63]. They report a large propagation vector of a spiral structure and a pitch of 87.7° close to $\pi/2$ like in LiVCuO_4 (84.5°). Anyhow, Yasui *et al.* have applied incorrectly the classical pitch-Eq. *NOT* valid here [64, 65] since their estimated $\alpha \approx 6(!)$ (is at odds with the reported and fitted $\chi(T)$ and specific heat data [32, 60]) corresponds to a situation of *extremely* weakly FM coupled interpenetrating coupled Heisenberg chains where quantum fluctuations at weak IC are very important. Our previous calculations for LiVCuO_4 demonstrated a strong reduction of the resulting "quantum" value of α [65]. Anyhow, we admit that our previous estimate of α and J_1 for $\text{Li}_2\text{ZrCuO}_4$ [60] should be considered also with some caution due to the uncertainty caused by fitting polycrystalline data and ignoring the sensitive IC, the symmetric and antisymmetric spin anisotropies allowed in a scenario with disorder as well as a weak 3rd neighbor coupling J_3 which slightly shifts the critical point.

A phenomenological analysis for LiCu_2O_2 [32] yields rather large J_2 -values: 6.9 to 10.3 meV at reasonably $J_1 \sim 17$ meV. We ascribe the former to well-known disorder effect for that compound containing very often some Li-ions on Cu(2)-sites and Cu(2) on Li-sites [66] due to similar ionic radii. This provides a realistic scenario for the observed multiferroicity. The failure of the simple J_1 - J_2 model to describe the propagation vector of the observed spiral state is not surprising and further theoretical studies are necessary also in view of the very complex magnetically ordered phases. For the isomorphic Na-compound without Cu-Na disorder a comparable value of $J_1 = -15$ meV but a much smaller $J_2 \approx 5$ meV has been calculated [62] which points again to the importance of disorder for enlarged J_2 -values.

-
- [1] R. Schumann, (2019), *et al.* in preparation.
- [2] Y. Mizuno, T. Tohyama, S. Maekawa, T. Osafune, H. Eisaki, and S. Uchida, Phys. Rev. B **57**, 5326 (1998).
- [3] W.E.A. Lorenz, R.O. Kuzian, S.-L. Drechsler, W.-D. Stein, N. Wizen, G. Behr, J. Málek *et al.*, EPL **88**, 27002 (2009).
- [4] W. Geertsma and D. Khomskii, Phys. Rev. B **54**, 3011 (1996).
- [5] S. Tornow, O. Entin-Wohlman, and A. Aharony, Phys. Rev. B **60**, 10206 (1999).
- [6] M. Braden, G. Wilkendorf, J. Lorenzana, M. Aïn, G.-J. McIntyre, M. Behruzi, G. Heger, *et al.*, *ibid.* **54** 1105 (1996).
- [7] T. Helgaker, P. Jorgensen, and J. Olsen, *Molecular Electronic-Structure Theory* (Wiley, Chichester, 2000).
- [8] Y. Gotoh, I. Yamaguchi, S. Takeya, H. Fujihisa, K. Honda, T. Ito, K. Oka *et al.*, J. Alloys and Comp. **408**, 1226 (2005).
- [9] F. Sapina, J. Rodriguez-Carvajal, M. Sanchis, R. Ibáñez, A. Beltrán, and A. Beltrán, Solid State Comm. **74**, 779 (1990).
- [10] N. B. Balabanov and K. A. Peterson, J. Chem. Phys. **123**, 064107 (2005).
- [11] T. H. Dunning Jr., The Journal of Chemical Physics **90**, 1007 (1989).
- [12] R. Dovesi, C. Ermondi, E. Ferrero, C. Pisani, and C. Roetti, Phys. Rev. B **29**, 3591 (1984).
- [13] C. J. Calzado, J. F. Sanz, and J. P. Malrieu, The Journal of Chemical Physics **112**, 5158 (2000).
- [14] J. Sanz and J. Malrieu, J. Phys. Chem. **97**, 99 (1993).
- [15] H.-J. Werner, P.J. Knowles, *et al.*, Wiley Interdisciplinary Reviews: Computational Molecular Science **2**, 242 (2012).
- [16] K. Koepnik and H. Eschrig, Phys. Rev. B **59**, 1743 (1999).
- [17] I. Ophale, K. Koepnik, and H. Eschrig, Phys. Rev. B **60**, 14035 (1999).
- [18] <http://www.fplo.de>.
- [19] J. Perdew and Y. Wang, Phys. Rev. B **45**, 13244 (1992).
- [20] J. Perdew, K. Burke, and M. Ernzerhof, Phys. Rev. Lett. **77**, 3865 (1996).
- [21] W. A. Harrison, *Electronic Structure and the Properties of Solids* (Freeman, San Francisco, 1980).
- [22] For completeness we mention that at least for external magnetic fields there is also a possibility of unusual for a Heisenberg like spin-model with localized spins various collinear SDW like states near the spiral chain state [67] (thereby the nature of the phases at almost vanishing magnetic fields near the QCP cannot be numerically resolved. Higher order multipolar states might be expected together with a rich variety (panoply) of phases predicted in Ref. 23 based on a Lifshits-field theory both caused by strong quantum fluctuations. Thereby an enlarged sensitivity to anti- and symmetric spin anisotropies and phase separations allowed by the low local-symmetry of composite symmetry might play a role, too. ()).
- [23] L. Balents and O. Starykh, Phys. Rev. Lett. **116**, 3457 (2016).
- [24] S. You, Z. Li, L. Yang, C. Dong, L. Chen, C. Jin, J. Hu, G. Shen, and H. Mao, J. Solid State Chem. **182**, 3085 (2009).
- [25] H. Rosner and U. Nitzsche, DPG-Spring Meeting Proc. **and**, private commun. (2011).
- [26] Z. Li, Y. S. Tse, S. You, C. Q. Jin, and T. Litaka, J. Mod. Phys. B **25**, 3409 (2011).
- [27] H. J. Xiang, C. Lee, and H.-J. Whangbo, Phys. Rev. B **76**, 220411(R) (2007).
- [28] M. Matsuda, T. Katsumata, T. Yokoo, S. M. Shapiro, and G. Shirane, Phys. Rev. B **54**, R15626 (1996).
- [29] M. Matsuda, K. Kakurai, J. E. Lorenzo, L. P. Regnault, A. Hiess, and G. Shirane, Phys. Rev. B **68**, 060406(R) (2003).
- [30] F. Heidrich-Meisner, A. Honecker, and T. Vekua, Phys. Rev. B **74**, 220403(R) (2006).
- [31] T. Lu, A. Wang, S. Qin, and T. Xiang, Phys. Rev. B **87**, 134425 (2006).
- [32] J. Sirker, Phys. Rev. B **81**, 014419 (2010).

- [33] J.M. Tomczak, private commun.; and S.-L. Drechsler *et al.*, unpublished.
- [34] In the 1D isotropic J_1 - J_2 model the peak position of $\chi(T)$ is a monotonous function of α . $\chi(T)$ shows a divergency at $T = 0$ for $\alpha \leq \alpha_c = 1/4$. [30, 60, 68] whereas the magnetic specific heat c_v exhibits *two* maxima for $\alpha \lesssim 0.4$. Its lower, sharper peak is field dependent reflecting the low-lying FM excitations above the spiral spin liquid GS. The Sommerfeld coefficient γ is also a monotonous function of α , diverging for $\alpha \rightarrow \alpha_c$.
- [35] S. Johnston, C. Monney, V. Bisogni, K.-J. Zhou, R. Kraus, G. Behr, V.N. Strocov *et al.*, nature comm. **7**, 10563 (2016).
- [36] N. Wizen, N. Leps, G. Behr, R. Klingeler, B. Büchner and W. Löser, J. Cryst. Growth **401**, 586 (2014).
- [37] N. Wizen, *Hochdruckkristallzüchtung von ausgewählten Oxiden*, PhD-dissertation, TU Dresden (2009).
- [38] H.-J. Schmidt, A. Lohmann, and J. Richter, Phys. Rev. B **84**, 104443 (2011).
- [39] A. Lohmann, H.-J. Schmidt, and J. Richter, Phys. Rev. B **89**, 014415 (2014).
- [40] For the 10th-order HTE see the HTE10 package from <http://www.uni-magdeburg.de/jschulen/HTE10/>.
- [41] K. Kudo, S. Kurogi, Y. Koike, T. Nishizaki, and N. Kobayashi, Phys. Rev. B **71**, 104413 (2005).
- [42] H.-J. Schmidt, J. Schnack, and M. Luban, Phys. Rev. B **64**, 224415 (2001).
- [43] S. Nishimoto, S.-L. Drechsler, R.O. Kuzian, J. van den Brink, J. Richter *et al.*, Phys. Rev. Lett. **107**, 097201 (2011).
- [44] The exact quantum one- and two-magnon saturation fields have been derived with the help of the hard-core boson technique in the 1D case for the FM J_1 -AFM J_2 -problem. In the quasi-1D case relevant here, the weak IC has been taken into account within the perturbation theory checked numerically by DMRG calculations for a bundle of chains with periodic boundary conditions perpendicular to the chains within planar (2D) and 3D arrangement of chains resulting in very accurate analytical expressions on which Eq. (23) is based. ().
- [45] K. Caslin, R.K. Kremer, F.S. Razavi, A. Schulz, A. Muñoz, F. Pertlik, J. Liu, *et al.*, Phys. Rev. B **89**, 014412 (2014).
- [46] K. Caslin, *Investigations of frustrated quasi-one-dimensional quantum spin-chain materials*, PhD-dissertation, Brock University, St. Catharines, Ontario, Canada (2015).
- [47] S.E. Dutton, M. Kumar, M. Mourigal, Z.S. Soos, J.-J. We, C.L. Broholm *et al.*, Phys. Rev. Lett. **108**, 187206 (2011).
- [48] M. Bosiočić, S. E. Dutton, R. J. Cava, P. Baker, M. Požek, and P. Mendels, Phys. Rev. B **96**, 224424 (2017).
- [49] H.-J. Grafe, S. Nishimoto, M. Jakovleva, E. Vavilova, L. Spillecke, A. Alfonsov, *et al.*, Sci. Rep. **7**, 6729 (2017).
- [50] K. Nawa, Y. Okamoto, A. Matsuo, and *etal.*, J. Phys. Soc. Jpn. **83**, 103702 (2014).
- [51] O. Janson, A. A. Tsirlin, M. Schmitt, and H. Rosner, Phys. Rev. B **82**, 014424 (2010).
- [52] H. Rosner, *Electronic structure and exchange integrals of low-dimensional cuprates*, PhD-dissertation, TU Dresden (1999).
- [53] Y. Kim, R. Birgeneau, F. Chou, M. Greven, M.A. Kastner, Y.S. Lee, B.O. Wells, *et al.*, Phys. Rev. B **64**, 024435 (2001).
- [54] P. Babkevich, N.E. Shaik, D. Lançon, D. Kikkawa, A. and Enderle, M. and Ewings, *et al.*, Phys. Rev. B **96**, 014410 (2017).
- [55] S. Fatale, C.G. Fatuzzo, N.E. Shaik, J. Pellicciari, X. Lu, D.E. McNally, T. Schmitt *et al.*, Phys. Rev. B **96**, 115149 (2017).
- [56] M. S. Hybertsen, E. B. Stechel, M. Schlüter, and D. R. Jennison, Phys. Rev. B **41**, 11068 (1992).
- [57] M. S. Hybertsen, E. B. Stechel, W. M. C. Foulkes, and M. Schlüter, Phys. Rev. B **45**, 10032 (1992).
- [58] A. N. Yaresko, A. Y. Perlov, R. Hayn, and H. Rosner, Phys. Rev. B **65**, 115111 (2002).
- [59] V. Y. Yushankhai and R. Hayn, EPL **47**, 116 (1999).
- [60] S.-L. Drechsler, O. Volkova, A.N. Vasiliev, J. Richter, M. Schmitt, H. Rosner *et al.*, Phys. Rev. Lett. **98**, 077202 (2007).
- [61] Y. Tarui, Y. Kobatashi, and M. Sato, J. Phys. Soc. Jpn. **77**, 043703 (2008).
- [62] M. Schmitt, *Microscopic Description of magnetic model compounds*, PhD-dissertation, TU Dresden (2011).
- [63] Y. Yasui, N. Igawa, and K. Kakurai, J. Phys. Conf. Proc. **8**, 034012 (2015).
- [64] R. Bursill, G.A. Gehring, D.J.J. Farnell, J.B. Parkinson, T. Xiang and C. Zeng, J. Phys.: Cond. Matter **7**, 8605 (1995).
- [65] S. Nishimoto, S.-L. Drechsler, R.O. Kuzian, J. Richter, J. Málek, M. Schmitt *et al.*, EPL **98**, 37007 (2012).
- [66] S. J. Hibble, J. Köhler, A. Simon, and S. Paiser, J. Solid State Chem. **88**, 534 (1990).
- [67] J. Sudan, A. Lüscher, and N. Lüscher, Phys. Rev. B **80**, 140402(R) (2009).
- [68] S.-L. Drechsler, J. Richter, R. Kuzian, J. Málek, N. Tristan, B. Büchner *et al.*, J. Magnet. Magn. Mat. **316**, 306 (2007).
- [69] D. Miloslavlevic, private communication. (2019).
- [70] S.-L. Drechsler, J. Málek, R.O. Kuzian, S. Nishimoto, U. Nitzsche, *et al.*, Physica C **470**, Suppl. **1**, S94 (2010).
- [71] A. Tsirlin, private communication. (2019).
- [72] A.A. Gippius, E.N. Morozova, A.S. Moskvina, A.V. Zalessky, A.A. Bush, *et al.*, Phys. Rev. B **75**, 204406(R) (2004).
- [73] L. Capogna, and M. Reehuis, A. Maliuk, R.K. Kremer, B. Ouladdiaf, M. Jansen *et al.*, Phys. Rev. B **82**, 014407 (2010).
- [74] M. Schäpers, H. Rosner, S.-L. Drechsler, S. Süllow, R. Vogel, B. Büchner *et al.*, Phys. Rev. B **90**, 224417 (2014).
- [75] K. Rule, B. Willenberg, and M. Schäpers, A. Wolter, B. Büchner, S.-L. Drechsler, *et al.*, Phys. Rev. B **95**, 024430 (2017).
- [76] C. Koo, and E. Zvereva, E. and I. Zhukhaev, M. Richter, M. Stratan, *et al.*, J. Phys. Soc. Jpn. **85**, 084702 (2016).
- [77] M. Schmitt, O. Janson, S. Golbs, *et al.*, Phys. Rev. B **89**, 174403 (2014).
- [78] I. A. Zaloznyak, H. Woo, T. G. Perring, C. L. Broholm, C. D. Frost, and H. Takagi, Phys. Rev. Lett. **93**, 0987202 (2004).
- [79] K. Sparta, A. Löffler, C. Gross, W. Aßmus, and G. Roth, Zs. f. Kristallografie **221**, 782 (2006).
- [80] E. Bordas, C. de Graaf, R. Cabasllol, and C. J. Colzado, Theor. Chim. Acc. **116**, 535 (2006).
- [81] K. Ruck, M. Wolf, M. Ruck, D. Eckert, G. Krabbes, and K. H. Müller, Mat. Res. Bull. **36**, 1995 (2001).
- [82] V. Bisogni, S. Kourtis, C. Wohlfeld, and *etal.*, Phys. Rev. Lett. **112**, 147401 (2013).
- [83] E. Bordas, C. de Graef, R. Caballol, and C. Calzado, Phys. Rev. B **60**, 3457 (1999).
- [84] G. Deng, D. Yu, R. Mole, E. Pomjakushina, K. Conder, M. Kenzelmann, S. Yano *et al.*, *ibid.* **98**, 184411 (2018).
- [85] G. Deng, V. Pomjakushin, V. and Petricek, E. Pomjakushina, M. Kenzelmann, *et al.*, *ibid.* **84**, 14411 (2011).
- [86] S. A. Carter, B. Batlogg, R. Cava, J. J. Krajewski, W. F. Peck Jr., and T. M. Rice, Phys. Rev. Lett. **77**, 1378 (1996).
- [87] S. Lebernegg, A. Tsirlin, O. Janson, and H. Rosner, Phys. Rev. B **88**, 224406 (2013).

- [88] E.S. Klyushina, A.T. Islam, J.T. Park, E.A. Goremychkin, E. Wheeler, B. Klemke, and B. Lake, *ibid.*, **98**, 104413 (2018).
- [89] O. Janson, (2019), private commun.
- [90] J. Holmlund, C.S. Knee, J. Andreasson, M. Granath, A.P. Livinchuk and L. Böresson, *Phys. Rev. B* **79**, 085109 (2009).

TABLE I. Empirical (e) and theoretical (t) values for J_1 in various edge-sharing cuprates: S (single chain - pure edge-sharing), AS (alternating FM-AFM single chain) D(L) (single double (zigzag)-chain / 2L(P2L)- two-leg, 3L (three-leg) of ladder (pseudo-ladder) edge- and single edge-sharing chains) and frustration ratio $\alpha = J_2 / |J_1|$ (In case of AS $\text{Li}(\text{Na})_3\text{Cu}_2\text{SbO}_6$ the second coupling J_2 measures the AFM NN coupling via the longer Cu-Cu bond bridging Sb or Te. The mineral notation *linarite* and *malachite* stand for the chemical notations PbCuSO_4OH and $\text{Cu}_3(\text{AsO}_4)(\text{OH})_3$, respectively, PW means "present work" and the rows with "GPa" refer to studies under pressure.

system	type (sharing)	$-J_1$ (meV)	J_2 (meV)	α	Φ $^\circ$	$d_{\text{Cu-Cu}}$ (Å)	$d_{\text{Cu-O}}$ (Å)	Ref.
CYCO	S	2.2(t)	4.7	2.14	94.5	2.82	1.92	[2]
CYCO	S	24 (e)	5.5	0.23	94.1, 92.1	2.818, 2.826	1.953	PW [8]
Li_2CuO_2	S	19.8 (e)	0.4	0.31	93.97	2.86	1.956	[3]
Li_2CuO_2	S	8.6 (t)	5.5	0.62	94	2.86	1.956	[2]
Li_2CuO_2	S	14.5 (t)	7.4	0.53	93.97	2.86	1.956	[27]
Li_2CuO_2	S	18.5 (t)	5.8	0.31	93.97	2.86	1.956	[69], PW
Li_2CuO_2	S	19.5 (t)	4.9	0.31	93.97	2.86	1.956	[70]
Li_2CuO_2	S	19.8 (t)	0.4	0.31	93.97	2.86	1.958	PW
Li_2CuO_2	S	19.8 (t)	5.6	0.31	93.97	2.86	1.956	[71]
Li_2CuO_2	S	–	–	–	94, 90.66	2.782, 2.86	1.955, 1.956	[24] 0, 32.5 GPa
Li_2CuO_2	S	–	–	–	92	2.785	1.938	[26] 28.8 GPa
Li_2CuO_2	S	20,15,11	5,7,9	0.34,0.5,0.9	–	–	–	[25] 0, 3, 5 GPa
$\text{Li}_2\text{ZrCuO}_4$	S	23.5 (e)	7.05	0.3	94	2.88	2.00	[32, 60]
$\text{Li}_2\text{ZrCuO}_4$	S	17 (t)	4.5	0.3	94.13	2.88	2.00	[62]
LiCu_2O_2	S	13.9	3.7	0.33	93	2.86	1.98	[66, 72], PW
LiCu_2O_2	S	~17.2	10.9	0.6	93	–	–	[32]
NaCu_2O_2	S	–	–	–	92.9	2.93	1.971	[73]
NaCu_2O_2	S	15	5	0.33	92.9	2.93	1.971	[62]
LiCuVO_4	S	6.4-15.5	5.2-7.8	0.5-0.85	96.	2.899	1.965	[32, 65]
<i>linarite</i>	S	10	5.5	0.36	90.8, 94.2	2.823	1.915, 1.961	[74, 75]
CuGeO_3	S	-10	4.99	0.241-0.36	97.654	2.935	–	[6]
$\text{Li}_3\text{Cu}_2\text{SbO}_6$	AS	24.56	13.8	0.56	88.95	2.92	2.014	[76]
$\text{Na}_3\text{Cu}_2\text{SbO}_6$	AS	17.8,18.7	14.7, 14.99	1.21	95.27, 95	2.96	2.003	[77]
$\text{Na}_3\text{Cu}_2\text{TeO}_6$	AS	18.7	15.0	1.25 1	95.27, 95	2.86	1.9	[77]
SrCuO_2	D	23-48	226	4-10	87.5, 92.96	2.795	1.896, 1.958	[78]
SrCu_2O_3	2L	35.8	166 (e); 155 (t)	4.03 (t)	88x	2.78	1.976(2L)	[79, 80]
SrCu_2O_3	2L	30.6	226	7.39	87.4	2.781	1.97(L), 1.87(R)	[2]
CaCu_2O_3	P2L	28.2 (t)	139 (t), 160 (e)	4.93 (t)	90	2.8	1.908	[80–82]
$\text{Sr}_2\text{Cu}_3\text{O}_5$	3L	35.8	166 (e); 155 (t)	4.03(t)	–	2.781	1.976 (2L)	[79, 80]
$\text{Sr}_{14}\text{Cu}_{24}\text{O}_{41}$	2L+S	30.6	130	2.8	53	90	–	[83]
$\text{Sr}_{14}\text{Cu}_{24}\text{O}_{41}$	2L+S	26.1	226	–	88.6	2.75	1.9(L)m 1.97(R)	[2]
$\text{SrCa}_{13}\text{Cu}_{24}\text{O}_{41}$	2L+S	-5.4(!?) (S)	? (S)	?	88, 95	2.746	1.9(L)m 1.97(r)	[84, 85]
$\text{La}_5\text{Ca}_9\text{Cu}_{24}\text{O}_{41}$	2L+S	26	112	–	88.6	2.761	–	[29]
$\text{La}_6\text{Ca}_8\text{Cu}_{24}\text{O}_{41}$	2L+S	1.8 (S)	0	0	91.6	2.76	1.927	[86]
$\text{La}_6\text{Ca}_8\text{Cu}_{24}\text{O}_{41}$	2L+S	~30(S), ~35(L)	~12(S), 139(L)	~0.4(S), ~4(L)	91.6	2.761	1.927	[28] PW
$\text{La}_6\text{Ca}_8\text{Cu}_{24}\text{O}_{41}$	2L+S	26(L) 18.5(S)	6.72	0.36(S)	91.6	2.76	1.927	[2]
$\text{La}_6\text{Ca}_8\text{Cu}_{24}\text{O}_{41}$	2L+S	26(L) 18.5(S)	6.72	0.36(S)	91.6	2.76	1.927	[2]
<i>green diopside</i>	AS	3.2	6.7	0.66	97.4, 107	2.76	1.96	[51]
CuAs_2O_4	S	8.96	2.24	0.25	91.5	2.7865	1.95	[45, 46]
CuSb_2O_4	AFFS	10.78	5.15	0.5-0.55	94.5	2.7893	1.877, 2.073	[46]
LiCuSbO_4	S	13.79	3.24	0.24	89.8, 95.0	2.87	1.95, 2.04	bond 1 [47, 49]
LiCuSbO_4	AFFS	7.76	3.24	0.42	92.0, 96.8	2.87	1.92, 2.0	bond 2 [47, 49]
<i>malachite</i>	AS	12.11	6.73	0.56	94.75, 106.41	2.787	1.95	[87]
$\text{NaCuMoO}_4(\text{OH})$	S	4.121	3.36	0.56	91.97, 103.65	2.787	1.899, 2.07	[50]
$\text{BaCu}_2\text{VO}_2\text{O}_8$	AS	11.97	40.92	0.295	93.7	2.86	1.94, 1.983,	[88]
$\text{BaCu}_2\text{VO}_2\text{O}_8$	AS	14.80	46.	0.0.322	93.7	2.87	1.94, 1.983	[89]
$\text{Ba}_2\text{Cu}_3\text{O}_4\text{Cl}_2$	2D	10.3	8.4	0.82	90.0	2.57	1.899	[54]
$\text{Ba}_2\text{Cu}_3\text{O}_4\text{Cl}_2$	2D	18	10.5	1.05	90.0	2.787	1.899	[58]
$\text{Ba}_2\text{Cu}_3\text{O}_4\text{Cl}_2$	2D	10.3	8.4	0.82	90.0	2.57	1.899	[54]
$\text{Sr}_2\text{Cu}_3\text{O}_4\text{Cl}_2$	2D	10-14	10.5	1.05	90.0	2.7285	1.929	[53]
$\text{Sr}_2\text{Cu}_3\text{O}_4\text{Cl}_2$	2D	10-14	13.7	1.05	90.0	2.7285	1.929	[90]